Studies on Electronic Structures of Quasi One-Dimensional Phthalocyanine Conductors, $NiPc(AsF_6)_{0.5}$ and $CoPc(AsF_6)_{0.5}$

Yukako Yonehara

DOCTOR OF PHILOSOPHY

Department of Structural Molecular Science
School of Mathematical and Physical Science
The Graduate University for Advanced Studies

1998

Acknowledgments

The present work has been carried out under the supervision of professor Kyuya Yakushi. The author would like to express her heartfelt thanks to him for his continuous interest, encouragement, and enlightening guidance and discussions at all stage of this work.

The author would like to express sincere gratitude to professor I. Kogan (Institute for Chemical Physics Research Chernogolovka, Moscow Region) for guidance of electrochemical experiment. The author would like to acknowledge Dr. Chikako Nakano and Mr. Mikio Uruichi for analyzing the X-ray structure of $Co_xNi_{1-x}Pc(AsF_6)_{0.5}$ and optical measurement. The author would like to thank Dr. M. Symonyan for assisting and teaching me in ESR and SQUID experiment. The author wishes to thank Mr. J. Ouyang for his kind help and Dr. Akito Ugawa (University of Florida) for his valuable suggestions. The author is grateful to Dr. Yasuhiro Nakazawa for his instructive suggestions.

The author would like to thank professor Kenji Yonemitsu, Dr. Takuhiro Ogawa for the theoretical suggestions of the gap formation of $CoPc(AsF_6)_{0.5}$ and their kind help.

The author deeply thanks professor Hayao Kobayashi for low-temperature X-ray study of $NiPc(AsF_6)_{0.5}$. The author would like to thank Dr. J. McArthur (Quantum Design) for his assistance of the heat capacity experiment of $NiPc(AsF_6)_{0.5}$.

Thanks go to all members of Institute for Molecular Science for various contribution and kindness.

Contents

Chapter 1	*General Introduction*	1
1-1	Organic charge transfer salts	2
1-2	The d-π coexistent system containing transition metal	5
1-3	The standpoint of the phthalocyanine salts in the study of organic conductors	6
1-4	Purpose and constitution of the present thesis	7
	References	13
Chapter 2	*High-pressure study of one-dimensional phthalocyanine conductor, $NiPc(AsF_6)_{0.5}$*	19
2-1	Introduction	20
2-2	Experimental	21
2-3	Results and discussion	22
2-3-1	Crystal structure and band structure	22
2-3-2	Insulating phase at ambient pressure	26
2-3-3	Metal-insulator transition under high pressure	28
2-4	Summery	30
	References	31
Chapter 3	*Optical, EPR, and structural properties of solid platinum phthalocyanine in the different oxidation states of electrochemical process*	43
3-1	Introduction	44
3-1-1	Scope of this study	44
3-1-2	General introduction for the electrochemistry	48
	References	52
3-2	Experimental	57
3-3	Results and discussion	58
3-3-1	The difference of the voltamograms between the cycles	58
3-3-2	The determination of the composition	60
3-3-3	The determination of the structures of mid- and full-oxidized state	61

3-3-4 The composition of the absorption spectra between film A and B 62
3-3-5 Another characteristic of the voltammogram 65
3-3-6 The development of a new method of the doping 67
3-3-7 From the viewpoint of the filling control 68
3-4 Summary 71
3-5 The problem to be solved in future 72
References 74

Chapter 4 *Optical spectra of mixed crystals of phthalocyanine conductors* 95

Part 1 *Optical spectra of phthalocyanine charge transfer salts; $NiPc(AsF_6)_{0.5}$ and $CoPc(AsF_6)_{0.5}$* 96

4-1-1 Introduction 97
4-1-2 Experimental 98
4-1-3 Results and discussion 100
(a) Anomalous spectrum of $CoPc(AsF_6)_{0.5}$ 100
(b) Vibrational investigation 105
4-1-4 Summary 107
References 108

Part 2 *Characterization of the mixed crystals of $NiPc(AsF_6)_{0.5}$ and $CoPc(AsF_6)_{0.5}$* 124

4-2-1 Introduction 125
4-2-2 Experimental 128
4-2-3 Results and discussion 129
References 138

Chapter 5 *Concluding remarks* 163

Chapter 1

General Introduction

1-1 Organic charge transfer salts

Organic conductors show various kinds of phase transitions because of the low-dimensional nature. As regards the metal-nonmetal phase transition, roughly speaking, there are three kinds of mechanisms at least; the metal-nonmetal transition caused by (1) the structural change. (2) the electron-electron correlation (3) the charge localization resulted from the random potentials. Physical properties of the real materials are characterized by several parameters such as on-site Coulomb energy U, nearest-neighbor V, and transfer integral t. The handy yardsticks which we can utilize for the evaluation of the physical properties which are governed by these parameters are temperature T and pressure P. By controlling the temperature T or pressure P, we can indirectly observe the profile of each material and predict the balance of each parameters. In fact, various kinds of phase transition were observed in the temperature and pressure-dependent resistivity measurement; metal-insulator transition due to the charge density wave (CDW) or spin density wave (SDW) instability, superconducting transition and order-disorder transition.

TTF-TCNQ is the first organic metal discovered in 1973[1] and showed metallic conductivity down to 58 K.[2] The metallic character of TTF-TCNQ is also revealed by the optical spectra.[3] A typical Drude-like edge is observed in the 1 eV range only for the polarization of the light parallel to the highly conducting direction of the single crystals. This property reflects the very anisotropic nature of the electronic structure of TTF-TCNQ. As suggested by the optical experiment, TTF-TCNQ is a one-dimensional metal, hence shows a Peierls transition and becomes a CDW insulator.[4] Peierls[5] and Fröhlich[6] have predicted that one-dimensional conductors are inherently unstable against a lattice

distortion that opens a band gap at Fermi level. To stabilize a metallic state against the Peierls transition, it was attempted to increase the dimensionallity by means of the molecular design or adding pressure. Superconductivity of organic compounds was detected for the first time in 1980 in $(TMTSF)_2PF_6$ under the pressure of 12 kbar at 0.9 K.[7] Later, $(TMTSF)_2ClO_4$ was found to show superconductivity at 1.3 K under ambient pressure.[8] The metal-insulator transition driven by SDW instead of CDW was first identified in $(TMTSF)_2PF_6$.[9] In 1982, a two-dimensional conductor based on BEDT-TTF was synthesized[10] and in 1983, superconductivity was observed in $(BEDT-TTF)_2ReO_4$ under high-pressure.[11] Since then, many BEDT-TTF based superconductors have been discovered[12] and now, many organic conductors as well as Mott insulators based on radical cation or anion salts have been obtained. The Mott insulator is caused by the electron-electron correlation. The Hubbard model incorporates the electron-electron interaction into the one-electron tight-binding model. The Hubbard model Hamiltonian is written as

$$H = -t \sum_{\langle ij \rangle, \sigma} c_{i\sigma}^{+} c_{j\sigma} + U \sum_{i} c_{i\uparrow}^{+} c_{i\uparrow} c_{i\downarrow}^{+} c_{i\downarrow}$$

where t represents the transfer integral between the wave functions on the neighboring sites in the lattice, U represents the Coulomb interaction between two electrons on the same site, and $c_{i\sigma}^{+}$, $c_{j\sigma}$ are the creation, destruction operators of electrons with spin σ ($\uparrow$, $\downarrow$) for localized states. In the half-filled case, if $t>>U$, the electrons are delocalized into a single conduction band; if $t<<U$, the system should become Mott insulator.

Related to high-T_c cuprate superconductors, the doping for the Mott insulator is one of the topics of the study of organic superconductors. $La_{2-x}Sr_xCuO_4$ shows

superconductivity in the composition of x = 0.1-0.3.[13] Non-doped La_2CuO_4 exhibits the antiferromagnetic(AF) insulating phases because of the strong electron-electron correlation. The high-T_c cuprates were achieved by the hole doping to the AF insulating phase (Mott insulator) through the unusual metallic state. In the case of organic compounds, superconducting phase is often located near the magnetically ordered phase. The noticeable difference is that the organic superconductors were achieved by controlling the ratio between bandwidth and on-site Coulomb energy (U/4t) not by doping but by pressure. In other word, the control of the band-filling should become another effective parameter to control the physical properties in addition to conventional temperature T and pressure P. However, in contrast to inorganic materials, the filling control in organic conductors is not so easy because the crystal structure is extremely sensitive to the substituents or interstitial dopants. If it becomes possible to control the band-filling in the organic material, it is very interesting from the topical viewpoint as mentioned above being expected the development of new high-T_c organic materials. The filling control is one of the open question in the field of the organic conductors. The typical methods of filling control are ① preparation of a mixed crystal ② ion channel using alkali metal ③ two-bulb method for the graphite and C_{60} [14] ④ the mixed valence of Cu^+ and Cu^{2+}. κ-(BEDT-TTF)$_2$Cu$_2$(CN)$_3$ is one of the rare example which shows the metallic property by carrier doping to the Mott insulator. Recently, (BEDT-TTF)$_y$[$(MCl_4^{2-})_{1-x}(MCl_4^{-})_x$] ($M^{2+}$ = Mn^{2+} or Zn^{2+}, M^{3+} = Fe^{3+} or Ga^{3+}) was reported as a example of the band-filling control.[15]

1-2 The d-π coexistent system containing transition metal

Another noticeable field of the study of the organic conductor is the d-π coexistent system containing transition metal. Localized d-electron and itinerant π-electron coexist in the same system and interact with each other around the Fermi level. The most typical example is the mixed-valent copper complex (R_1, R_2-DCNQI)$_2$Cu system. In this system, there are a lot of derivatives that have different substituents; -CH_3, halogen, and so on. All the derivatives belong to the same crystal system with the space group, $I4_1/a$, however, the physical properties are very different from each other. (DMe-DCNQI)$_2$Cu remains metallic down to liquid helium temperature in spite of an apparent low-dimensional structure.[16] The Peierls instability due to the one-dimensionality was not observed. The stability of the metallic state in (DMe-DCNQI)$_2$Cu comes from the hybridization of Cu 3d-orbital and 1D organic π-band.[17] XPS and infrared studies have verified that the Cu has the mixed valent state $Cu^{4/3+}$ in the metallic state.[17,18] Therefore, the d-electron of Cu is expected to take part in the electronic states at the Fermi level. A first principle band calculation has shown this intuitive expectation is valid.[19] The reflectance spectrum of (DMe-DCNQI)$_2$Cu is different from one-dimensional compounds and does not show a strong anisotropy for the polarized direction.[20] This result also suggests the existence of the three-dimensional Fermi surface produced by the hybridization between π– and d-electronic systems. In the case of (DMe-DCNQI)$_2$Ag, the strong anisotropy was observed in the reflectance spectrum and indicates the existence of a one-dimensional electronic structure along the stacking direction in spite of the same crystal structure with (DMe-DCNQI)$_2$Cu.[5] This outstanding contrast is attributed to the difference of the energy levels of the copper 3d-

and silver 4d-orbitals of DMe-DCNQI's LUMO. As described above, the energy levels of the π- and d-electron systems provide a remarkable influence on the π-d interaction.

Another examples of π-d electron system are $M(dmit)_2$ salts (M =Ni, Pd *et.al*). In these salts, the hybridization occurs within one molecule. The energy gap between LUMO and HOMO is small, and only LUMO is able to hybridize with d_{xz}-orbital of central metal due to the request of the symmetry of the orbital. Therefore, the energy gap between LUMO and HOMO depends on the kind of the central metal.

1-3 The standpoint of the phthalocyanine salts in the study of organic materials

$NiPc(AsF_6)_{0.5}$ which is one of the subject materials of this thesis is a typical one-dimensional metal down to 40 K. In spite of the high one-dimensionallity, the matal-non-metallic transition of $NiPc(AsF_6)_{0.5}$ seems not to be the Peierls transition. On increasing pressure, the metal-nonmatal transition temperature moves to high temperature side. To investigate the property of this insulating phase is one of the main scope of the present thesis.

The important matter in the filling control is to keep the band structure and to be able to control the filling continuously. Judging from the fact that the $NiPc(AsF_6)_{0.5}$ does not show Peierls transition, the phthalocyanine is a rather hard compound against the lattice distortion. It seems to be favorable for the band-filling control.

Phthalocyanine salts are also a representative of the π-d system. In a similar way to $M(dmit)_2$ salts, the phthalocyanine salt is a remarkable material which contains both d- and π-electron systems in one molecule. The central metal and maclocycle produce one-dimensional 3d and π-bands, respectively. However, because of the symmetry

restriction, they don't mix in the same molecule. The HOMO of a phthalocyanine has a_{1u} symmetry, whereas $3d_z^2$ orbital of the central metal has a_{1g} symmetry. In the previous work of our group, a pressure-induced charge transfer was reported in $NiPc(AsF_6)_{0.5}$ and $CoPc(AsF_6)_{0.5}$ which means the change of the oxidation site. In addition to this interesting phenomenon in the phthalocyanine salts, there are some noticeable properties that is impossible to explain without the interaction between d- and π-electrons, for example, the difference of the conductivity between $NiPc(AsF_6)_{0.5}$ and $CoPc(AsF_6)_{0.5}$. Therefore, the electronic state of d- and π-electrons in this system should be one of the main scope of this thesis.

Based on the above points, purpose and constitution of the present thesis will be presented in the next section.

1-4 Purpose and constitution of the present thesis

The charge-transfer salts of metallo-phthalocyanines (MPcs) make up a family of quasi-one-dimensional organic conductors such as $MPc(X)_y$ (M = H_2, Ni, Co, Cu, Pt; X = I_3, BF_4, ClO_4, AsF_6, SbF_6; y = 0.33-1.0). Among these compounds, charge-transfer salts of NiPc, CoPc, and PtPc with y = 0.33 and 0.5 form double-chain and two-band systems: the central metal and macrocycle produce one-dimensional 3d and π-bands, respectively. Moreover, some phthalocyanine molecules contain unpaired d-electrons in the conjugated π-electron system. Due to this special nature, the itinerant π-electrons and localized unpaired d-electrons coexist in solid phthalocyanine salts.

$NiPc(AsF_6)_{0.5}$ shows metallic property at room temperature and undergoes a metal-insulator transition at 40 K.[21] The narrow 3d-band is located near the Fermi level

of the π-band. Due to this closeness, high pressure induces a metal-ligand charge-transfer between the 3d and π-bands, which was proved by the vibrational spectrum in the infrared region, plasmon absorption in the near-infrared region, and interband transition in the visible region.[22,23] The high-pressure optical experiment suggests that a metal-insulator transition accompanies the pressure-induced metal-ligand charge transfer.

In chapter 2, the results of high-pressure experiments of electrical resistivity and thermopower were presented to characterize this pressure-induced insulating phase. The metal-insulator transition temperature goes up to high temperature side on increasing pressure. The thermopower under high pressure decreased linearly against temperature and did not show any anomaly around the metal-insulator transition temperature. The metal-insulator transition under high-pressure is not accompanied by the opening of a gap at the Fermi level. Therefore, Peierls transition is not compatible with the behavior of the thermopower. There is a possibility that the insulating phase of $NiPc(AsF_6)_{0.5}$ is some kind of localized state probably due to the small amount of Ni^{3+}, in other words, a small amount of holes in the metal chain or narrow 3d band. The localized Ni^{3+} will be distributed randomly in the crystal and this excess charge produces random potentials, which make an influence on the coherent motions of the charge carriers in the π-band. Since the number of Ni^{3+} sites increases due to the metal-ligand charge transfer induced by high pressure, the insulating phase expands to the high-temperature region in a *P-T* phase diagram.

Pressure induced d-π charge transfer is regarded as a "band-filling control" by pressure. It is very interesting to investigate the physical properties in the various band

fillings which result in the different density of state or effective on-site Coulomb repulsion. However, under high-pressure, the practicable measurement is limited. Therefore, we tried to control the band filling at ambient pressure.

In Chapter 3, a new doping method in the solid state was presented and the possibility of the filling control was discussed. In the conventional electrochemical method through solution state, the crystal composition settled down one stable phase as a necessary result through an equilibrium condition. Therefore, as the first stage, we tried to develop a new doping method in the "solid state". We used the MPc-PBC composite films (M = Pt, Ni) as the starting material for doping. $TBAPF_6$ and $TBAAsF_6$ were adopted as supporting electrolytes. The doped film was characterized by X-ray diffraction, EPMA, ICP, ESR, and conductivity measurement. It showed almost the same properties as the crystals produced by the conventional electrochemical crystallization method. As the second stage, we tried to control the band filling by potential control in the range of the oxidation wave. Judging from the result of the X-ray diffraction study, MPc-PBC could not keep the same crystal structure over the potential range of the anodic peak giving the mixture pattern of undoped and doped one. As a result, we succeeded in the development of a new doping method based in solid state, though the continuous filling control by potential control could not be realized by this method.

In contrast to metallic $NiPc(AsF_6)_{0.5}$, nearly isostructural $CoPc(AsF_6)_{0.5}$ is a non-metal already at room temperature. The different point between two compounds is that the 3d-orbital of the central metal is singly occupied in $CoPc(AsF_6)_{0.5}$ and fully occupied in $NiPc(AsF_6)_{0.5}$. Figure 2 show the conductivity and thermopower of both salts

measured by H. Yamakado *et. al.*[24] The room-temperature value of conductivity of $CoPc(AsF_6)_{0.5}$ is *ca.* 100 S cm^{-1} and has a broad peak around room temperature. The thermopower of $CoPc(AsF_6)_{0.5}$ is almost temperature independent above 100 K. This property is very different from that of metallic $NiPc(AsF_6)_{0.5}$, in which the thermopower depends strongly on the temperature just below room temperature. The almost temperature-independent thermopower in the high-temperature region has been observed in large-U compounds such as $(TMTTF)_2BF_4$ and $Ag(DMe\text{-}DCNQI)_2$.[25,26] and suggest the localized nature of the charge carriers. Though CuPcI also has a magnetic moment on the central metal, it shows metallic behavior down to 20 K.[27] The thermopower of CuPcI resembles that of NiPcI rather than $CoPc(AsF_6)_{0.5}$. The magnetic susceptibility of CuPcI is described by two components: a temperature-dependent component from localized Cu^{2+} spins expressed well in a Curie-Weiss form, and a temperature-independent Pauli susceptibility. This suggests that the interaction between the spins on the neighboring Cu is very small. The temperature that the susceptibility deviates from the Curie-Weiss low is below 10 K suggesting the weak antiferromagnetic interactions between the neighboring Cu spins. This antiferromagnetic d-d interaction may contain direct interaction between the neighboring Cu ions and indirect interaction through the π-carriers. These results suggest that the influence of the local magnetic moment on the charge carriers is very weak in CuPcI. In the case of $CoPc(AsF_6)_{0.5}$, the Curie constant is one order of magnitude smaller than that of CuPcI. This suggests that the antiferromagnetic interaction between the neighboring Co spins is rather strong compared with CuPcI this strong interaction between the the neighboring Co spins may be due to the short Co-Co distance and the big overlap between the $3d_{z^2}$

orbitals which has unpaired electron of $CoPc(AsF_6)_{0.5}$. (The unpaired electron of CuPcI exists in the $3d_{x^2-y^2}$ orbital.) Judging from the non-metallic behavior of $CoPc(AsF_6)_{0.5}$, it seems that the strong interaction between the neighboring Co spins influences on the property of π-carriers. To promote our understanding for the interaction between the d-electrons which may contain both direct $J_{d\text{-}d}$ and indirect $J_{d\text{-}d}$ through $J_{\pi\text{-}d}$, we prepared the mixed crystals of $CoPc(AsF_6)_{0.5}$ and $NiPc(AsF_6)_{0.5}$.

In Chapter 4, the results of optical study of these mixed crystals were presented. The plasma frequency of $CoPc(AsF_6)_{0.5}$ is nearly 30 % larger than that of $NiPc(AsF_6)_{0.5}$. This result indicates the formation of one-dimensional d-band in $CoPc(AsF_6)_{0.5}$. The plasma edge of $Co_xNi_{1-x}Pc(AsF_6)_{0.5}$ is close to that of $NiPc(AsF_6)_{0.5}$ in spite of the small contents of Ni ions. This means that the overlap of Co d_{z^2}-orbital was interrupted by the introduction of non-magnetic Ni ions.

Abbreviations of donors and acceptors

Donor

TTF	Tetrathiafulvalene
TMTSF	Tetramethyltetraselenafulvalene
BEDT-TTF	Bis(ethylenedithio)tetrathiafulvalene
MPc	Metal Phthalocyanine

Acceptor

TCNQ	7,7,8,8-tetracyano-p-quinodimethane
DCNQI	N,N'-dicyano-p-quinodiimine
DMe-DCNQI	2,5-dimethyl-N,N'-dicyano-p-quinodiimine
dmit	1,3-dithiol-2-thione-4,5-dithiolate (=dimercaptoisotrithione)

References

[1] J. Ferraris, D. O. Cowan, V. Walatka, Jr. And J. H. Perlstein, *J. Am. Chem. Soc.*, **95**, 948 (1973).

[2] S. Etemad, *Phys. Rev. B*, **13**, 2254 (1976).

[3] D. B. Tanner, C. S. Jacobsen, A. F. Garito, A. J. Heeger, *Phys. Rev. B*, **13**, 3381 (1976).

[4] P. A. Lee, T. M. Rice, P. W. Anderson, *Solid State Commun.*, **14**, 703 (1974).

[5] R. E. Peierls, *Quantum Chemistry of Solids* (Clarendon, New York, 1964); *Quantum Theory of Solids* (Oxford Univ. Press, 1955)

[6] H. Fröhlich, *Proc. R. Soc. London*, **A223**, 296 (1954).

[7] D. Jérome, A. Mazaud, M. Ribault, K. Bechgaard, *J. Physique Lett.*, **41**, 95 (1980).

[8] K. Bechgaard, K. Carneiro, F. B. Rasmussen, M. Olsen, G. Rindorf, C. S. Jacobsen, H. J. Pederson, J. C. Scott, I. *Am. Chem. Soc.*, **103**, 1440 (1981).

[9] A. Andrieux, D. Jérome, K. Bechgaard, *J. Physique lett.*, **42**, 87 (1981).

[10] G. Saito, T. Enoki, K. Toriumi, H. Inokuchi, *Solid State Commun.*, **42**, 557 (1982).

[11] S. S. P. Parkin, E. M. Engler, R. R. Schumaker, R. Lagier, V. Y. Lee, J. C. Scott, R. L. Greene, *Phys. Rev. Lett.*, **50**, 270 (1983).

[12] T. Ishiguro, K. Yamaji, *Organic Superconductors*, Solid State Science 88, springer-Verlag (1990).

[13] (a) M. W. Shafer, T. Penney, B. L. Olson, *Phys. Rev. B* **36**, 4047 (1987).

(b) H. Takagi, T. Ido, S. Ishibashi, M. Uota, S. Uchida, Y. Tokura, *Phys. Rev. B* **40**, 2254 (1989).

(c) J. B. Torance, Y. Tokura, A. I. Nazzal, A. Bezinge, T. C. Huang, S. S. P. Parkin, *Phys. Rev. Lett.* **61**, 1127 (1988).

(d) J. B. Torance, A. Bezinge, A. I. Nazzal, T. C. Huang, S. S. P. Parkin, D. T. Keane, S. J. LaPlaca, P. M. Horn, G. A. Held, *Phys. Rev. B* **40**, 8872 (1989).

(e) R. B. van Dover, R. J. Cava, B. Batlogg, E. A. Reitman, *Phys. Rev. B* **35**, 5337 (1987).

[14] D. E. Nixon, G. S. Parry, *Br. J. Appl. Phys. Ser. 2* **1**, 291 (1968).

[15] R. Kumai, A. Asamitsu, Y. Tokura, submitted to *J. Am. Chem. Soc.*

[16] A. Aumüller, *Angew. Chem. Int. Ed. Engel.* **25**, 740 (1986).

[17] H. Kobayashi, A. Miyamoto, R. Kato, F. Sakai, A. Kobayashi, Y. Yamamoto, Y. Furukawa, T. Tasumi, T. Watanabe, *Phys. Rev. B* **47**, 3495 (1993).

[18] I. H. Inoue, A. Kakizaki, H. Namatame, A. Fujimori, A. Kobayashi, R. Kato, H. Kobayashi, *Phys. Rev. B* **45**, 5828 (1992).

[19] T. Miyazaki, K. Terakura, Y. Morikawa, T. Yamasaki, *Phys Rev. Lett.* **74**, 5104 (1995).

[20] K. Yakushi, A. Ugawa, G. Ojima, T. Ida, H. Tajima, H. Kuroda, R. Kato, H. Kobayashi, *Mol. Cryst. Liq. Cryst.*, **181**, pp.217 (1990).

[21] K. Yakushi, H. Yamakado, M. Yoshitake, N. Kosugi, H. Kuroda, T. Sugano, M. Kinoshita, A. Kawamoto, J. Tanaka, *Bull Chem. Soc. Jpn.* **62**, 687 (1989).

[22] T. Hiejima, K. Yakushi, *Solid State Commun.*, **95**, 661 (1995).

[23] T. Hiejima, K. Yakushi, *J. Chem. Phys.* **103**, 3950 (1995).

[24] H. Yamakado, T. Ida, A. Ugawa, K. Yakushi, K. Awaga, Y. Maruyama, K. Imaeda, H. Inokuchi, *Synth. Met.* **62**, 169 (1994).

[25] K. Mortensen, E. M. Conwell, J. M. Fabre, *Phys. Rev. B*, **28**, 5856 (1983).

[26] T. Mori, H. Inokuchi, A. Kobayashi, R. Kato, H. Kobayashi, *Phys. Rev. B*, **38**, 5913 (1988).

[27] M. Y. Ogawa, J. Martinsen, S. M. Palmer, J. L. Stanton, J. Tanaka, R. L. Greene, B. M. Hoffman, J. A. Ibers, *J. Am. Chem. Soc.*, **109**, 1115 (1987).

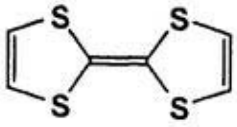

TTF

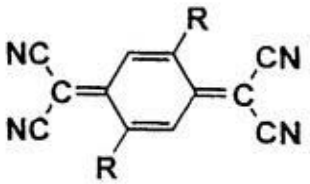

TCNQ (R = H)
DMeTCNQ (R = CH_3)

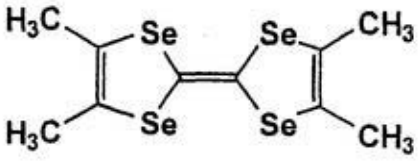

TMTSF

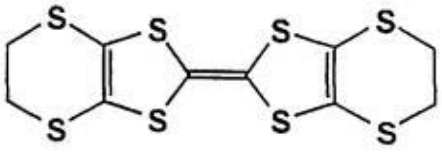

BEDT-TTF

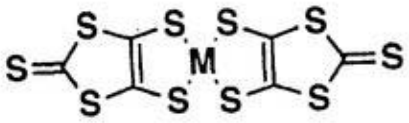

$M(dmit)_2$

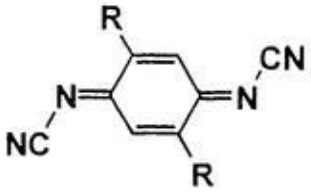

DCNQI (R = H)
DMeDCNQI (R = CH_3)

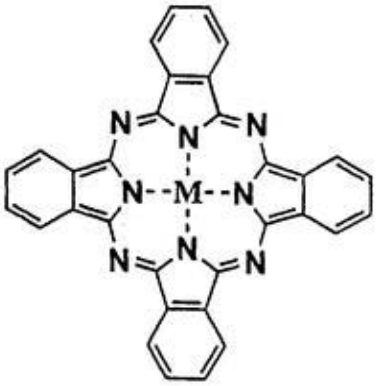

Metal-phthalocyanine
(M = H_2, Co, Ni, Cu, Pt)

Fig. 1 Molecular structures of organic donor and acceptors

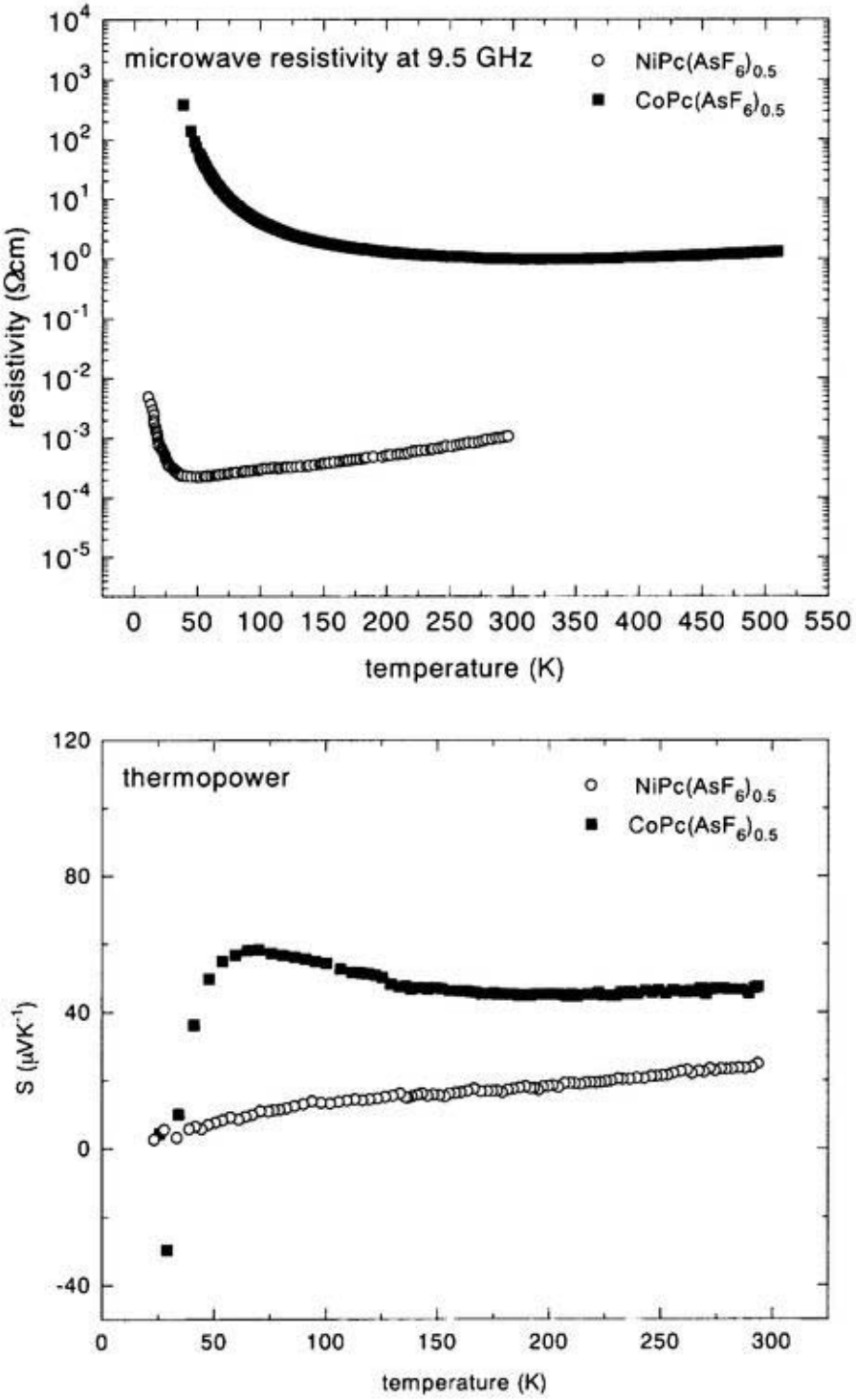

Fig. 2 The resistivity and thermopower of $CoPc(AsF_6)_{0.5}$ and $NiPc(AsF_6)_{0.5}$

Chapter 2

High-pressure study of one-dimensional phthalocyanine conductor, $NiPc(AsF_6)_{0.5}$

薬師久弥、米原由華子
フタロシアニン導体における圧力誘起電荷移動
高圧力の科学と技術第 6 巻第 3 号（1997 年）167-175.

Y. Yonehara, K. Yakushi
High-pressure study of one-dimensional phthalocyanine conductor, $NiPc(AsF_6)_{0.5}$
Synth. Met., **94** (1998) 149-155.

2-1 Introduction

The charge-transfer salts of metallo-phthalocyanines (MPcs) make up a family of quasi-one-dimensional organic conductors such as $MPc(X)_y$ (M = H_2, Ni, Co, Cu, Pt; X = I_3, BF_4, ClO_4, AsF_6, SbF_6; y = 0.33-1.0). Among these compounds, charge-transfer salts of NiPc, CoPc, and PtPc with y = 0.33 and 0.5 form double-chain and two-band systems: the central metal and maclocycle produce one-dimensional 3d and π-bands, respectively. In $NiPc(AsF_6)_{0.5}$, positive holes are doped into this π-band at ambient pressure, being metallic above the metal-insulator transition temperature of 40K.[1] The narrow 3d-band is located near the Fermi level of the π-band. Due to this closeness, high pressure induces a metal-ligand charge-transfer between the 3d and π-bands was proved by the vibrational spectrum in the infrared region, plasmon absorption in the near-infrared region and interband transition in the visible region.[2, 3] When pressure is applied to this compound, these π-holes being to flow into the 3d-band at about 0.5 GPa and this charge flow continues up to about 7 GPa.

The high pressure optical experiment suggests that a metal-insulator transition accompanies the pressure-induced metal-ligand charge transfer. To characterize this pressure-induced insulating phase, we have conducted high pressure experiments of powder X-ray diffraction, electrical resistivity and thermopower. It becomes more obvious from these experiments that the low temperature insulating phase at ambient pressure evolves by high pressure to the high temperature region. In this Chapter, we review the band structure of this two-band system and the optical experiment of the pressure-induced charge transfer, and then discuss the nature of the nonmetallic state.

2-2 Experimental

The finely powdered nickel phthalocyanine (NiPc) was sublimated in vacuum (about 10^{-4} Pa) three times. The radical salts of NiPc were prepared by the method of electrochemical crystallization at 120 ℃ under Ar atmosphere using an electrochemical cell separated into two compartments by a glass filter. 1-Chloronaphthalene used as the solvent was refluxed with CaH_2 and purified by vacuum distillation. The concentrations of the electrolytes, $(n\text{-}C_4H_9)_4NAsF_6$, and NiPc were 2.5 $\times 10^{-3}$ and 3×10^{-4} mol/l, respectively. The crystal grown near the glass filter in the anode compartment after about two weeks with a galvanostatic mode of 2-4 μA.

The high-pressure electrical resistivity of the $NiPc(AsF_6)_{0.5}$ single crystal was measured by means of a four-probe method using a clamped piston cylinder made of BeCu alloy. Idemitsu Daphne oil No. 7373 was used as a pressure medium. The pressure in the cell was monitored with the resistance change of a manganin wire (0.025mm ϕ, noncoating). The pressure drop which is caused by the decrease in the volume of the pressure medium was *ca.* 3 kbar from 295 to 2 K (Fig. 1A). The absolute pressure was corrected by NH_4F which shows phase transition at 3.61 kbar with uncontinuous volume change. The digital indicator of the press shows 88 kgf/cm^2 at the phase transition point of NH_4F using the 6 mm ϕ Teflon cell (Fig. 1B). Therefore, 100 kgf/cm^2 is corrected to 0.414 GPa. The high pressure cell was installed on the sample pack of Quantun Design PPMS. The resistance was measured using the resistance measurement system equipped in PPMS.

The thermopower was measured along the conducting axis by modifying the method of Chaikin and Kwak by applying a small temperature difference of less than

0.5 K.[4] Both edges of a single crystal were bonded to the 1mm gold foils attached to boron nitride heat sink blocks in which a carbon heater (100 Ω) was embedded. A temperature difference was measured by Au(Fe)-chromel thermocouple. This apparatus was mounted on a sample pack of PPMS. The voltage between the electrodes was measured on a Keithley 2001 multimeter. The software program for controlling the heater current and for sampling the voltage was combined with the temperature control system of PPMS. The high pressure thermopower device was made of a glass epoxy plate, both sides of which were coated with copper. As shown in Fig. 1C, one of the arms was heated by manganin wire (0.1mm ϕ, polyester coating) to make a temperature difference, which was measured by a Cu-constantan thermocouple. The pressure dependence of the thermopower of this thermocouple was neglected. The inner pressure was monitored by the resistance of the manganin wire installed on the back side. The arms were bridged by the sample through 1 μm gold foil.

2-3 Results and Discussion

2-3-1 Crystal structure and band structure

The crystal of $NiPc(AsF_6)_{0.5}$ belongs to an orthorhombic system, the lattice parameters being a = 14.015 Å, b = 28.485 Å, c = 6.466 Å, and Z = 4. The neighboring molecules along the c-axis are connected with each other by a glide plane symmetry.[1] Due to the requirement of this symmetry, the blanches of the energy band folded at $k = \pi/c$ are not split. So the band structure is equivalent to that of the regular stack with a half (c/2) periodic unit. This molecular arrangement produces two chains: metal (Ni) chain and macrocycle (Pc) chain. According to the molecular orbital calculation with the

Xα method by Kutzler and Ellis[5], the HOMO of Ni is $3d_z^2$ with a_{1g} symmetry which is elongated to the adjacent Ni, and the HOMO of Pc with a_{1u} symmetry has nodes at the eight nitrogen atoms. Thus, the a_{1u} molecular orbital of Pc is spatially separated from the $3d_z^2$ orbital of Ni in addition to the orthogonal symmetry. Therefore, these two orbitals cannot be hybridized with each other. According to their calculation of the one-dimensional band, the 3d band is quite narrow whereas the π-band produced by the a_{1u} HOMO is wide enough. In $NiPc(AsF_6)_{0.5}$, holes are introduced mainly in the π-band, forming a 3/4-filled metallic band. From the analysis of the polarized reflectance spectrum of E//*c*, the band width of this π-band was estimated to be 1.35 eV as mentioned in Chapter 4. As pointed out in Ref. 1, however, some holes are partly introduced in the 3d-band, which strongly depends upon the sample crystals. We suppose that this sample dependence comes from the non-stoichiometry, namely, a slight deviation from x = 0.5 in $NiPc(AsF_6)_x$, although it has not been experimentally proved yet. In this experiment, we used the crystal in which holes are mainly doped in the π-band which is characterized from the ESR line width of 1-3 G. This result suggests that the 3d-band is located just below the Fermi level of the π-band, as schematically shown in Fig. 2.

The high pressure reflectivity measurement of the single crystal of $NiPc(AsF_6)_{0.5}$ showed an unusual behavior.[6, 7, 8] The plasma edge of the reflection spectrum of E//*c* polarization shifted to a lower wavenumber at 1.6 GPa, contrary to an ordinary organic conductor such as TTF-TCNQ.[9] The interband transition from the filled lower band to the 3/4-filled conduction band weakened and disappeared above 0.5 GPa. It was suggested that the oxidation site changed from Pc to Ni.[6, 7, 8] A more detailed

experiment was conducted using powdered samples.[3] This interpretation was proved by the pressure dependencies of the molecular vibration and of plasmon absorption by conduction electrons. The pressure dependence of plasmon absorption and intensity in Fig. 3 and Fig. 4, in which the correction of the integrated intensity (open circles) is newly added. The correction is necessary, since the integrated intensity depends upon the dielectric constant of the pressure medium which increases upon pressure. The absorption spectrum of powder samples dispersed in transparent medium is given by the formula:

$$\alpha(\omega) \propto \frac{\varepsilon_a^{3/2}\varepsilon_{2z}(\omega)\omega}{\left[\varepsilon_{1z}(\omega)+2\varepsilon_a\right]^2+\varepsilon_{2z}^{\ 2}(\omega)}$$

according to the effective medium theory[10], where ε_0 is the dielectric constant of pressure medium, $\varepsilon_{1z}(\omega)$ and $\varepsilon_{2z}(\omega)$ the z-components (c-axis) of the real and imaginary parts of the dielectric function of sample crystal. Based on this equation, the absorption spectrum was simulated using the Drude-type dielectric function which is described following equation,

$$\varepsilon(\omega) = \varepsilon_c - \omega_p^{\ 2}/\left(\omega^2 + i\omega\tau\right)$$

where τ is the relaxation time of the carriers, and ω_p is the plasma frequency. From the analysis of the polarized reflectance spectra of the single crystal, the Drude parameters were obtained as ω_p = 7170 cm^{-1} for plasma frequency, $1/\tau$ = 450 cm^{-1} for the relaxation rate, and ε_c = 2.18 for the dielectric constant coming from the high frequency region. In the pre-correction data, the dielectric constant of the pressure medium was approximated by the square of the refractive index of solid paraffin (n_0 = 1.433 at 589 nm).

The correction did not change the previous result qualitatively. Since the integrated intensity of plasmon absorption is proportional to the square of the plasma frequency $\omega_p^2 = Ne^2/\varepsilon_0 m^*$, where ε_0 is the dielectric constant of vacuum, the open circles are proportional to the carrier concentration divided by effective mass N / m^*. Below 1GPa, as shown in this figure, N / m^* increases due to the decrease of the effective mass, but above 1.0 GPa it turns down and reaches almost zero above 1.0 GPa it turns down and reaches almost zero above 6 GPa. On the other hand, the peak position of the plasmon absorption is proportional to ω_p according to the effective medium theory.[10] This means that the absorption peak should shift to lower wavenumber, if this compound maintains metallicity. However, this absorption does not shift to lower wavenumber, but rather to slightly higher wavenumber. This behavior suggests a phase change from metal to insulator.[3]

The structural information in the high pressure region is available from the high pressure experiment of X-ray diffraction. All the diffraction lines of the powder sample show monotonic high-angle shift with increasing pressure, and any anomaly such as the disappearance or splitting of some diffraction lines was not observed in the pressure region up to 4.1 GPa. These results indicate that the crystal structure is maintained in the entire pressure region. In an organic conductor, an insulating phase is often brought about by Peierls instability, which cannot be detected by the powder X-ray diffraction, since the lattice distortion is very small. The sensitive probe for this kind of lattice distortion is the vibronic mode which is strongly coupled with conduction electrons. However, the infrared spectrum shows monotonic high-frequency shift and no vibronic mode was observed up to 4 GPa.[3] These two results indicate that the metal-insulator

transition suggested by the plasmon absorption is ascribable to an electronic origin.

The X-ray diffraction patterns are indexed based on the lattice parameters of ambient pressure. Since the lattice parameter *a* is very close to *b*/2 and, thus, for example, (200) and (040), and (141) and (221) could not be resolved from each other, we analyzed the X-ray diffraction lines assuming a tetragonal symmetry. The result is shown in Fig. 5. The lattice parameters are not linearly changed against the pressure contrary to the linear change in the low pressure range (0-2 GPa) of organic conductors such as β-(BEDT-TTF)$_2$I$_3$[11], (TMTTF)$_2$PF$_6$[12], and TTF-TCNQ.[13] The lattice contraction in the pressure region above 2 GPa is very similar to the above compounds. A more detailed experiment using a single crystal is necessary to elucidate the unusual behavior in the low pressure region. High pressure shortens the crystal lattice significantly, for example, *c*-axis changes from 6.466 to 5.82 Å, i. e., about a 10 % contraction.

2-3-2 Insulating phase at ambient pressure

Let us discuss the metal-insulator transition at ambient pressure and the properties of the low temperature phase. The top panel of Fig. 6 shows the temperature dependence of the microwave resistivity at 9.5 GHz.[14] NiPc(AsF$_6$)$_{0.5}$ is metallic down to about 40 K and undergoes a metal-insulator transition. The result of the reflectance spectroscopic study of single crystal shows that the metal-insulator transition of NiPc(AsF$_6$)$_{0.5}$ at 40 K accompanied extremely small or no lattice dimerization along the *c*-axis as described in Chapter 4. The thermopower displayed in the bottom panel of Fig. 6 behaves like a metal even below 40 K. Since thermopower is sensitive to the density of states at the Fermi level, this metal-insulator transition is not accompanied by the opening of a gap at

the Fermi level. These properties resemble $Li_{1+x}Ti_{2-x}O_4$, the thermopower of which exhibits linear decrease in the nonmetallic region of x = 0.15, 0.20, 0.22 and 0.25 in the same way as the metallic region of x = 0.[15,16] A finite density of states was suggested at the Fermi level of these nonmetallic compounds. Magnetic susceptibility also provides information on the density of states at the Fermi level.

Fig. 7 shows the paramagnetic susceptibility, which is very well reproduced by the model, $\chi_m(T) = 0.00285 / (T + 0.855) + 4.99\times10^{-5}$, shown by the solid line. The triangles are the residuals subtracted by the Curie-Weiss term from the observed susceptibility: $\chi_{obs}(T) - 0.00285 / (T + 0.855)$. The inset shows this almost temperature-independent component on an expanded scale. This is close to the paramagnetic susceptibility of 5.8×10^{-5} emu / mol, which is calculated using the formula $\chi_p = N\mu_B^2 / [t\pi\sin(3\pi/4)]$ based on the one-dimensional tight-binding band. So this temperature-independent term in the metallic region is regarded as a Pauli paramagnetism. In the insulating phase below 40 K, however, the magnetic susceptibility still remains finite. These separate properties of charge and spin excitation look like a Mott transition in a quasi-one-dimensional system. However, Mott transition is not compatible with the behavior of the thermopower. The temperature-independent property in the insulating phase also resembles the magnetic properties of insulating $Li_{1+x}Ti_{2-x}O_4$.[17] In these materials, the nonmetallic state is attributed to the localized states.[15] Thus, we propose that the low-temperature insulating phase is some kind of localized state probably due to the small amount of Ni^{3+}, in other words, a small amount of holes in the metal chain or narrow 3d band. The localized Ni^{3+} will be distributed randomly in the crystal and this excess charge produces random potentials, which make

an influence on the coherent motions of the charge carriers in the π-band.

The preliminary data of heat capacity and low-temperature X-ray diffraction study indicate that the possibility of some kind of structural change around the metal-insulator transition temperature such as a torsion of the phthalocyanine molecular "gear" in the *a,b*-plane accompanying the change of crystal system from orthorhombic to monoclinic. Fig. 8 shows the temperature-dependent heat capacity of $NiPc(AsF_6)_{0.5}$. Optical experiment which is very sensitive to the lattice dimerization also did not show any evidence of lattice dimerization. Consequently, these structural change will not directly influence on the electronic state of the one-dimensional chain.

2-3-3 Metal-insulator transition under high pressure

The resistance at room temperature continuously decreases when we slowly apply the pressure, and shows about 20 % decrease at 1.1 GPa. As shown in Fig. 9, the metal-insulator transition temperature goes up to about 230 K at 1.0 GPa. To characterize the high pressure insulating phase, we measured the thermopower, the result being shown in Fig. 10. The linear decrease against temperature and no anomaly around the metal-insulator transition temperature are the same as those characteristics taken at ambient pressure. This result indicates that the insulating phase at ambient pressure is the same as the high pressure insulating phase and that the insulating phase expands to the high temperature region in the *P-T* phase diagram. Probably the metal-insulator transition temperature will become higher than room temperature when the pressure is higher than 1 GPa. The elevation of the transition temperature will be connected to the room temperature metal-insulator transition point against the pressure in the *P-T* phase

diagram. The extension of the insulating phase under high pressure is understandable based on the pressure-induced metal-ligand charge transfer as will be mentioned in the next section.

Since the pressure below 10 GPa has little effect on the covalent bond within the molecule, the M-N distance within the phthalocyanine (MPc) molecule will not change under pressure below 10 GPa. The contraction along the *a*- or *b*-axis makes the molecular columns closer, but does not shorten the M-N distance. On the other hand, the contraction along the *c*-axis directly shortens the metal-metal distance. Consequently, the hydrostatic pressure gives the same effect as the uniaxial stress along the *c*-axis. The environment of the metal ion is the Ni_2N_4 octahedral coordination elongated along the c-axis as shown in Fig. as the exrernal pressure increases, only the metal-metal distance is shortened: Ni-N = 2.00 Å, Ni-Ni = 3.23 Å at ambient pressure and Ni-N = 2.00 Å, Ni-Ni = 2.91 Å at 4.1 GPa. According to the ligand field theory, this geometrical change pushes up the orbital energy of $3d_z^2$. Since the 3dz2 orbital is located near the Fermi level of the π-band, the electrons in the 3d band will flow into the vacant state of the π-band. Since the 3d-band is narrow, the holes produced by this mechanism will be localized and enhance the numbers of random potential. The enhanced randomness by pressure will increase the metal-insulator transition temperature. The extension of the insulating phase will be interpreted in this way. Incidentally, it should be noted that the metal-ligand charge transfer seems to be difficult when we take into account the electron correlation in the narrow 3d-band and the increase of the bandwidth of the π-band. High pressure widens the bandwidth of the π-band, and thus lifts up the Fermi level. Furthermore, when the 3d-electron moves into the π-band, the 3d-band will be stabilized

due to the decrease of the on-site Coulomb energy. Both are against the charge transfer from the 3d to π-band. Pushing up the 3d-band should overcome this difficulty to complete the metal-ligand charge transfer. The continuous charge transfer in a wide pressure range can be understood by this situation.

Finally, we comment on the high pressure phase in the range higher than 2 GPa. Upon increasing pressure, the degree of the metal-ligand charge transfer increases and thus the 3d hole concentration increases. To minimize the electrostatic repulsion, the 3d holes possibly make a lattice, which erases the randomness. Therefore, this material might be metallic again, if this 3d-hole lattice is produced before all the π-holes change into 3d-holes. This possibility is suggested by the continuous decrease of the resistance of the powdered sample up to 7.6 GPa.[18]

2-4 Summery

The analysis of the plasmon absorption has suggested the metal-insulator transition in $NiPc(AsF_6)_{0.5}$. From the high-pressure experiments of electrical resistivity and thermopower, it is more likely that this insulating phase is the same as the low temperature phase at ambient pressure, which is regarded as some kind of localization comes from the random potential generated by the randomly distributed Ni^{3+}. Since the number of Ni^{3+} sites increases due to the metal-ligand charge transfer induced by high pressure, the insulating phase expands to the high-temperature region in a *P-T* phase diagram.

References

[1] K. Yakushi, H. Yamakado, M. Yoshitake, N. Kosugi, H. Kuroda, T. Sugano, M. Kinoshita, A. Kawamoto, J. Tanaka, *Bull Chem. Soc. Jpn.* **62**, 687 (1989).

[2] T. Hiejima, K. Yakushi, *Solid State Commun.* **95**, 661 (1995).

[3] T. Hiejima, K. Yakushi, *J. Chem. Phys.* **103**, 3950 (1995).

[4] P. M. Chaikin, J. F. Kwak, *Rev. Sci. Instrum.* **46**, 218 (1975).

[5] F. W. Kutzler, D. E. Ellis, *J. Chem. Phys.* **84**, 1033 (1986).

[6] K. Yakushi, H. Yamakado, T. Ida, A. Ugawa, H. Masuda, H. Kuroda, *Spring Proceedings in Physics*, Vol. **51**, Springer, Berlin. 1990, p.54.

[7] T. Ida, H. Yamakado, H. Masuda, K. Yakushi, D. Kanazawa, H. Tajima, H. Kuroda, *Mol. Cryst. Liq. Cryst.* **181**, 243 (1990).

[8] T. Ida, Thesis, University of Tokyo, 1991.

[9] B. Welber, P. E. Seiden, P. M. Grant, *Phys. Rev. B* **18**, 2692 (1978).

[10] G. C. Papavassiliou, *Prog. Solid State Chem.* **12**, 185 (1979).

[11] H. Tanino, K. Kato, M. Tokumoto, H. Anzai, G. Saito, *J. Phys. Soc. Jpn.* **54**, 2390 (1985).

[12] B. Morosin, J. E. Schirber, R. L. Greene, E. M. Engler, *Phys. Rev. B* **26**, 2660 (1982).

[13] D. Debray, R. Millet, D. Jérome, S. Barisic, L. Giral, J. M. Fabre, *J. Phys.* **38**, L227 (1977).

[14] H. Yamakado, Thesis, Graduate University for Advanced Studies, 1991. We have not succeeded in obtaining the temperature-dependent d. c. resistivity in the whole temperature range due to frequent resistivity jumps.

[15] I. Maekawa, F. Takagi, Y. Sakai, N. Tsuda, *J. Phys. Soc. Jpn.* **56**, 2119 (1987).

[16] M. Watanabe, K. Kaneda, H. Takeda, N. Tsuda, *J. Phys. Soc. Jpn.* **53**, 2437 (1984).

[17] M. R. Harrison, P. P. Edwards, J. B. Goodenough, *Philos. Mag. B* **52**, 679 (1985).

[18] T. Hiejima, K. Yakushi, T. Adachi, O. Shimomura, K. Takeda, I. Shirotani, K. Imaeda, H. Inokuchi, *Mol. Cryst. Liq. Cryst.* **296**, 255 (1997).

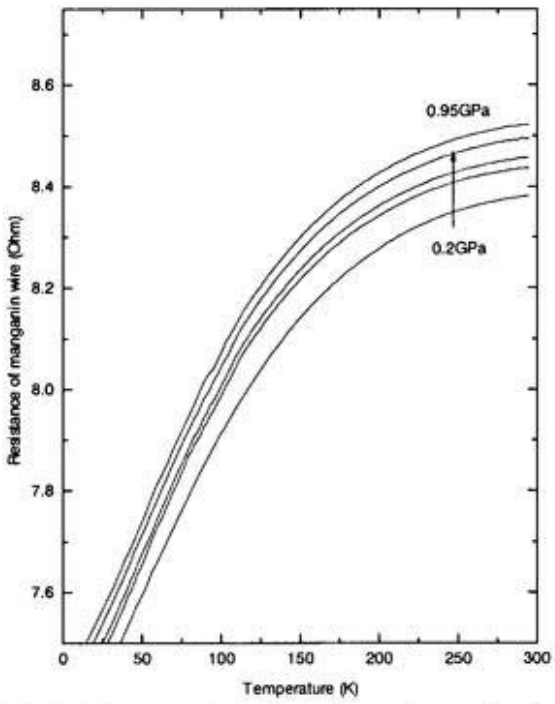

Fig. 1A Temperature-dependent resistance of manganine wire

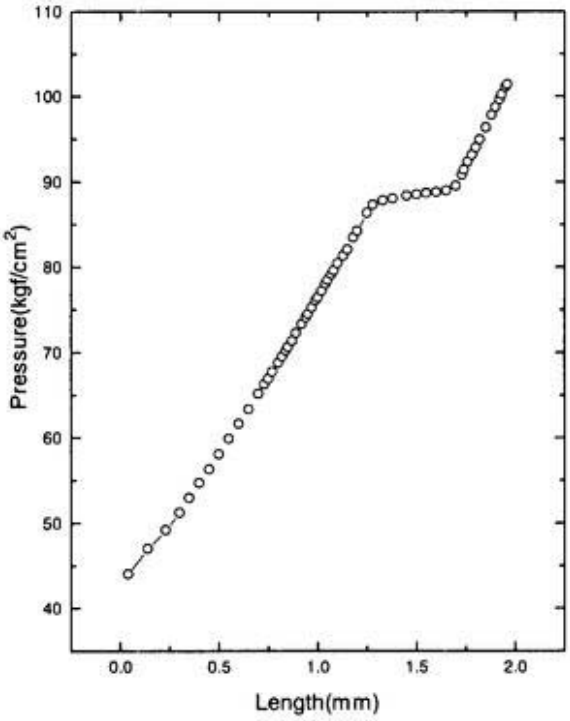

Fig.1B The phase transition point of NH_4F

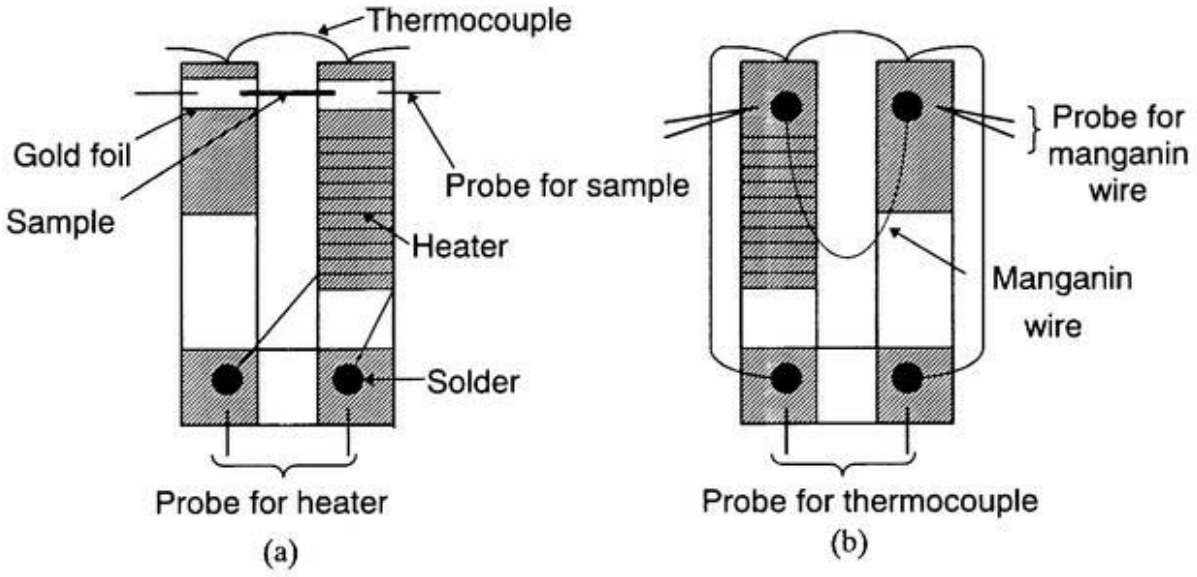

Fig. 1C Sketch of the high pressure device for the measurement of thermopower: (a) front side; (b) back side

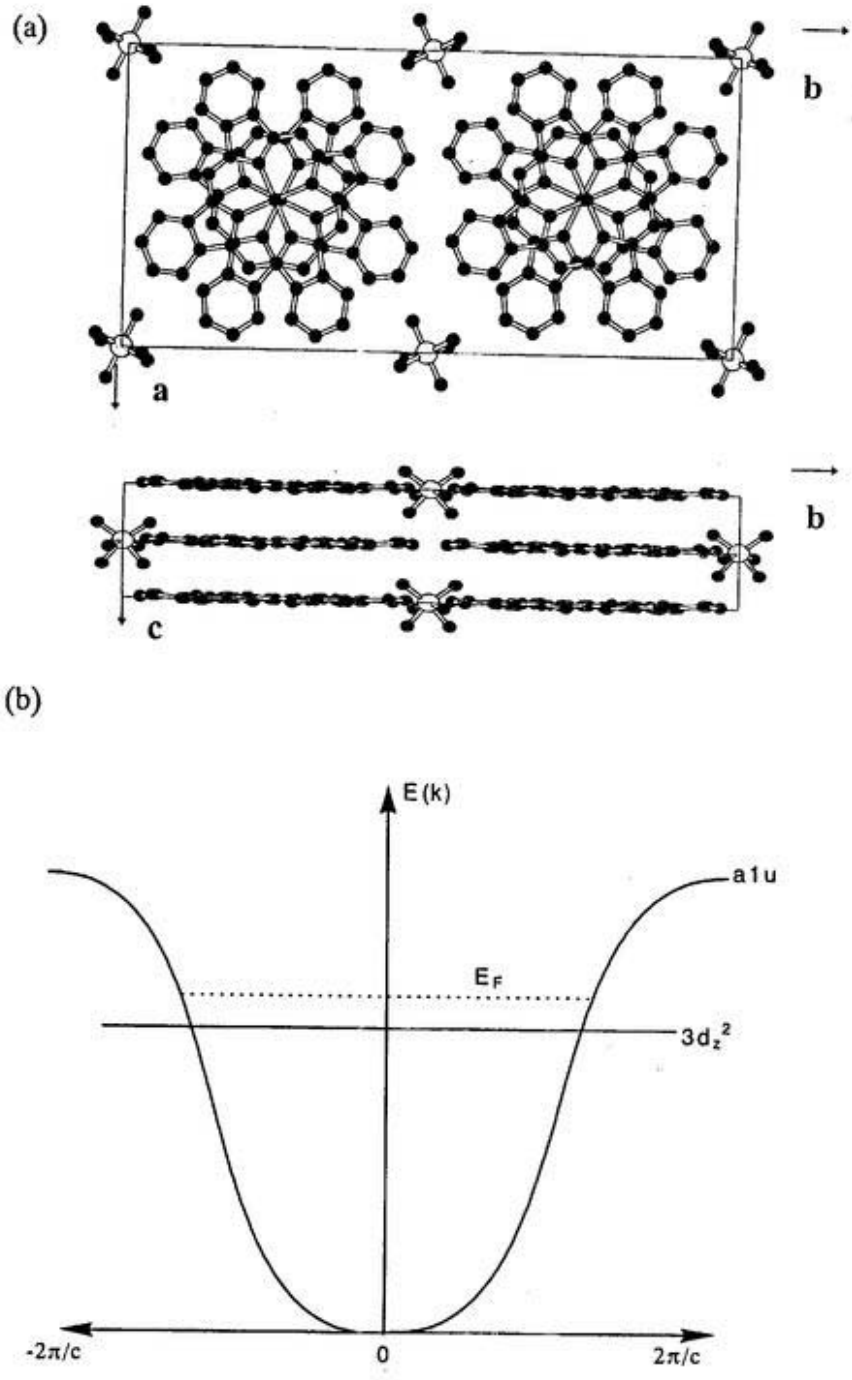

Fig. 2 The crystal structure (a) and schematic drawing of the band structure (b) of $NiPc(AsF_6)_{0.5}$, which shows the two-band system

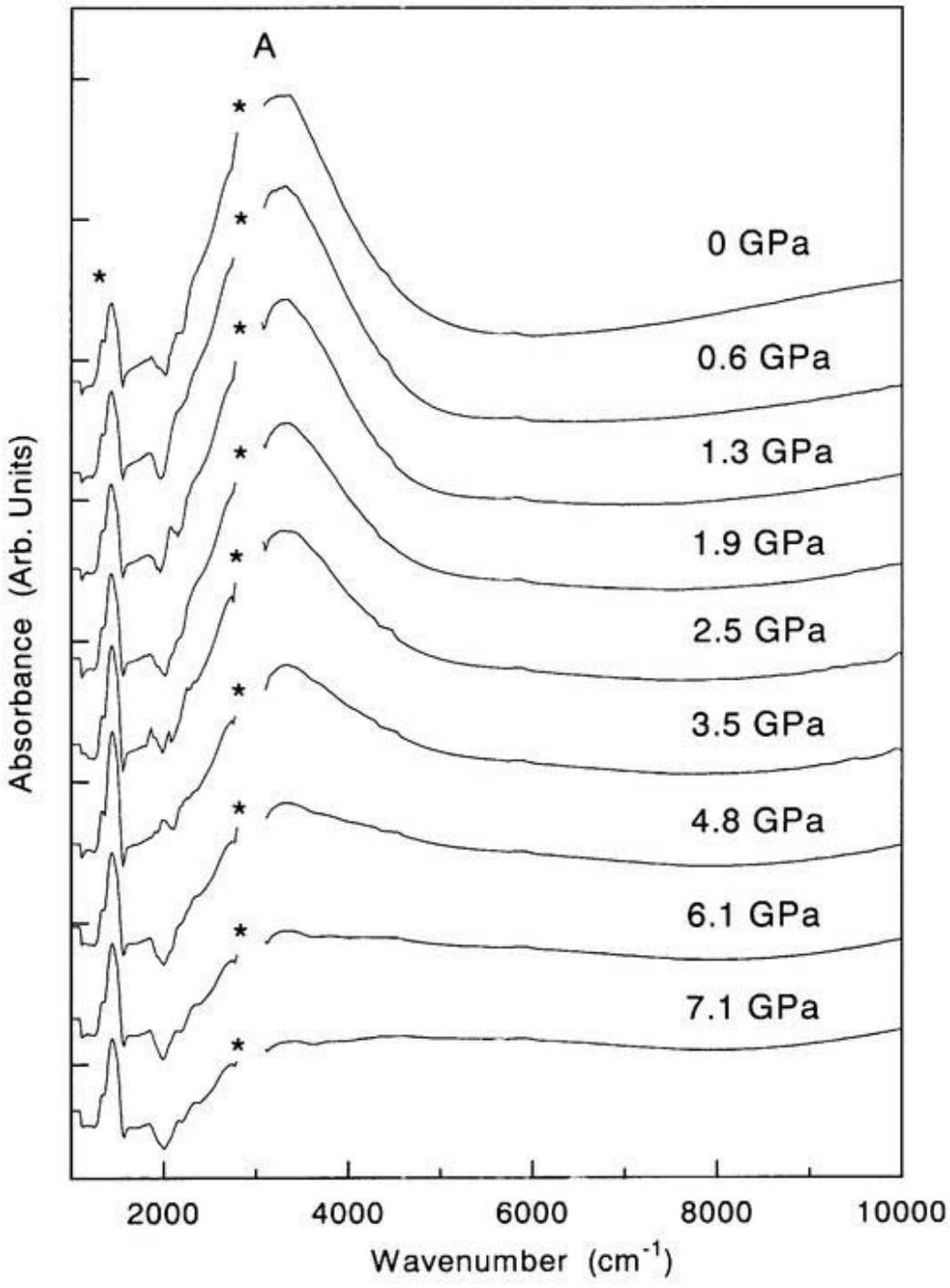

Fig. 3 Pressure dependence of plasmon absorption

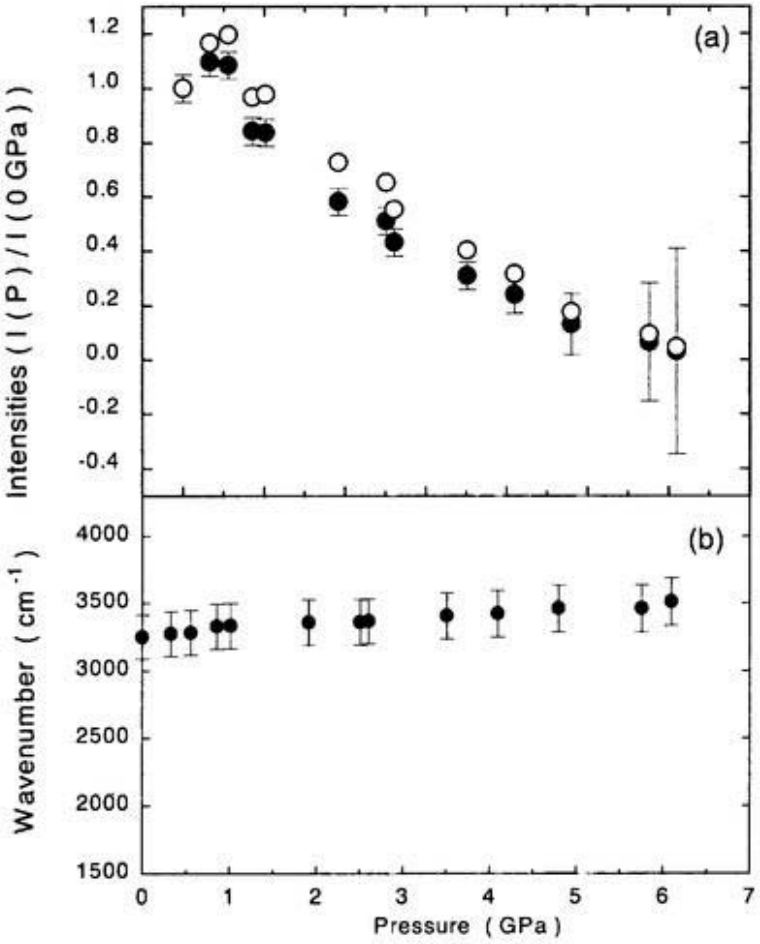

Fig. 4 Pressure dependence of the integrated intensity(a) and peak position(b). The open circles are corrected taking account of the increase of the dielectric constant of pressure medium.

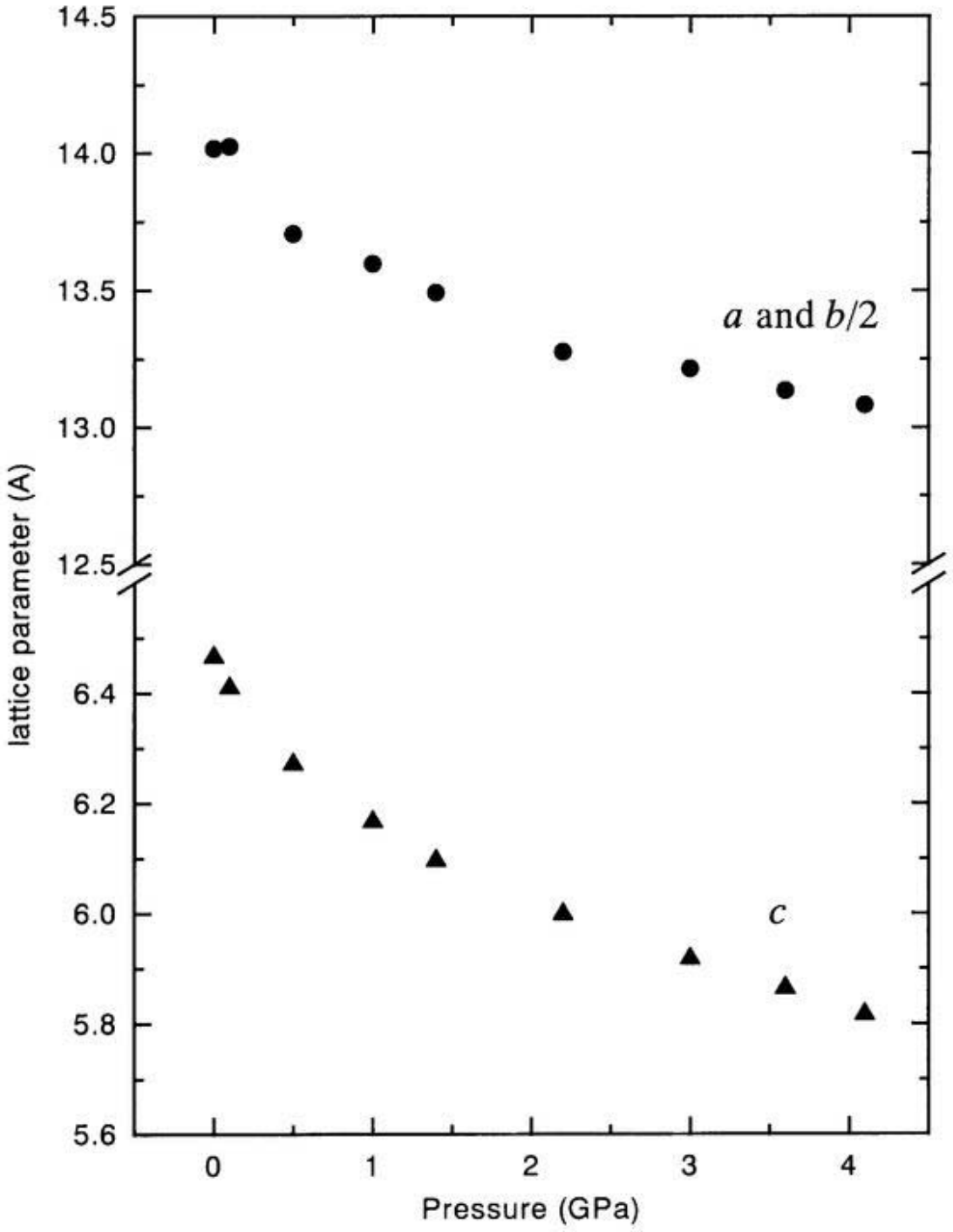

Fig. 5 Pressure dependence of the lattice parameters. Tetragpnal symmetry is assumed.

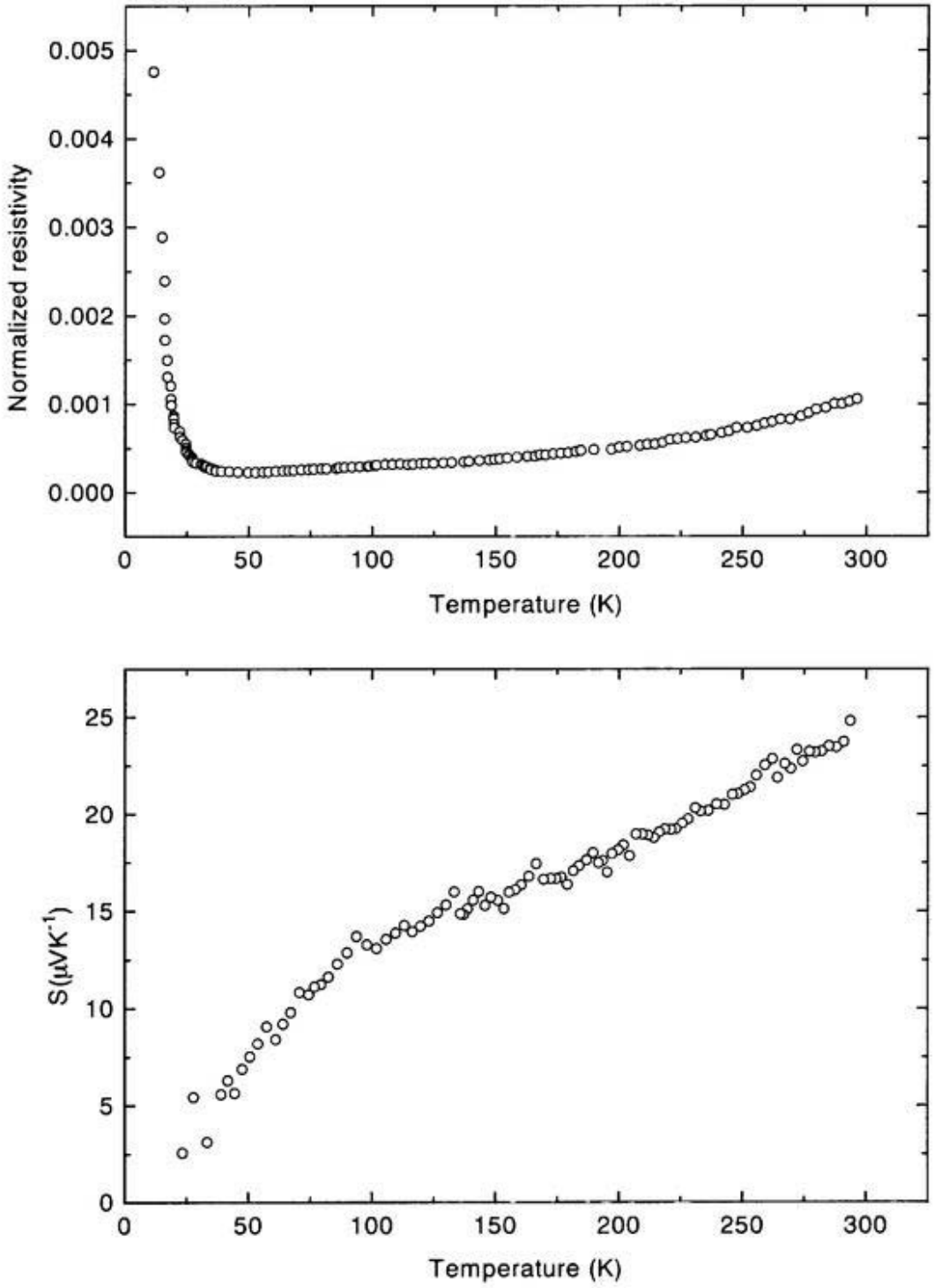

Fig. 6 Microwave resistance and thermopower of ambient pressure $NiPc(AsF_6)_{0.5}$

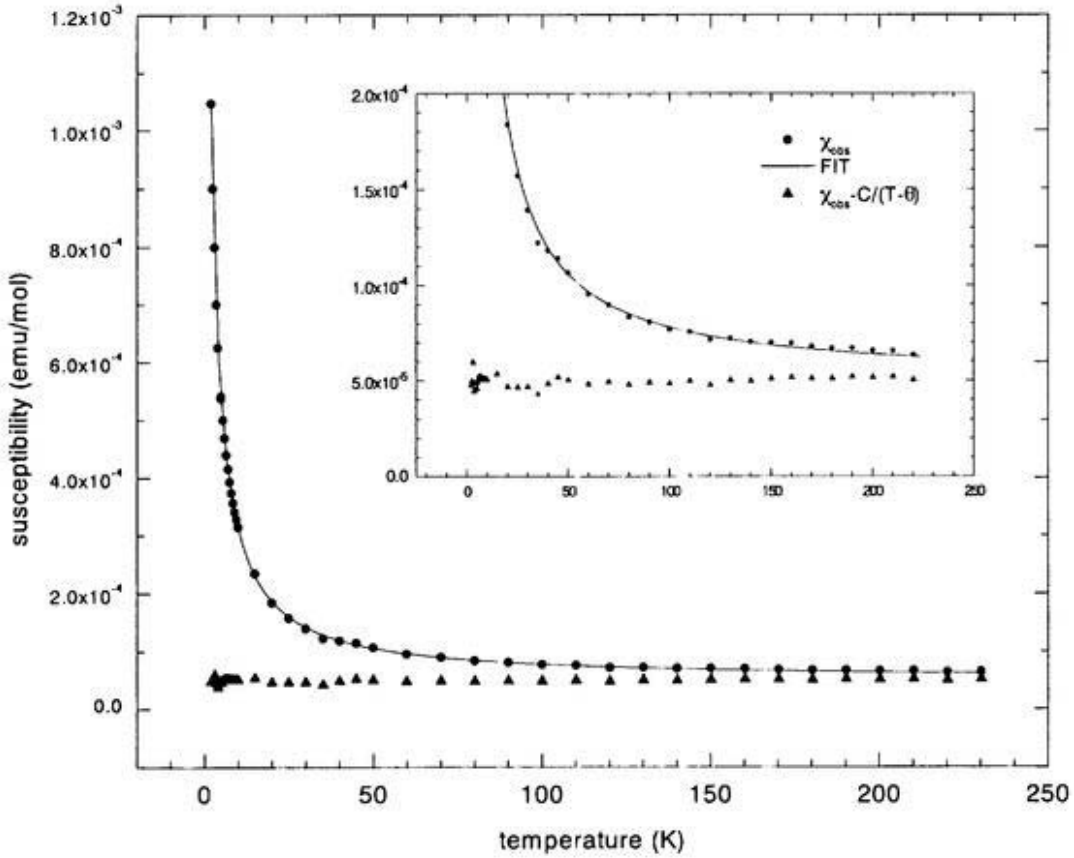

Fig. 7 Paramagnetic susceptibility of $NiPc(AsF_6)_{0.5}$. The diamagnetic contribution is subtracted. The solid line is the model function of $\chi_m=\chi_p+C/(T-\theta)$.The triangles are the residuals subtracted by $C/(T-\theta)$.

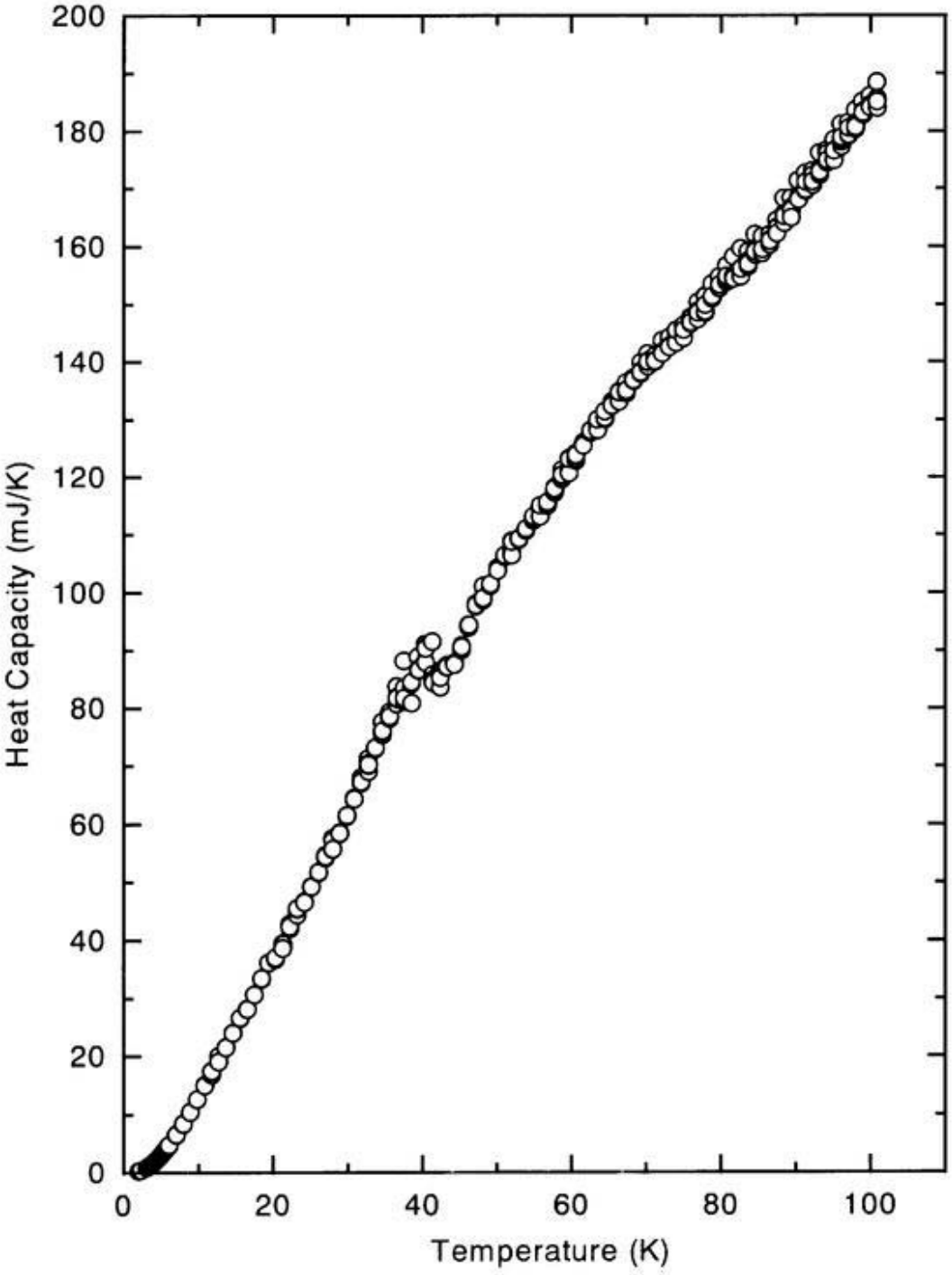

Fig. 8 Temperature-dependent heat capacity of $NiPc(AsF_6)_{0.5}$

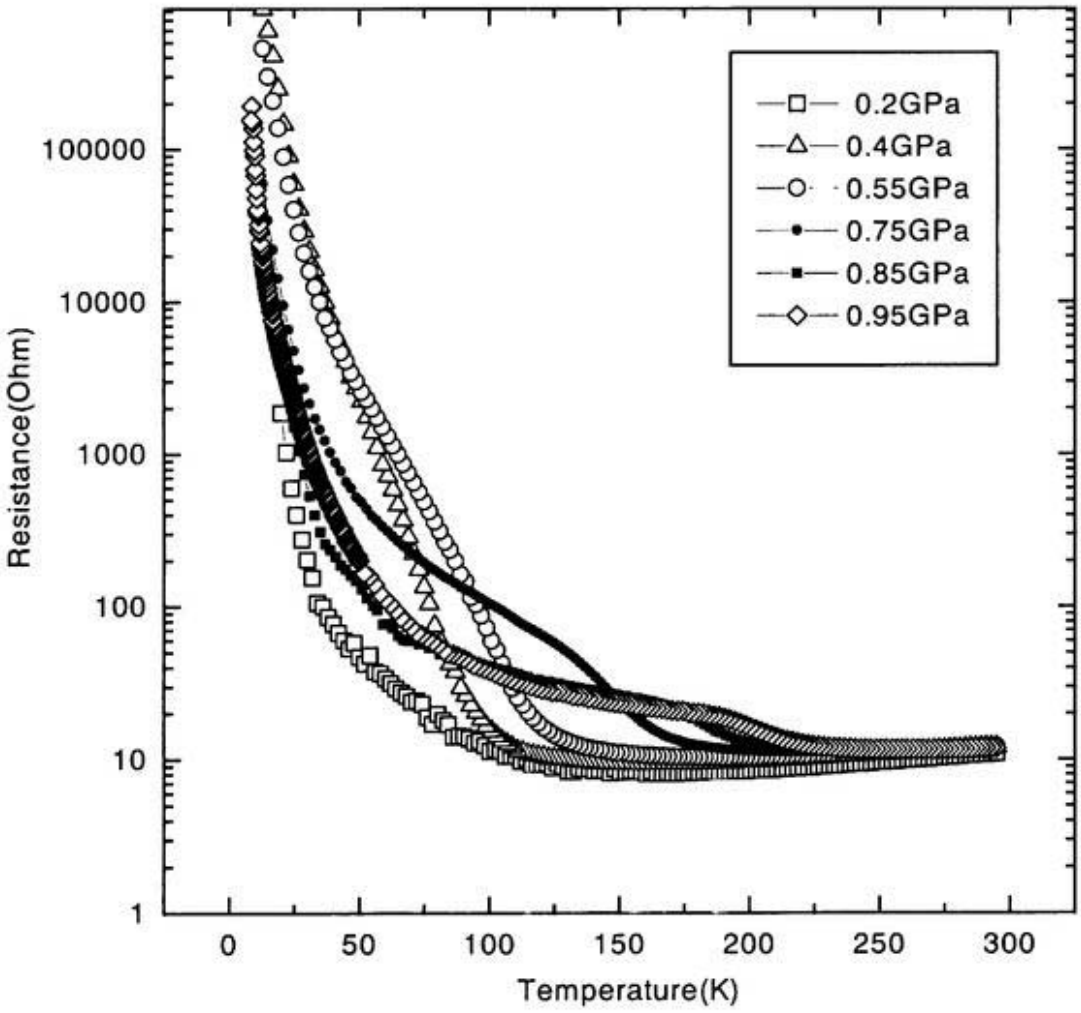

Fig. 9 Pressure dependence of resistance of $NiPc(AsF_6)_{0.5}$

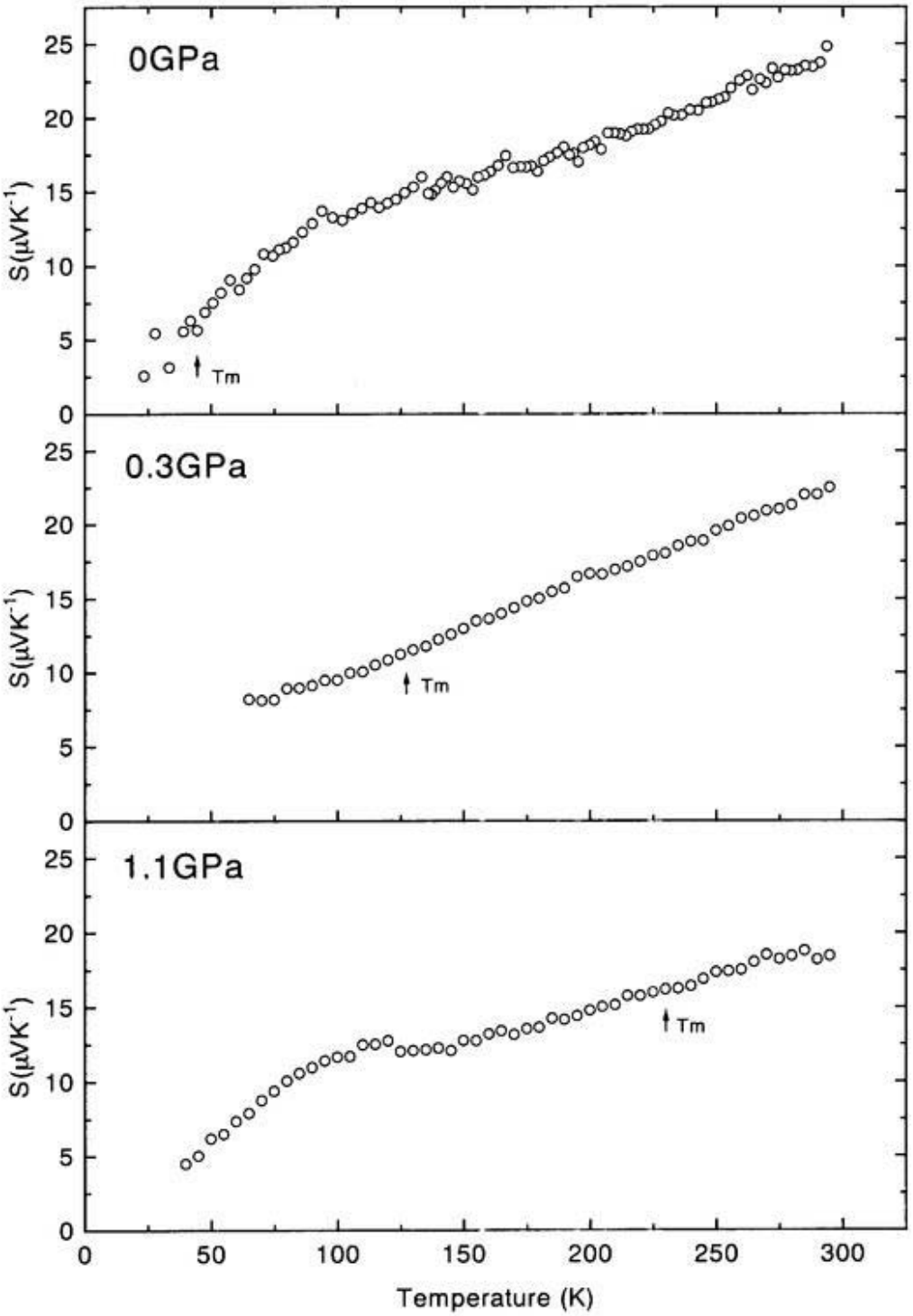

Fig. 10 High pressure thermopower. Arrows denote the resistivity minimum temperature at which no anomaly was found.

Chapter 3

Optical, EPR, and structural properties of solid platinum phthalocyanine in the different oxidation states of electrochemical process

Y. Yonehara, I. Kogan, K. Yakushi

Optical, EPR, and structural properties of solid platinum phthalocyanine in the different oxidation states of electrochemical process
submitted to *Solid State Ionics*

3-1 Introduction

3-1-1 Scope of this study

Recently the electrochemical conversions of phthalocyanines (Pc) has attracted much attention due to their high stability, a number of interesting physical properties, and a variety of practical applications.[1] Solid state phenomena, for instance, electrical conductivity, optical spectrum, crystal structure have been studied for neutral metal phthalocyanine (MPc) or metallic charge transfer (CT) salts with formula ($MPc(A)_{0.5}$) where A is an anion. Generally the electrochemical properties of the solid molecular crystal are less studied than those of conducting polymers, in certain of them a band filling can be continuously controlled by electrochemical potential.[2]

Moreover, general procedure to form these materials is electrochemical crystallization from 1-chloronaphtalene solution at 120℃[3] that takes very long time and PtPc CT salts do not crystallize easily.

Therefore, to investigate the redox states of crystalline compounds, we try to develop a new technique for the electrode formation in which a single crystal or an array of the relatively large crystals were encapsulated into transparent and electrochemically inactive polymer matrix.

The another purpose of this study is to control the filling of the band. Now, many organic conductors as well as Mott insulators based on radical cation or anion salts have been obtained. However, it is difficult to control the filling of the conduction electron band or the effective valence because of extreme sensitivity of the crystal structure to substituents or intersticial dopants. In other words, the organic compounds are very soft

compared with inorganic compounds and a modification of counter anions or cations usually results in a change of crystal structure. For example, in the case of Li, Cu mixed crystal of DMe-DCNQI, the band structure changes from 1D to 3D by mixing different valences. This is the reason why the high pressure measurement to the extent of just around 1GPa gives many interesting results in the field of the organic phase transition. However, this softness is not so convenient to investigate physical properties of the salt systematically. The important matter in the filling control is to keep the band structure and to be able to control the filling continuously. When these requirements are satisfied, the systematic research will be achieved from the physical stand point. The typical methods of filling control are ① preparation of a mixed crystal ② ion channel using alkali metal ③ two-bulb method for the graphite and C_{60} [4] ④ the mixed valence of Cu^{+} and Cu^{2+}.

In the case of cuprate superconductor, the carrier doping achieved the high transition temperature.[5] Compared with inorganic compounds, in the case of the organic compounds, at present, the control of the ratio between band width and on-site coulomb is the ordinary methods to control the phase diagram. κ-(BEDT-TTF)$_2$Cu$_2$(CN)$_3$ is one of the rare example which shows the metallic property by carrier doping to the Mott insulator. In the case of inorganic compounds, it is relatively easy to prepare the non-stoichiometric composition because of the crystallization which contains defects or substitution of the elements. In contrast to this, in organic compounds, the stoichiometric equilibrium condition is necessarily established by way of the preparation. That is, the electrochemical crystallization proceeds invariably through the solution state.

The continuous filling control in the organic compounds is difficult by this restriction concerning the preparation method itself. If the filling control comes true in the organic conductors, the variety of the material will be expanded through the change of the density of state or the on-site coulomb repulsion. Moreover, it is expected that the development of the new materials which show some interesting properties such as high T_c superconductor from the physical standpoint. Therefore, we planed for solid state doping by electrochemical method as to polymer composite film based on the phthalocyanine salts.

There are three reason why the phthalocyanine was selected for the object of the trial of the band filling control. The first reason is the d-π charge transfer observed under high pressure. The second is the hardness of the molecular as you know through the optical measurement. The third is the dispersion of the line width of the ESR in the $NiPc(AsF_6)_{0.5}$.

The most striking feature of phthalocyanine CT salts is a two-band system, in which a narrow 3d-band is located just below the Fermi level of π-band. Figure 1 shows the band structure of $NiPc(AsF_6)_{0.5}$ schematically. These two bands do not hybridize each other because of the difference of symmetry. So it is expected that the physical properties change extremely by which band is oxidized. In general, in the case of phthalocyanine salts, the difference of the oxidized site seems to effect upon the lattice constant. So, we tried to control the oxidized site by adding pressure. In fact, the metal-nonmetal transition temperature of $NiPc(AsF_6)_{0.5}$ which shows metallic behavior below 40K at ambient pressure moved higher side gradually as increasing pressure. The

energies of narrow 3d-band and π-band are close. Based on the ligand field theory, high pressure lifts up the 3d-band to upper side of the π-band and causes the gradual charge transfer from 3d- to π-band as shown in Fig. 1. A small amount of 3d-holes (Ni^{3+}) produced by pressure is distributed randomly and localized in the narrow 3d-band. It is considered that the gradual change of the concentration of this localized potential leads to the shift of the transition temperature. The experiment of X-ray diffraction do not show any symmetrical change between 0 to 3.5GPa showing the monotonous decreasing of the lattice constant.[6] This pressure induced d-π charge transfer is able to be regarded as the filling control of the π-band if we neglect the possibility of the change of band structure owing to the interaction between d-and π-band after the charge transfer induced by pressure. There is no direct evidence of the change of the Fermi level in the π-band though the formation of Ni^{3+} was observed in the infrared spectrum under high pressure.[7]

There is a report that the line width of the ESR signal of $NiPc(AsF_6)_{0.5}$ shows distribution from 1G to over 100G.[8] There is possibility that this distribution of the line width of the ESR is related to the difference of the composition. Directly speaking, the AsF_6 anion contents is not just 0.5 for one molecule of phthalocyanine and distributed around 0.5. In this case, the filling of the π-band is change between samples. As a result of the difference of the d-π interaction caused by the difference of the band filling, it is considered that the line width of ESR show wide dispersion. Assuming that this is true, in the study for phthalocyanine salts, ESR is an effective method that we can observe the change of the π-band filling, directly.

Based on these experimental background, in the phthalocyanine salts, there is possibility to reach the filling control.

3-1-2 General introduction for the electrochemistry

Electrochemistry is a well-developed area of chemistry with a complete set of theories and quantitative relationships. Especially, linear sweep or cyclic voltammetry is the most popular method because only one experimental run gives a current response containing much information over a wide potential range in the simple equipment. It is capable of evaluating total amounts of electroactive species contained in the film by intergrating effective areas of voltammgrams if there is no supply of electroactive species from the solution into the film.

In order to estimate the total electroactive species exactly, it is important that the equilibrium condition must be achieved. Under equilibulium condition, the Ilkovic equation is applicable, and quantitative analysis may become possible. The redox reaction contains two processes. One is "mass transfer" and the other is "electron transfer". "Mass transfer" is the process that the ion moves to the surface of the electrode, that is, the migration or the diffusion process in the solution and "electron transfer" is the electron delivery process on the surface of the electrode. The rate of the reaction is determined by the slower process. Whether the redox reaction is equilibrium or not was determined by which transfer is the rate-determining step. If we have some electroactive compounds in solution, we may distinguish two cases. The first case is that electrochemical reaction is controlled solely by mass transfer, that is, the electrolytic

current is controlled solely by diffusion, and at that time, the current is called "diffusion current". The diffusion current is proportional to the concentration of the electroactive material by Ilkovic equation. In this case, the reaction is called reversible and equilibrium condition is achieved. The second case is that electrochemical reaction is controlled by electron transfer. In this case, the reaction is called irreversible. Intermediate case is quasi equilibrium condition.

Generally, electrolytic analysis based on the combination of the oxidation and reduction reaction. All cells are considered as the combination of two half-cells, with each of the latter represented by a half-reaction written as a reduction.

$$Ox + ne^- \rightarrow Red$$

the potential of each half cell can be calculated by means of the Nernst equation in the reversible condition,

$$E = E^0 + \frac{RT}{nF} \ln \frac{[Ox]}{[Red]}$$

where E^0 is the standard electrode potential of hydrogen electrode, R is the gas constant, T is temperature, n is the number of the electrons, F is the Faraday constant, Ox and Red are oxidized and reduced species, respectively.

The solid state reaction such as polymer films on the electrode is more complicated than the solution case. In addition to the conventional classification (reversible, quasi-reversible, irreversible) for the equilibrium of the electrode reactions, we have to consider the diffusion process in the film. From the diffusional viewpoint inside the film, the voltammograms can be classified into the three cases of semi-infinite

diffusion, finite diffusion and the surface waves.[9,10] In most films, electrochemical charge transport occur by electron self-exchange reactions between neighbor oxidized and reduced sites as shown in Fig. 2. This electron hopping process is mathematically representable by diffusion laws in which a charge transport diffusion coefficient D_{ct} is introduced to measure its rate.[11,12,13] Time- and potential-dependent profiles of the concentration of fixed oxidized (C_O) and reduced (C_R) sites in the films can consequently be prepared which depend on the parameter $D_{ct}\tau/d^2$, where τ is the experimental time scale (related to the time for the potential scan to traverse the wave) and d is the polymer film thickness. Figure 3 is the schematic drawings. When $D_{ct}\tau/d^2>>1$ (Fig.(c)), all electroactive sites in the film are, for a reversible reaction, in equilibrium with the electrode potential and the voltammmetric behavior is like that of an immobilized monolayer, i.e., the anodic and cathodic peaks must basically coincide ($\Delta E_p = E_{anodic}-E_{cathodic} = 0$) and the potential of the peak is independent of scan rate (ν) and peak currents (i_p) are proportional to scan rate. If $D_{ct}\tau/d^2<<1$ (Fig.(a)), a negative potential scan traverses the wave before oxidized sites at the film's outer boundary are reduced at all; that is, a semi-infinite electrochemical charge diffusion condition prevails. The voltammetric peak current is the proportional to square root of scan rate. At intermediate values of $D_{ct}\tau/d^2$, intermediate i_p vs. ν dependence occurs. Based on these phenomena, it is often found that the diffusion layer spreads up to the film/solution interface in a time scale of a measurement, i. e. the diffusion behavior is varied from semi-infinite to finite as time lapses. The increase of the potential sweep may lead to transition to the infinite diffusion when the border between solid film and

electrolyte do not influence the process. The equilibrium condition (i_p proportional to ν) must be achieved in order to estimate the whole charge by the voltammogram. It will be achieved at the slower scan rate or on thinner films as a rule. Using this relation (i_p proportional to ν), we can check that the equilibrium condition is achieved or not.

The formation of polymer films on electrode surfaces and the use of polymer-film-coated electrodes for analytical purposes has been known for some time.[14,15,16] The polymer on electrodes can be alternatively classified as "redox polymers" and "ion exchange polymers". Redox polymers contain the electroactive center as a part of the polymer chain backbone, or the electroactive center may be coupled to a functionalized polymer either before or after the polymer is applied to the electrode surface. Poly-vinyl ferrocene is one of the example of redox polymer. Ion exchange polymer films on electrodes depend on drawing ionic redox substances from their solutions into the film as counter ions having favorable ion exchange partition coefficients. Poly 4-vinyl pyridin is belong to this group. The distinctive characteristic of modern polymer-coated electrodes is that the polymer films contain electrochemically reactive centers. However, in this study, contrary to polymer modified electrodes, the crystals were mechanically mixed in transparent polymer matrix in these electrodes.

References

[1] A. B. P. Lever, E. R. Milaeva and G. P. Speier, in "*Phthalocyanines: Properties and Applications*" (Edited by C. C. Leznoff and A. B. P. Lever), Vol. 3, p.1, VCH Publishers, Inc, New York, (1993).

[2] T. J. Marks, *Angew. Chem., Int. Ed. Engl.* 29, 857 (1990).

[3] H. Yamakado, K. Yakushi, N. Kosugi, H. Kuroda, A. Kawamoto, J, Tanaka, T. Sugano, M. Kinoshita and S. Hino, *Bull. Chem. Soc. Jpn.* 62, 2267 (1989) .

[4] D. E. Nixon, G. S. Parry, *Br. J. Appl. Phys. Ser. 2* 1, 291 (1968).

[5] J. G. Bednorz and K. A. Muller, *Z. Phys.* B64, 189 (1986).

[6] T. Hiejima, K. Yakushi et al. *Mol. Cryst. Liq. Cryst.* Vol. 296, pp.255-268 (1997).

[7] T. Hiejima, K. Yakushi, *Solid State Commun.* 95, 661-666 (1995).

[8] K. Yakushi, H. Yamakado, M. Yoshitake, N. Kosugi, H. Kuroda, T. Sugano, M. Kinoshita, A. Kawamoto, and J. Tanaka, *Bull. Chem. Soc, Jpn.* 62, 687-696 (1989).

[9] K. Aoki, T. Tokuda, H. Matsuda, *J. Electroanal. Chem.* 146, 417 (1983).

[10] K. Aoki, T. Tokuda, H. Matsuda, *J. Electroanal. Chem.* 160, 33-45 (1984).

[11] P. Daum, J. R. Lenhard, D. R. Rolison, and R. W. Murray, *J. Am. Chem. Soc.* 102, 483 (1980).

[12] R. J. Nowak, F. A. Schultz, M. Umana, R. Lam, and R. W. Murry, *Anal. Chem.* 52, 315 (1980).

[13] N. Oyama and F. C. Anson, *J. Electrochem. Soc.* 127, 640 (1980).

[14] M. Bazier, *Organic Electrochemistry*, Marcel Dekker, New York, 947 (1973).

[15] L. C. Clark, R. G. Weld, and Z. Taylor, *J. Appl. Physiol.* 6,189 (1953).

[16] R. C. Bowers and A. M. Wilson, *J. Am. Chem. Soc.* 81, 1840 (1959).

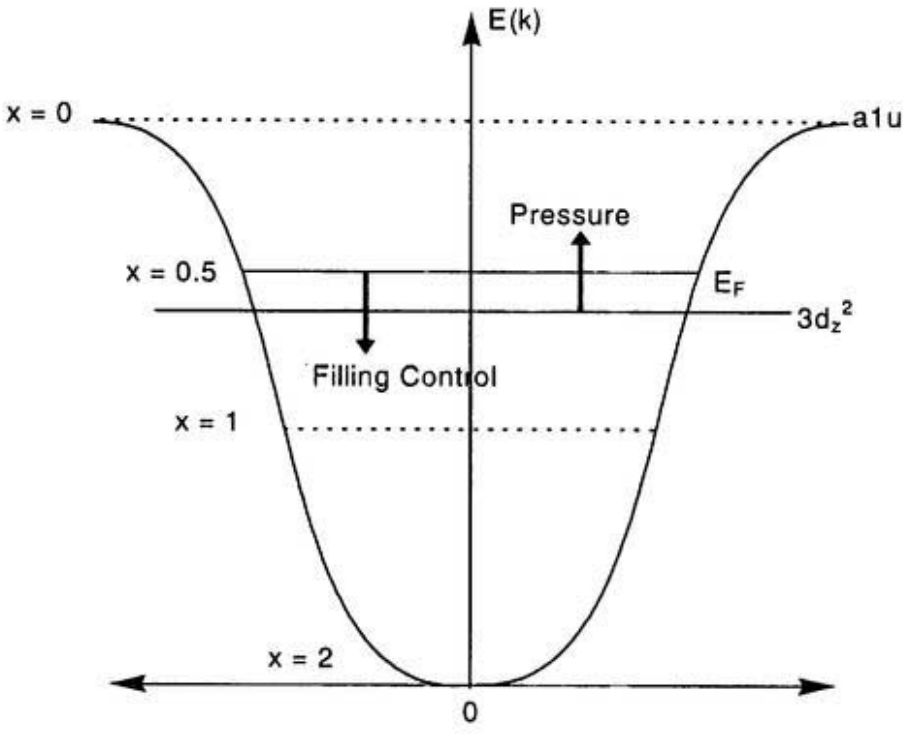

Fig. 1 Schematic Band Structure of $NiPc(AsF_6)_{0.5}$

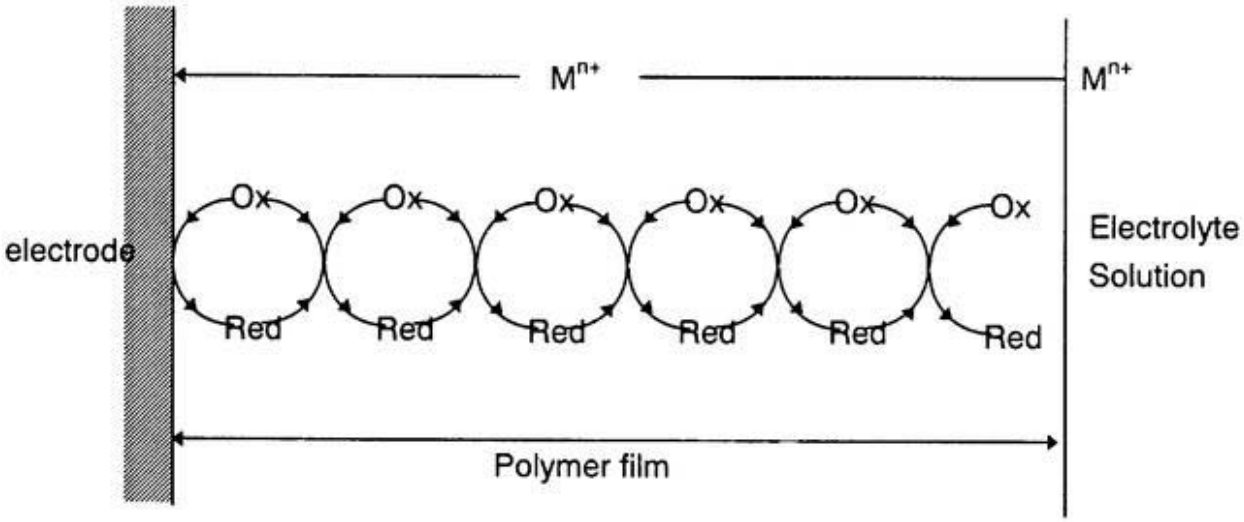

Fig. 2 Electron Transport Process in the Polymer Film

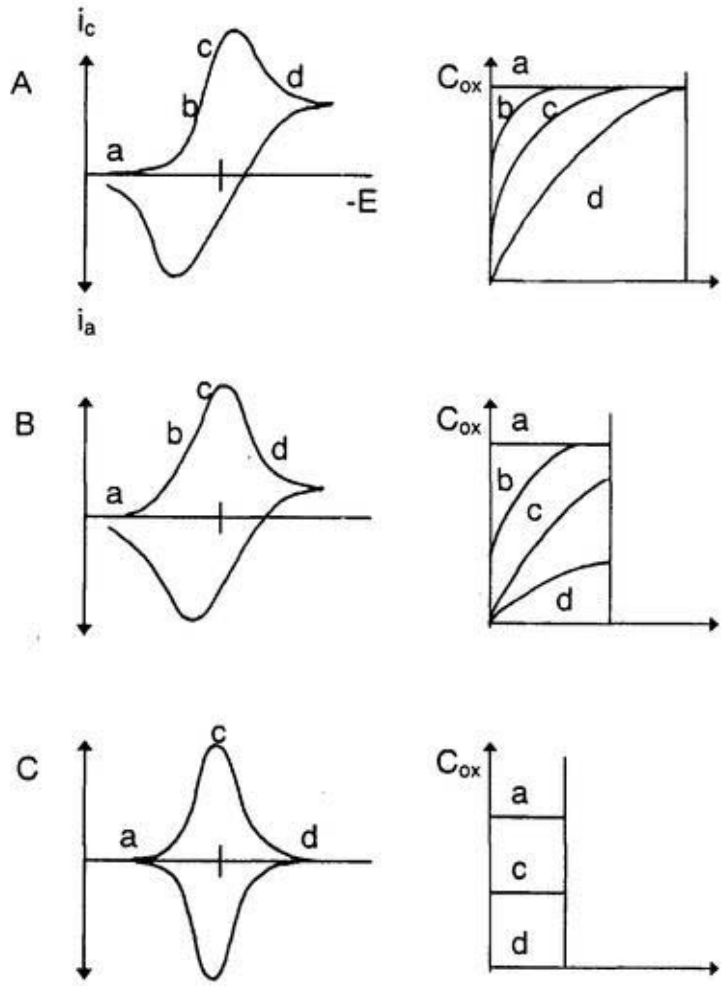

Fig. 3 Schematic reversible cyclic voltammograms and concentration-distance plot for oxidized sites (during negative sweep) for a redox polymer film.

3-2 Experimental

We used the MPc-PBC (poly-bisphenol-A-carbonate; Aldrich) composite film as starting materials for the electrochemical doping (M = Pt, Ni). PtPc was synthesized from phthalonitrile (nacalai tesque) and $PtCl_2$ (nacalai tesque),[1] and purified three times by vacuum sublimation. The purified PtPc was identified by elemental analysis. The results were C : 54.23%, N : 2.54% and N : 15.78%, and these values agree closely with the theoretical one (C : 54.32%, N : 2.28% and N : 15.84%). NiPc(Aldrich) was also used after three times vacuum sublimation. PBC was used without additional purification. PtPc and NiPc were finely ground in an agate motor and dispersed in CH_2Cl_2 with PBC. The final concentration of PtPc (or NiPc) and PBC in dichlorometane solution were 2-3 mass %. Thin semi-transparent composite film of 0.1-0.05 mm thickness for the spectrochemical experiment and more thick film for the X-ray measurement were cast from suspension, dried in the air, and pumped out in the dynamic vacuum for 2-3 h. To evaluate the effect of particle size on the electrochemical and spectrochemical phenomena, two different films were prepared : the film A consisted of PtPc electrochemically dispersed to nearly molecular level while the film B was formed finely ground crystals. In the film A, the PtPc molecules were separated out from the crystal surface and distributed in the polymer matrix as a result of relatively fast scans of potentials during electrochemical pretreatment.

The electrochemical doping was carried out in the hermetic three compartment electrochemical cell (Figure. 1) using 0.1 M tetrabutylammonium hexafluorophosphate ($TBAPF_6$;Aldrich) or tetrabutylammonium hexafluoroarcenate ($TBAAsF_6$) solution of propylene carbonate (nacalai tesque) as a supporting electrolyte. $TBAAsF_6$ was obtained

by mixing the equimolar aqueous solutions of (n-butyl)$_4$NBr and $KAsF_6$ and recrystallized from ethanol for three times. $TBAPF_6$ was used as supporting electrolyte for PtPc-PBC. Both $TBAPF_6$ and $TBAAsF_6$ were used for NiPc-PBC. Propylene carbonate was used after vacuum distillation with molecular sieves 4A. $Ag/10^{-3}$ M $AgClO_4$ + 0.1 M $LiClO_4$ + propylene carbonate was used for the reference electrode which shows +0.77 V against the standard Ag/AgCl + 3 M KCl. In the case of spectrochemical experiment a standard quartz cuvette was used as a body. A similar cell filled with electrolyte was placed in the reference beam of Hitachi U-3400 spectrometer. EPR signal was studied in the tubular cell with inner diameter D = 4 mm installed in the cylindrical cavity of the Varian EPR spectrometer. A gold wire (0.3 mmϕ) in the form of helix (4 mm in diameter and 1 mm in pitch) was used as the working electrode. Grassy carbon or glass plates covered with ITO transparent films (surface resistance : 10 Ω) were employed as the current collectors. The instruments were as follows. Potentiostat/Galvanostat: HA 501 (Hokuto Denko LTD); Resistivity measurement system: Physical Property Measurement System, Model 6000 (quantum design); EPR spectrometer: VARIAN with a cylindrical cavity; powder X-ray diffractometer: MXP^3VA, (Mac Science, Cu-K_α radiation).

3-3 Results and discussion

3-3-1 The difference of the voltamograms between the cycles

Figure 2 is a typical cyclic voltammogram showing the redox process of PtPc-PBC being used $TBAPF_6$ as supporting electrolyte. The scan rate is 0.05 mV/sec. In the first cycle, the oxidation of PtPc gave only one anodic peak (0.43 V) and two cathodic

peaks followed by a formation of a violet film at the highest voltage. In the second and successive cycles, it shows two anodic (0.36 V, 0.63 V) and relevant two cathodic peaks (0.13 V, -0.18 V). The peak position and current were summarized in Table. 1. Let us call the intermediate state of solid PtPc salt formed after the first anodic peak at 0.36 V and before the second anodic peak at 0.63 V as "the mid-oxidation state" and that built after the second anodic peak as "the full-oxidation state". In the film which contains relatively large crystals of PtPc, the same kind of voltammograms were observed.[2]

This construction difference between the first and the second (or successive) cycle (peak position and number) does not depend on the scan rate (ν), although the peak currents (i_p) does. As described in the introduction, the relation between ν and i_p gives us the information that the equilibrium has been reached or not. In the case that i_p is proportional to ν, the diffusion is limited, that is, the oxidation is accomplished during one cycle because of the big charge transport diffusion coefficient D_{ct} or experimental condition such as the thin film or slow scan rate. In the case that i_p is proportional to the square root of ν, the diffusion is semi-infinite. In the case of the oxidation in the solid state PtPc, the scan rate accomplished the limited diffusion is below 0.05 mV/sec that is very slow compared with the general molecular oxidation. Our experiment was carried out under the condition that i_p is proportional to ν. So, the construction difference is not due to an incomplete oxidation in the first cycle. In evidence, the charge required for full oxidation (the sum of the area of the first and second peaks ; *ca.* 0.7 *e*) in the second run was equal to that in the first cycle, the color of the electrode film at 0.7 V being violet as well. A large potential difference (*ca.* 0.5 V) between relevant andic and cathodic maxima could not be eliminated at the slowest scan rate (44 h registration of a

cycle). Perhaps the initial rigid crystal lattice may require the overvoltage higher than the potential of the full-oxidized state, and the worse crystallinity allows the mid-oxidized state to be realized.

3-3-2 The determination of the composition

In the second cycle, the area of the second anodic peak was nearly half of the first one while the charge (n) required for full oxidation was 0.70 *e* per a molecule, i. e. less than 1.0 *e* estimated in our previous experiments using film A.[2] For more accuracy the Coulometric experiments were performed at relatively low currents for 24 h until the leakage current was decreased down to 1-3 μA. In the previous experiments, the mid-oxidized state was determined as $PtPc(PF_6)_{0.5}$.[2] Some characteristic properties of this compound (lattice parameters and g factors) are very close to those of metallic CT salt $PtPc(ClO_4)_{0.5}$. It is more difficult to determine the composition of PF_6 in the full-oxidized state, since it is unstable in the atmosphere as shown by the following X-ray experiment. In the full-oxidized state, the number of electrons per a molecule of PtPc calculated from the voltammogram (0.7 *e*) is close either to 0.67 or 0.75 which respectively correspond to the formula $(PtPc)_3(PF_6)_2$ or $(PtPc)_4(PF_6)_3$. If we take the anodic charge ratio ($r = C_2/C_1 = 0.5$), $(PtPc)_2PF_6$ and $(PtPc)_4(PF_6)_3$ can be suggested for the compositions of mid- and full-oxidized states, respectively. However, the charge ratio ($r = 0.96$) between the cathodic peaks is higher than the ratio between the anodic peaks, the reason is not clear at the moment. If we take this cathodic ratio (0.96), $(PtPc)_2PF_6$ and $(PtPc)_3(PF_6)_2$ can be supposed for the compositions of mid- and full-oxidation states. In this estimation we corrected the contribution of the current coming

from the unavoidable charging of the double layer capacitance. The anodic peaks are sharp enough to be separated from this background current. We believed that the compositions $(PtPc)_2PF_6$ and $(PtPc)_4(PF_6)_3$ are more reliable for the mid- and full-oxidized states. In this case, the energies consumed in the doping process are equal between first and second cycle: $n\phi$ = 0.33 eV for the first cycle and $n_1\phi_1 + n_2\phi_2$ = 0.32 eV for the second one, where n = 0.75 e, n_1 = 0.5 e (the number of electrons in the first scan) and n_2 = 0.25 e(the number of electrons in the second scan), ϕ = 0.43 V, ϕ_1 = 0.36 V, ϕ_2 = 0.63 V (related potentials).

3-3-3 The determination of the structures of mid- and full-oxidized state

To promote our understanding for the oxidation states, the powder X-ray experiments was carried out on three kind of the free standing films of $PtPc(PF_6)_x$-PBC. PtPc-PBC films were oxidized at the following three predefined potentials; (1) just after the anodic peak in the first cycle (0.5 V) and (2) just after the first anodic peak in the second cycle (0.5 V) and (3) full-oxidized state in the second cycle (0.73 V) as shown in Figure 3. Figure 4c shows the X-ray diffraction pattern of the film oxidized at 0.5 V after the single anodic peak in the first cycle (film (1)). This diffraction pattern agreed with that of the full-oxidized state in the second cycle (0.73 V, film(3)). These diffraction patterns were different from both of the monoclinic lattice of the reduced state (pristine solid PtPc, Figure 4a) and the tetragonal lattice of the film oxidized at 0.5 V in the second cycle (film(2)) that is correspond to "the mid-oxidized state" (Figure 4b). The full-oxidized state observed in both film (1) and (3) (Figure 4c) was unstable in the air and transformed into the mid-oxidized tetragonal $PtPc(PF_6)_x$ state observed in

film (2) after 24 h of exposition. Figure 5 shows the time-dependent powder X-ray diffraction pattern of the full-oxidation state.

The reduction of the full-oxidition state resulted in the dedoping brought about a drastic change in the EPR signal as shown in Figure 6. The potential change from +0.8 V to -0.12 V, which produced mid-oxidized state , led to a significant (nearly an order of magnitude) increase of the signal intensity. The successive reduction diminished the signal intensity to the initial level. It should be noted that pristine PtPc kept a very small unknown EPR signal in spite of the repeated sublimation under vacuum. In contrast to the reduction process, the oxidation of solid PtPc did not give such a large increase of the EPR signal. In defiance of this strange behavior, the general picture of the intensity changes was very reproducible from cycle to cycle.

3-3-4 The comparison of the absorption spectra between film A and B

Film A and B gave various absorption spectra in the highest oxidation states as shown in Fig. 7. The optical spectra of film A (Figure 7-1) were described in our previous paper.[2] The spectra of film B (Figure 7-2) were a little different from those of film A. In the reduced state (ϕ = -0.8 V), the position of the important absorption peaks (line a of Figure 7-2) almost agree with those of solid PtPc: 606 nm (Q band), 680 nm (650 nm for film A) and shoulder at 741 nm. The oxidation at 0.5 V resulted in the new band at 559 nm (line b of Figure 7-2), which was the same as the spectrum (line b of Figure 7-1) of film A. However, the full-oxidized state of film B (line c of Figure 7-2) was characterized by two peaks, as opposed to the spectrum of film A (line c of Figure 7-1) where only one absorption band was detected at 550 nm. As for this difference

between film A and B, it is necessary to remind the variance in the particle size and the fashion of the coverage in the transparent electrode. The size of the PtPc crystals in the samples studied in the previous work is so large (about 100-200 μm in length) that they are almost non-transparent in the optical experiment. Furthermore, there is a large transparent window space between crystals in this electrode. The compounds distributing in this window area are mainly responsible for the absorption spectrum shown in Figure 7-1. We assume that these substances are the PtPc or oxidized PtPc molecules produced by full oxidation-reduction and distributed in the polymer matrix. These molecules are likely to be prevented from aggregation inside the matrix due to interaction with polycarbonate polymer. Nevertheless, this interaction is enough weak because these molecules can be washed out of the matrix with acetonitrile, in which these molecules aggregate to the colloidal particles. On the other hand, the spectrum of film B shown in Figure 7-2 is ascribed to the optical absorption of the crystals, because of uniform and complete covering the film by semitransparent microcrystals. Since the particle size of the film A is much smaller than that of film B, the spectrum of film A shows a clear peak and valley, whereas the spectrum of film B is smeared out due to the strong light scattering. Related to the unstability of the full-oxidized state, we found that submicron colloidal particles were separated from the fully oxidized crystals at 0.5 V in the first cycle. These particles were washed out from the oxidized solid with acetonitrile (CH_3CN), and passed through a filter of 0.5 μm mesh. Figure 8 showed the optical absorption spectrum of the suspension consisted of two peaks at 554 nm and 597 nm (dotted line). In the atmosphere, the color was changed from violet to blue, and simultaneously the optical absorption at 554 nm decreased significantly (solid line).

In the case of individual molecules only one or two electrons can be electrochemically released from HOMO, and this process results in the cation radical or dication of PtPc. We considered that the lines a, b, and c in Figure 7-1 mainly correspond to the absorptions by $PtPc^0$, $PtPc^+$, and $PtPc^{2+}$, respectively. So, the number of electrons required for full oxidation of PtPc molecule must be $n = 2$. In the solid PtPc, the electrons are extracted from the valence band until the next stable compound is produced. Thus the number of oxidized electrons per molecule can be fractional. Actually, 0.7 e per a molecule is consumed to give full-oxidized state. As a result the 650 nm peak does not disappear in the full-oxidized state unlike the film A (line c), thereby the spectrum exhibits two peaks.

The disagreement in the degree of oxidation of molecule ($n = 2$) and crystal ($n = 0.7$) at the same potential is attributed to the difference in energy of HOMO of PtPc molecule and Fermi energy of solid PtPc. As we discussed above, the optical spectrum suggests the schematic energy diagram shown in Figure 9, the molecule is more deeply oxidizable than solid. It is difficult to estimate the energy difference quantitatively, because many factors should be taken into account, polarization energy, Coulomb energy in the field of positively charged PtPc and negatively charged PF_6, and bandwidth of the conduction band in crystal.

If the range of the solvent stability is expanded to the higher potentials, the next oxidation step can be registered. Considering the above discussion, it becomes easy to understand the various values of the degree of oxidation n presented in literature. The quantity of the charge required for full oxidation is $n = 1.21$ in ZnPc[3], $n = 1.8$ (an additional electron may be released from the central atom) in CoPc[3], $n = 0.67$ (1.25) for

CuPc[4], and n = 0.75 (1.62) for NiPc.[4] Values 1.25 and 1.62 in the parenthesis are likely to be associated with next oxidation step realized in the acetonitrile which has a more wide potential range of stability in comparison with propylenecarbonate.

3-3-5 Another characteristic of the voltammogram

CV of this system is characterized by a very large potential difference between anodic and cathodic peaks (*pd* = 0.4 V) independent of scan rate at ν = 0.02-0.05 mVs^{-1} and a very narrow width (25-50 mV). This hysteretic phenomenon in cyclic voltammetry was reviewed by Feldberg and Rubinstein.[5] They introduced a rather general approach based on the N-shaped free energy dependence of a system with hysteretic behavior to the process of the electrochemical interaction. According to this proposal, the doping of a compound proceeds discontinuously at a specific potential as a phase transition, when the system is characterized by an N-shaped free energy upon dopant concentration. The specific N-shape of the energy dependence results in the constant potential difference between oxidation and reduction potentials and ultra narrow peaks (theoretically δ function) in CV. Figure 10 is the schematic picture which shows the relation between N-shaped free energy and peak position. A very narrow width and large *pd* in CV of film B is consistent with this idea. In fact, the doping does not proceed continuously unlike the doping of conducting polymer as described following section. A new phase related to the next oxidation state is formed at the very initial stage of intercalation and no intermediate state can be registered in CV. We have to mention some other possible explanations on large *pd* in CV. It has been reported that *pd* of the evaporated CuPc film depends upon the dopant size.[6] The potential difference

may arise from the potential drop at the polymer-electrolyte interface, i. e. Donnan potential. However, the potential difference is too large to be considered from this point of view.

Let us briefly discuss the weak peak at ϕ = 0 V appeared after several fast scans. In the paper[2], it is suggested that this weak peak was likely to be attributed to small particles or molecules of PtPc. We succeeded to wash out these substances with acetonitrile in form of colloidal particles. We consider that PtPc molecules are separated out from the surface area of the crystal and distributed in the polymer matrix by applying high anodic potentials. The small *pd* in CV of this weak peak, which was shown in Figure 2, strongly supports this conjecture. The less anodic potential than other strong two peaks is consistent with the schematic energy diagram shown in Figure 9 as well. Probably the second oxidation peak is hidden under the oxidation peaks responsible for the oxidation of the solid. It remains to note that CV with a negligible difference between anodic and cathodic maxima related to this peak is typical for polymer modified electrodes.

As mentioned in the introduction, one of our purpose of this solid state doping is to develop the new method to get the same compound as the crystals produced from the conventional crystallization in the solution. So far, we have found to get the stable tetragonal phase (mid-oxidized state) by the solid state doping. We tried to verify whether this mid-oxidized state certainly show the same properties as the crystals prepared from the solution.

3-3-6 The development of a new method of the doping

-The characterizations by X-ray diffraction, EPMA, ESR, and conductivity measurement-

The compound produced at 0.5 V (just after the first anodic peak in the second cycle) was characterized by X-ray diffraction, EPMA, ICP, ESR, and conductivity measurement and it showed the same properties as the one of $PtPc(PF_6)_{0.5}$ produced by the conventional electrochemical crystallization method. The detailed results will be described below.

From the powder X-ray measurement, the crystal structure changes from monoclinic to tetragonal before and after the first anodic peak in the second cycle (The first anodic peak position of $PtPc(PF_6)_x$ -PBC ; 0.36 V, and that of $NiPc(PF_6)_x$-PBC ; 0.3 V). The undoped film has the same pattern as α-PtPc which belongs to monoclinic system with space group C2/n, the lattice paramerters being a = 26.29, b = 3.818, c = 23.92, $\beta = 94.6^\circ$, Z = 4. In the case of $PtPc(PF_6)$x-PBC oxidized at 0.5V, the peak positions obtained from powder X-ray measurement are in fair agreement with the calculated values based on the lattice parameter of the single crystal of $PtPc(ClO_4)_{0.5}$ which belongs to the tetragonal system with space group $P4/mcc$, the lattice parameters being a = 14.062, b = 14.062, c = 6.510, Z = 2.[7]

EPMA qualitatively detects the phosphorus atom in the crystals, which also evidences the formation of CT salt.

The chemical analysis of Pt and P were conducted with the aid of ICP atomic emission spectroscopy. The films oxidized at 0.5V and 0.7V containing 20mg PtPc were dissolved in conc. H_2SO_4, then decomposed in conc. HNO_3 and diluted with pure water. The emission lines, 203.646, 253.565 nm were used for the detection of Pt and P. The

results shown in Table 2 indicate that the ratio of P is rather high relative to predicted value in both 0.5 and 0.7 V films. We consider that this extensive P comes from the un-reacted electrolyte contained in the polymer. Actually, we were able to remove some amount of P by washing with pure water, although the contents of P is still too high. However, it was verified that the film oxidized at 0.7 V contains much amount of P compared with the one oxidized at 0.5 V qualitatively.

The CT salt formation accompanies the growth of conductivity at least by 6 order of magnitude up to 0.5-1 $S \cdot cm^{-1}$. Thermoelectric power is 10 μ $V \cdot K^{-1}$ at 300 K and quasi linearly decreases in the temperature range 150-300 K.

ESR signal becomes narrower on decreasing the temperature and shows well-defined uniaxial symmetry. Principal g values g// = 2.0165 and g $\perp$ = 1.989 are close to those of $PtPc(ClO_4)_{0.5}$ (g// = 2.0225 and g $\perp$ = 1.992). The integrated intensity is almost constant down to 100 K with subsequent growth in the range 100-3 K.

Both the linear decrease of thermoelectric power and Pauli like behavior of magnetic susceptibility indicate the metallic character of $PtPc(PF_6)$x-PBC.

Based on these results, we concluded that the compound just after the peak is $PtPc(PF_6)_{0.5}$-PBC. The solid state doping is a new method to get the compound which shows the same physical properties with the crystals produced by the electrochemical crystallization from solution.

3-3-7 From the viewpoint of the filling control

As mentioned in the introduction, our another purpose in this study was filling-control. Therefore, we tried to control the degree of oxidation by potential control. In

cyclic voltammetry, the oxidation proceeds at the potentials observed the oxidation wave. In the case of MPc-PBC, the oxidation wave extends for the potential range ca. 100 mV. Therefore, we expected that the anion composition will be able to control by potential control within the range that the oxidation wave is observed. Moreover, phthalocyanine complex is rather hard compared with other organic compounds apparently from optical measurement. X-ray analysis under high pressure also supports the hardness of phthalocyanine complex. If the phthalocyanine complex is able to keep the same crystal structure over some potential range, it is possible to control the filling. The ESR signal of single crystal of $NiPc(AsF_6)_{0.5}$ shows the wide distribution of the line width from about 1 G to over 100 G.[8] We considered that the distribution of the line width comes from the difference of the band filling. The energies of narrow 3d-band and π-band are close. The interaction between π-band and 3d-band should change the degree of the oxidation, as a result, the line width shows some distribution. If this hypothesis is true, the change of the π-band filling will be able to be captured by ESR measurement.

From these viewpoint, we carried out X-ray and ESR measurement as to the MPc-PBC films oxidized at various potentials.

As for PtPc-PBC composite film, five kind of films were prepared at following predefined potentials; 0.26 V (just before the first anodic peak), 0.35 V (middle of the uphill of the peak), 0.38 V (maximum of the peak), 0.39 V (middle of the downhill of the peak), and 0.4 V (just after the peak) as shown in Figure 11 using $TBAPF_6$ as a supporting electrolyte. Figure 12 shows the powder X-ray pattern of these films. The films oxidized at 0.26V, 0.38V, and 0.4V showed monoclinic, mixture of monoclinic

and tetragonal, and tetragonal pattern, respectively. Judging from these X-ray results, $PtPc(PF_6)_x$-PBC can not keep the same crystal structure over the potential range of the anodic giving the mixture pattern of monoclinic and tetragonal at the potential of the middle of the anodic wave. As a result, it is difficult to control the filling in $PtPc(PF_6)_x$-PBC. One of the most important point to control the filling is to keep the same band structure, therefore, the mixed system is out of the question. In the same way as PtPc-PBC, NiPc-PBC oxidized films were prepared using two kind of supporting electrolyte ($TBAPF_6$ and $TBAAsF_6$). Figure 13 and Figure 14 are voltamograms of NiPc-PBC oxidized by $TBAPF_6$ and $TBAAsF_6$, respectively. The voltamogram of $NiPc(PF_6)_x$-PBC has a strong resemblance to that of $PtPc(PF_6)_x$-PBC. The powder X-ray pattern of oxidized just after the first anodic peak (0.46 V) shows tetragonal pattern as shown in Figure 15. The voltamogram of $NiPc(AsF_6)_x$-PBC differ in the shape. It has wide peak width and the valley between first and second anodic peak is not clear. The wide peak width means that the control range of the potential is more wide, and the unclear valley between the two anodic peaks means that the oxidation proceeds to the next step continuously. By these reasons, we considered that $NiPc(AsF_6)_x$-PBC is more suitable material for filling control in comparison with $PtPc(PF_6)_x$-PBC and $NiPc(PF_6)_x$-PBC. We prepared three kind of oxidized film of $NiPc(AsF_6)_x$-PBC. The oxidized potential were 0.23, 0.3, 0.4 V. Figure 16 shows the powder X-ray patterns of these films. However, in the same way as $PtPc(PF_6)_x$-PBC, the X-ray pattern at 0.3 V shows mixed pattern of 0.23 and 0.4 V.

The ESR was measured on the films of $NiPc(PF_6)_x$-PBC (oxidized at 0.43 V) and $NiPc(AsF_6)_x$-PBC (oxidized at 0.23, 0.3 and 0.4 V) at room temperature. The potential

dependent ESR pattern of $NiPc(AsF_6)_x$-PBC is shown in Figure 17. If the interaction between d- and π-band change before and after the potentials of the anodic wave, resulting from the change of the π-band filling, we should observe the change of the band width. However, we could not observe any change of band width before and after the potentials of the anodic wave. However, both of the $NiPc(PF_6)_x$-PBC and $NiPc(AsF_6)_x$-PBC oxidized at the potential just after the peak (0.43 and 0.4 V, respectively) showed a typical polycrystallin signal which contains two anisotropic g value just like $PtPc(PF_6)_x$-PBC, that is, from the viewpoint of the development of a new doping method, we succeeded to verify that the solid state doping is effective as for these NiPc composite films. Figure 18 shows the ESR signal of $NiPc(AsF_6)_x$-PBC (0.40 V) measured at several different temperatures. The two component was not separate even at the lowest temperature (4 K).

3-4 Summary

We describe the characteristic properties of solid state electrochemistry in organic crystalline material PtPc and NiPc encapsulated in the polymer matrix. Although some similar properties in the interaction process of a molecular crystal are known and are observed earlier, we will mention some of them for more complete description. (1) The redox transformation of the crystalline electroactive material (or electrochemical doping of the crystalline solid) brings about a partial oxidation or reduction per a molecule, and often results in the formation of material with an incompletely filled energy band. (2) there is a constant potential difference (*pd*) between relevant anodic and cathodic peaks. In contrast to inorganic compounds or conducting polymer, organic crystals usually

discontinuously change the structure upon doping. This stepwise structural change as a result of phase transition seems to be the reason of the constant *pd*. (3) in the same condition as solid, molecules are more deeply oxidizable than crystal at the defined potential. This trend probably holds in other crystalline organic compounds as well.

3-5 The problem to be solved in future

We succeeded to develop a new doping method by potential control in the solid state. However, we couldn't succeed the continuous filling control for PtPc-PBC and NiPc-PBC because of the structural change at the anodic peak potential. Therefore, it is necessary to verify whether the composition control by potential (not by concentration) is possible or not for organic complexes. In the case of the crystallization through the solution state, the composition is controlled by the concentration of the solution. The first step is to find out the compounds that is able to control the composition (not filling) by potential. DCNQI complex is one of the good example that the mixed crystals are prepared by control of the solution concentration. In this case, the band structure changes accompanied with the formation of the mixed crystal but the crystal structure does not change so much. The Cu and Li play roles in the injection of the carrier. This atomic level exchange suppress the strain of the lattice at a minimum and contribute to the maintenance of the crystal structure. In consideration of these reason, DCNQI complex is the best sample as for the first trial of the composition control by potential. Once checked the effectiveness of the composition control by potential for DCNQI system, the next step is to search the materials that are suitable for the filling control by potential. The molecule which shows strong self-aggregation-ability, for example, BO

complex strongly attracts our interest.

To accomplish the filling control, the competitive relation between the maintenance of the lattice and the injection of the carrier is very important. Generally speaking, both effects conflict with each other. The maintenance of the lattice tends to shut out the invasion of the carrier keeping the static condition and on the contrary, the injection of the carrier promote the destruction of the lattice. From this viewpoint, the material which has big flexibility, for example, polymer or graphite are also interesting in contrast to the materials which has a hard lattice just as phthalocyanine complexes.

References

[1] J. Brown, *J. Chem. Soc. (A)*, 2494 (1968).

[2] I. L. Kogan and K. Yakushi, *J. Mater. Chem.*, 7, 2231 (1997).

[3] J. M. Green, L. R. Faulkner, *J. Amer. Chem. Soc.*, 105, 2950(1983).

[4] R. Jansen, F. Beck, *Synthetic. Metals*, 41-43, 2903(1991).

[5] S. W. Feldberg, I. Rubinstein, *J. Electroanal. Chem.*, 240, 1(1988).

[6] N. Toshima, T. Tominaga, and S. Kawamura, *Bull. Chem. Soc. Jpn.*, 59, 245(1996).

[7] K. Yakushi, T. Ida, A. Ugawa, H. Ishii, H. Yamakado and H. Kuroda, *J. Phys. Chem.*, 95, 7636 (1991).

[8] K. Yakushi, H. Yamakado, M. Yoshitake, N. Kosugi, H. Kuroda, T. Sugano, M. Kinoshita, A. Kawamoto, and J. Tanaka, *Bull. Chem. Soc. Jpn.* 62, 687-696 (1989).

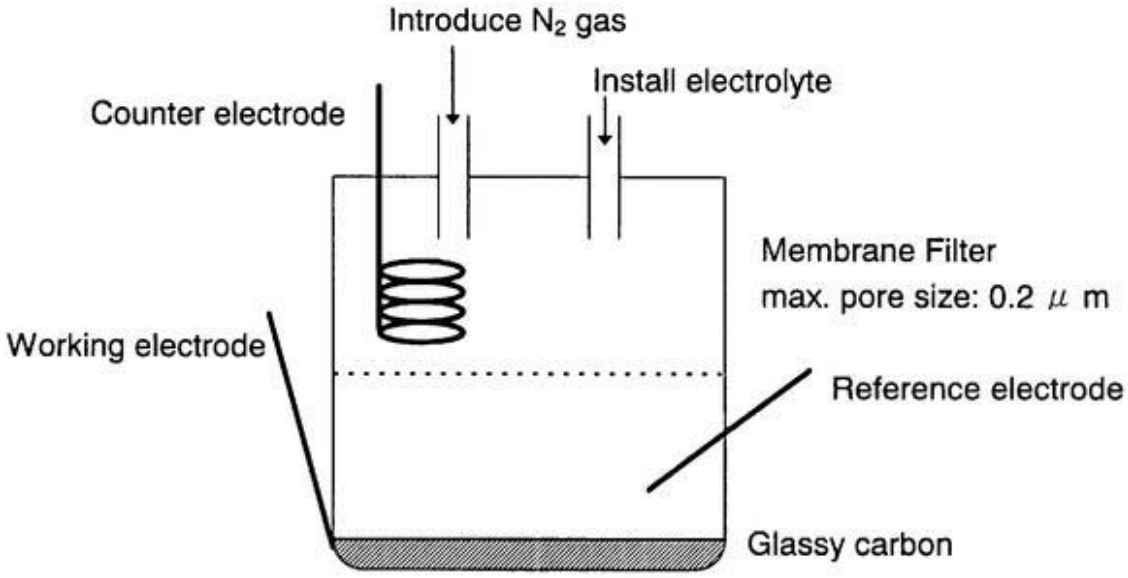

Fig. 1 The electrochemical cell

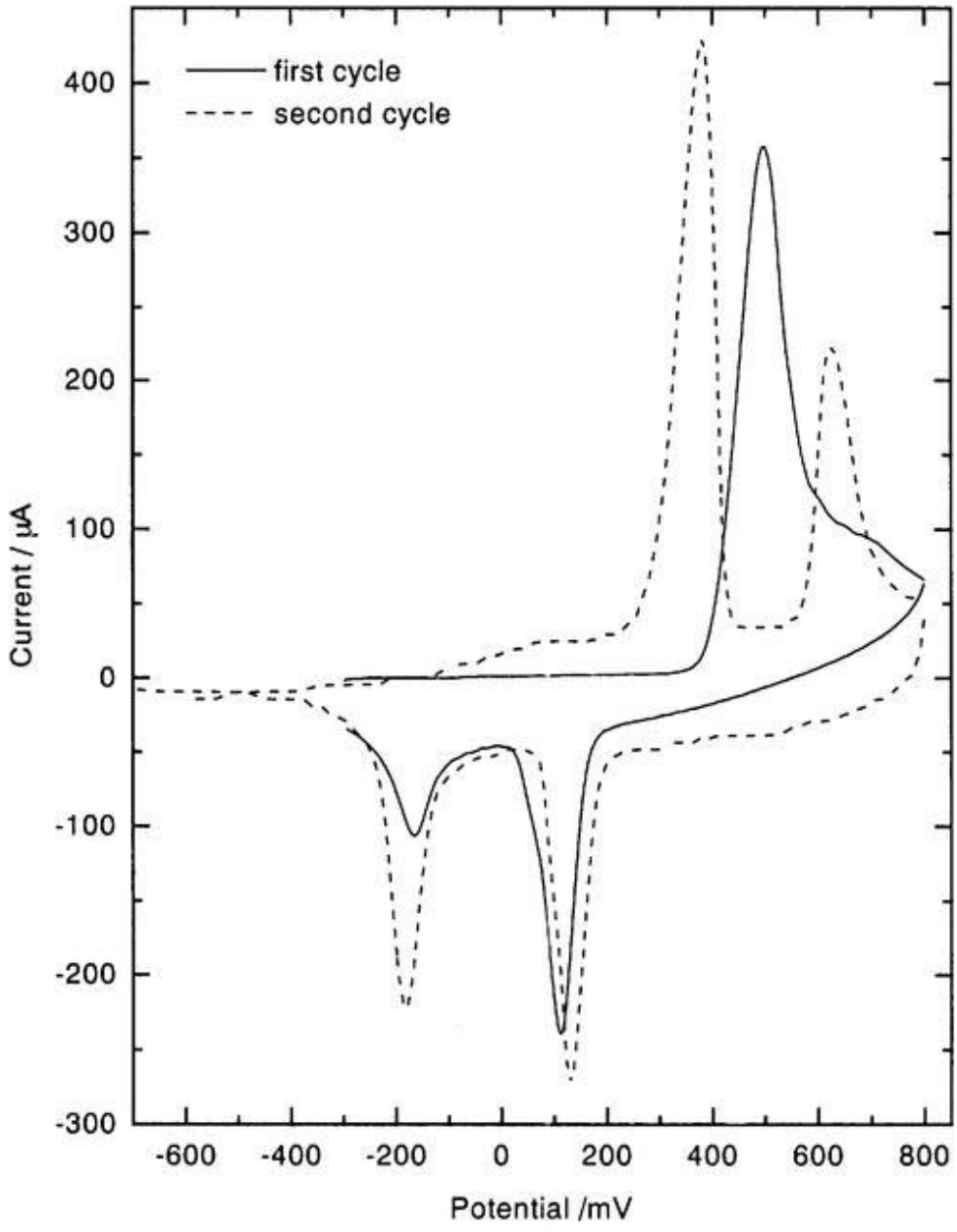

Fig. 2 Voltammograms of PtPc-PBC

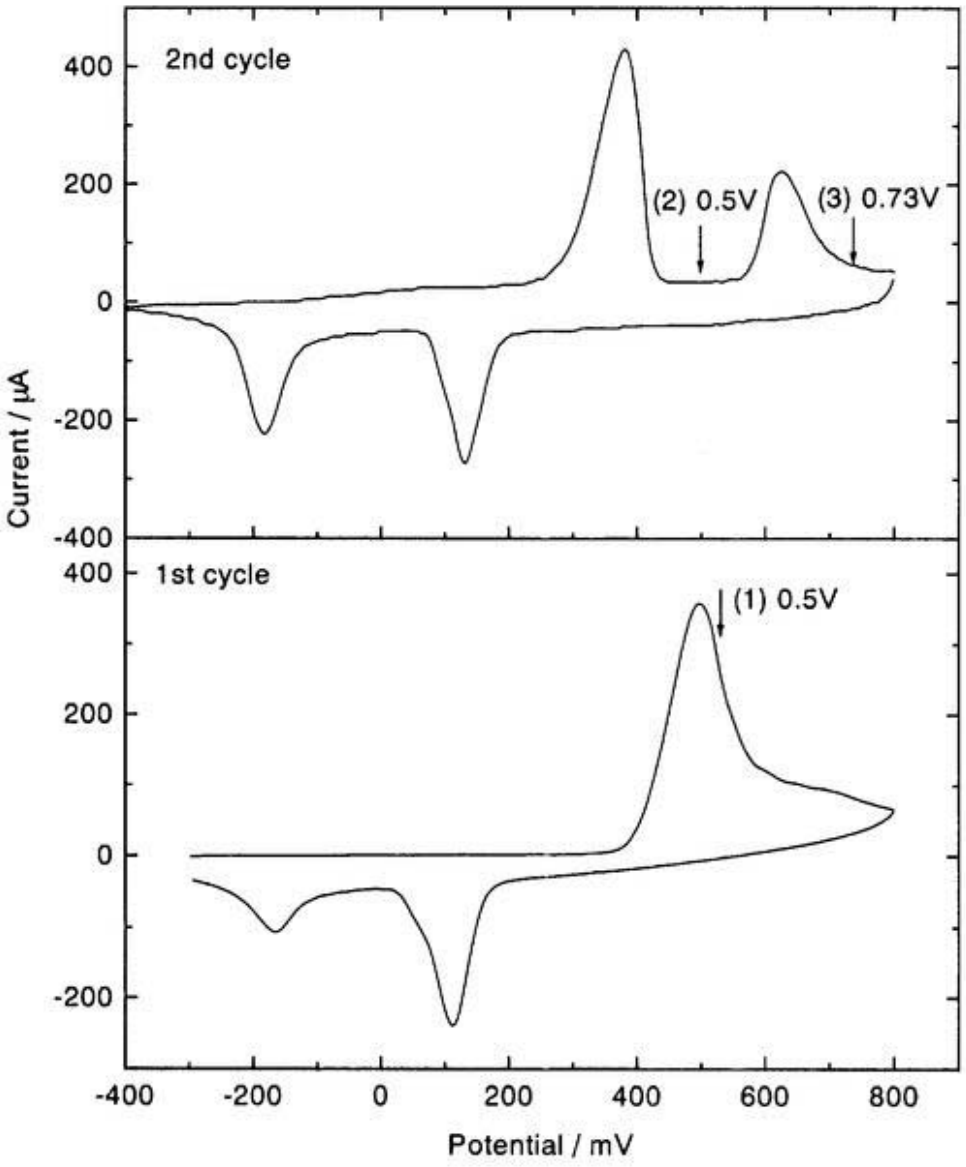

Fig. 3 The predifined potencials for the powder X-ray experiment

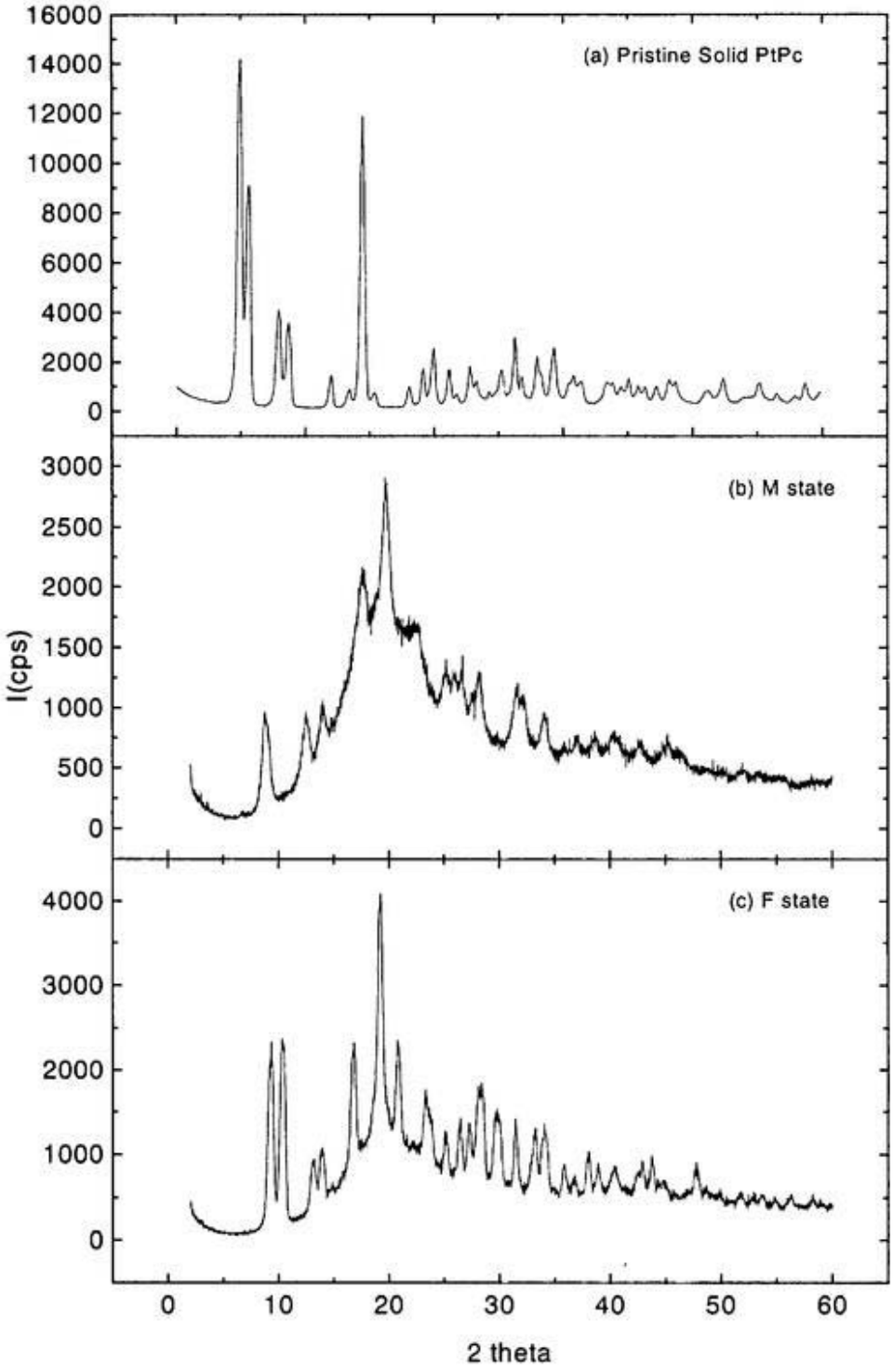

Fig. 4 The X-ray diffraction pattern of pristine solid PtPc(a), mid-oxidized state(b), full-oxidized state(c).

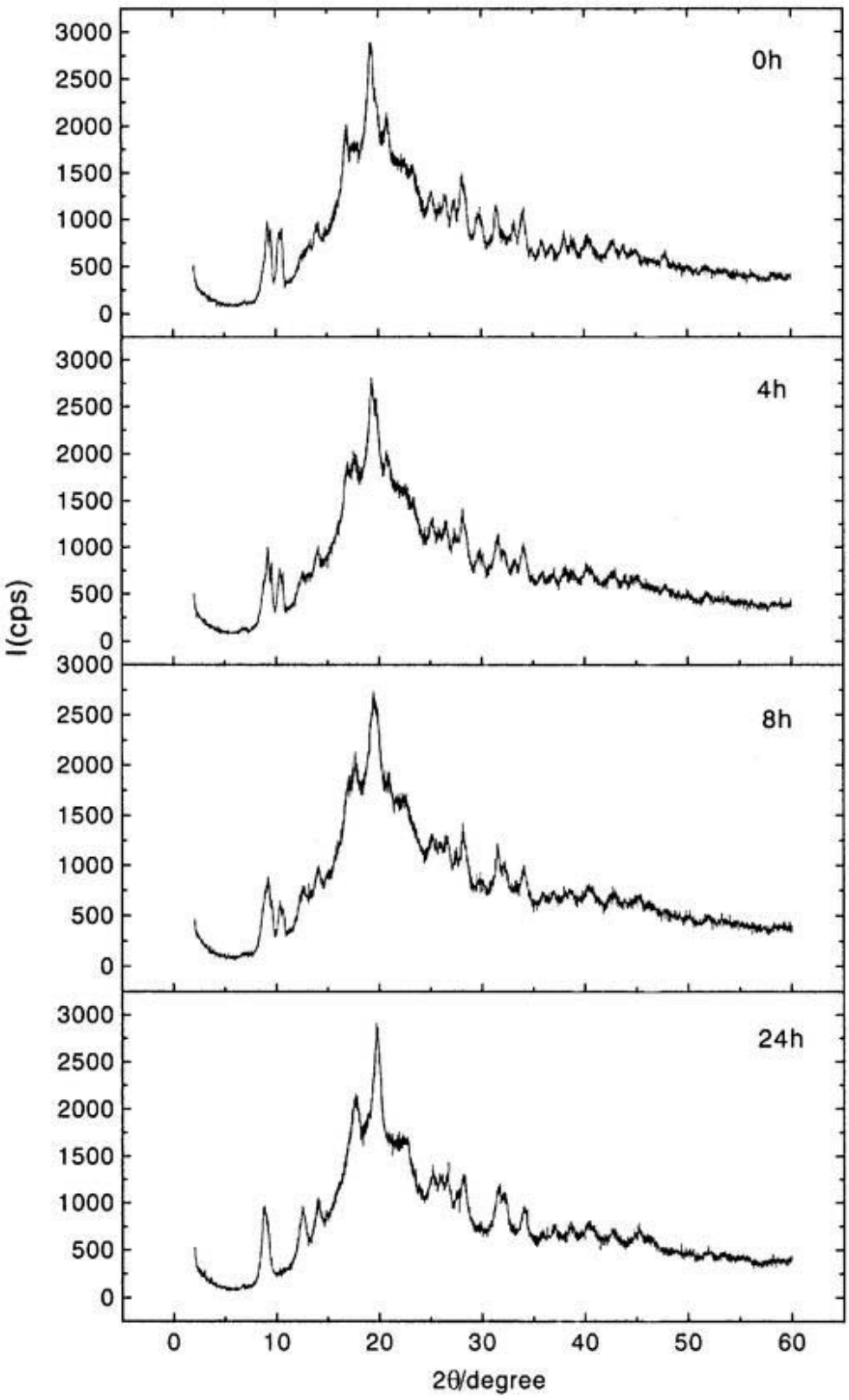

Fig. 5 The time-dependent powder X-ray diffraction pattern of the full-oxidation state

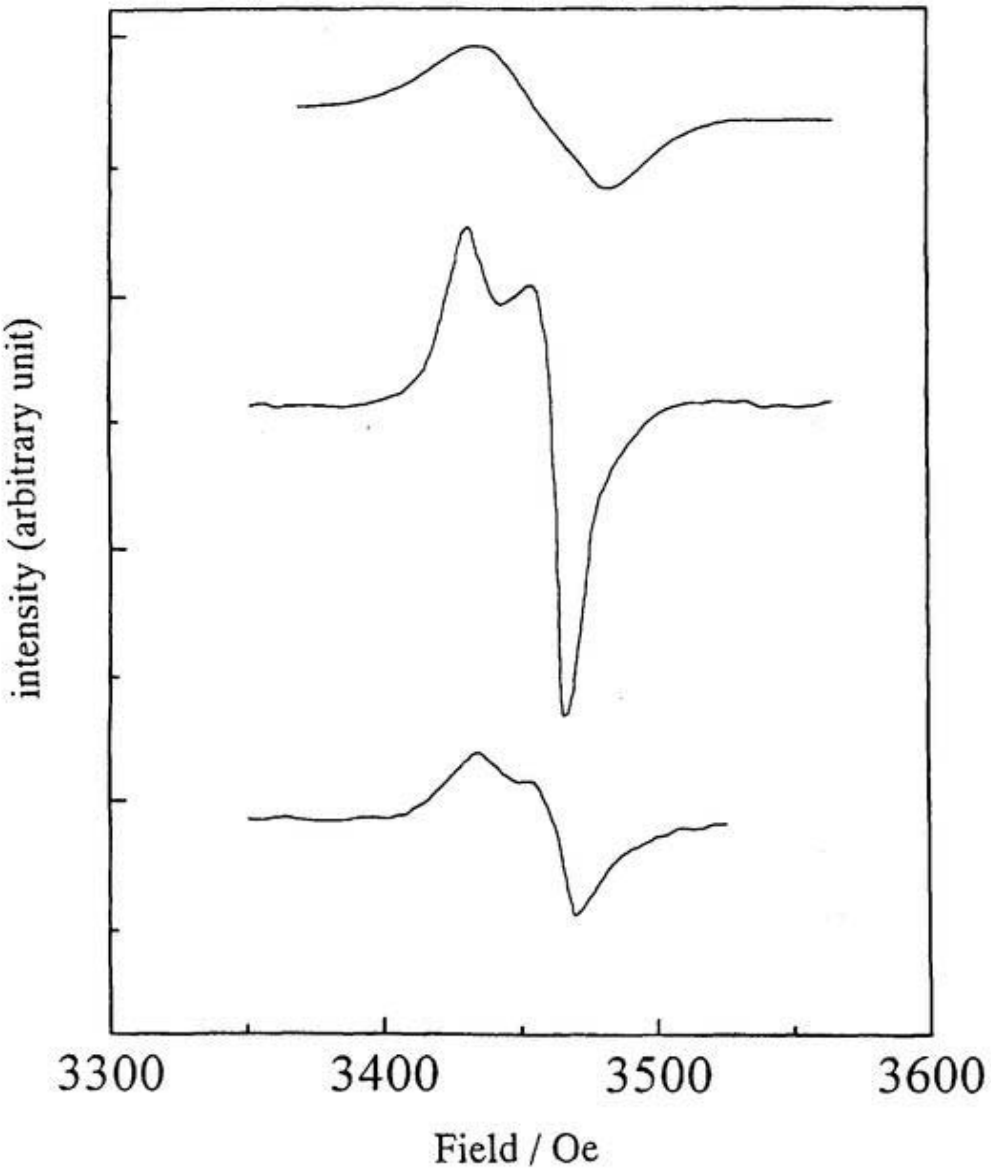

Fig. 6 Reduction potential dependence of EPR spectra
full-oxidation state at ϕ = +0.8 V (top)
mid-oxidation state at ϕ = -0.12 V (middle)
reduced state at ϕ = -2.00 V (bottom)

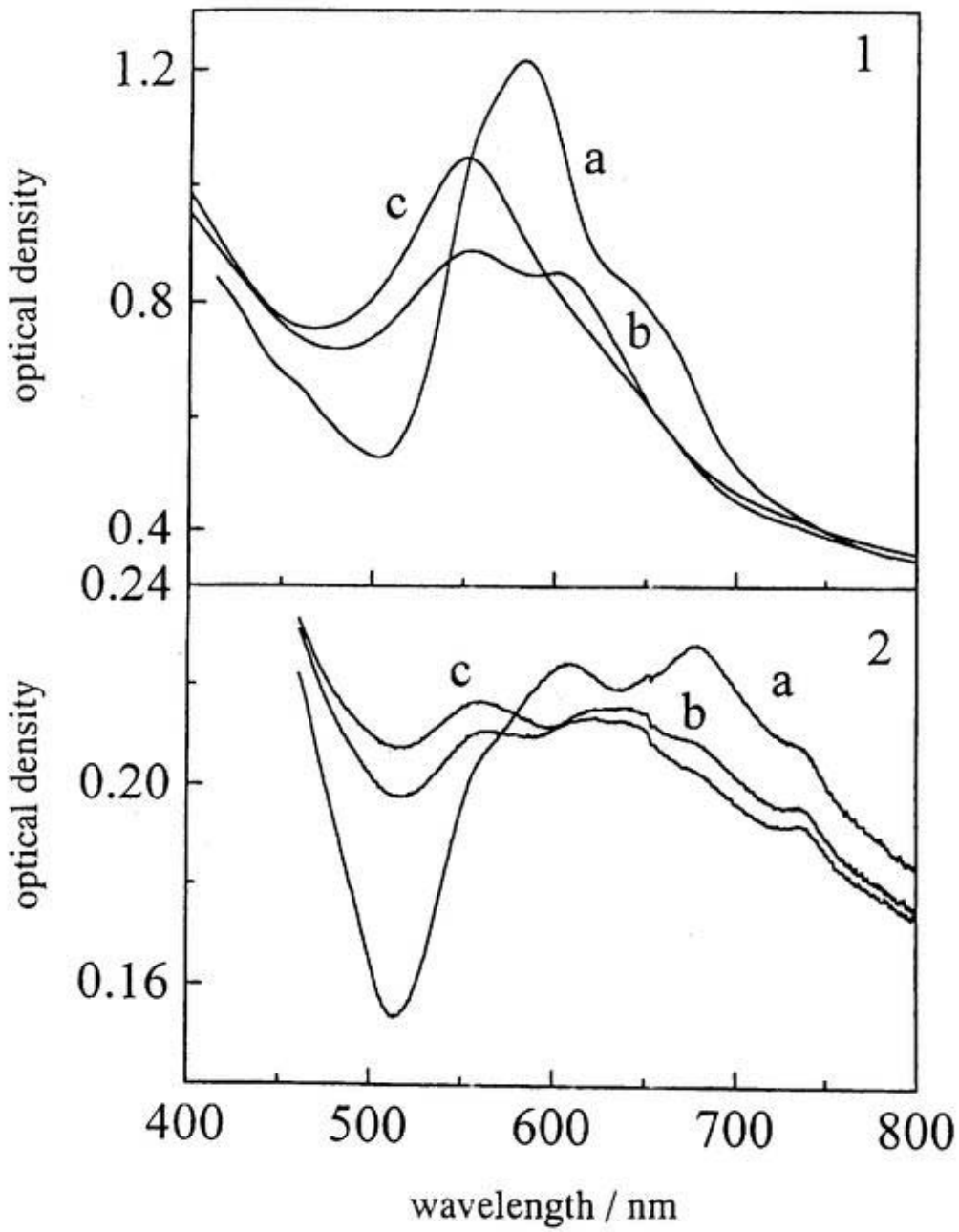

Fig. 7 In-situ optical absorption spectra of (1) film A and (2) film B at potentials a: -0.8 V, b: +0.4 V, c: +0.8 V

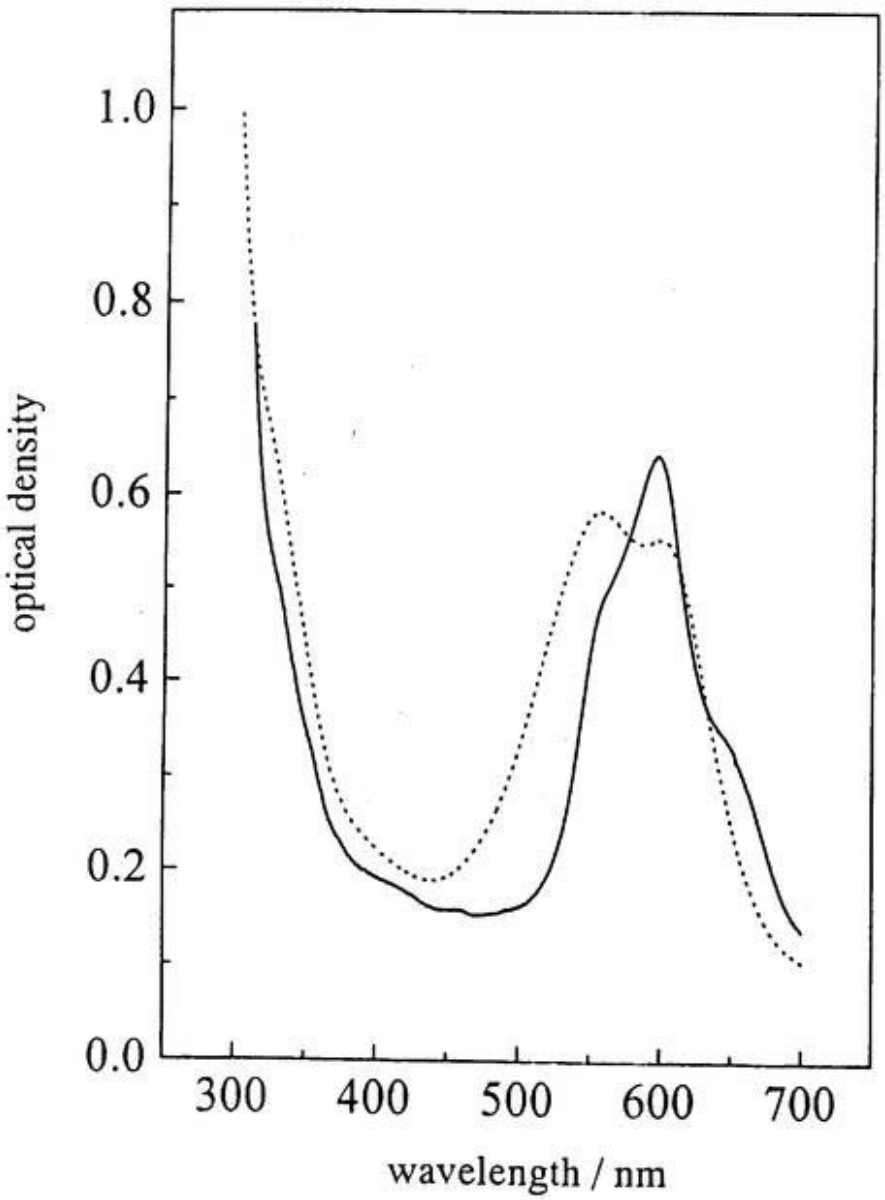

Fig. 8 Optical absorption spectra of colloidal PtPc particles dispersed in acetonitrile solution, before (dashed line; violet color) and after (solid line; blue color) exposing in the atmosphere for 24 h

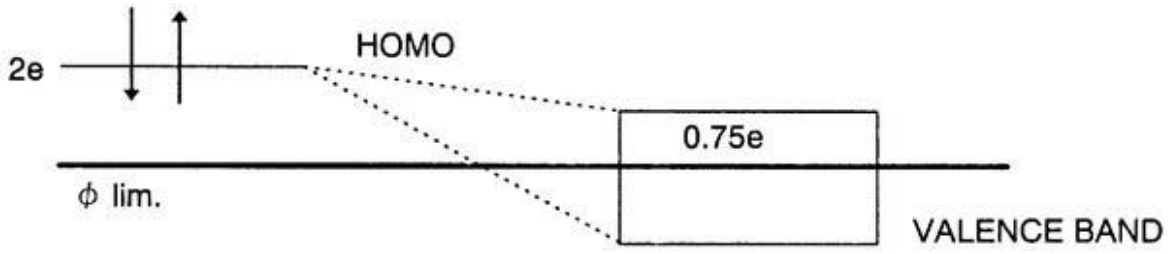

Fig. 9 Schematic energy diagram

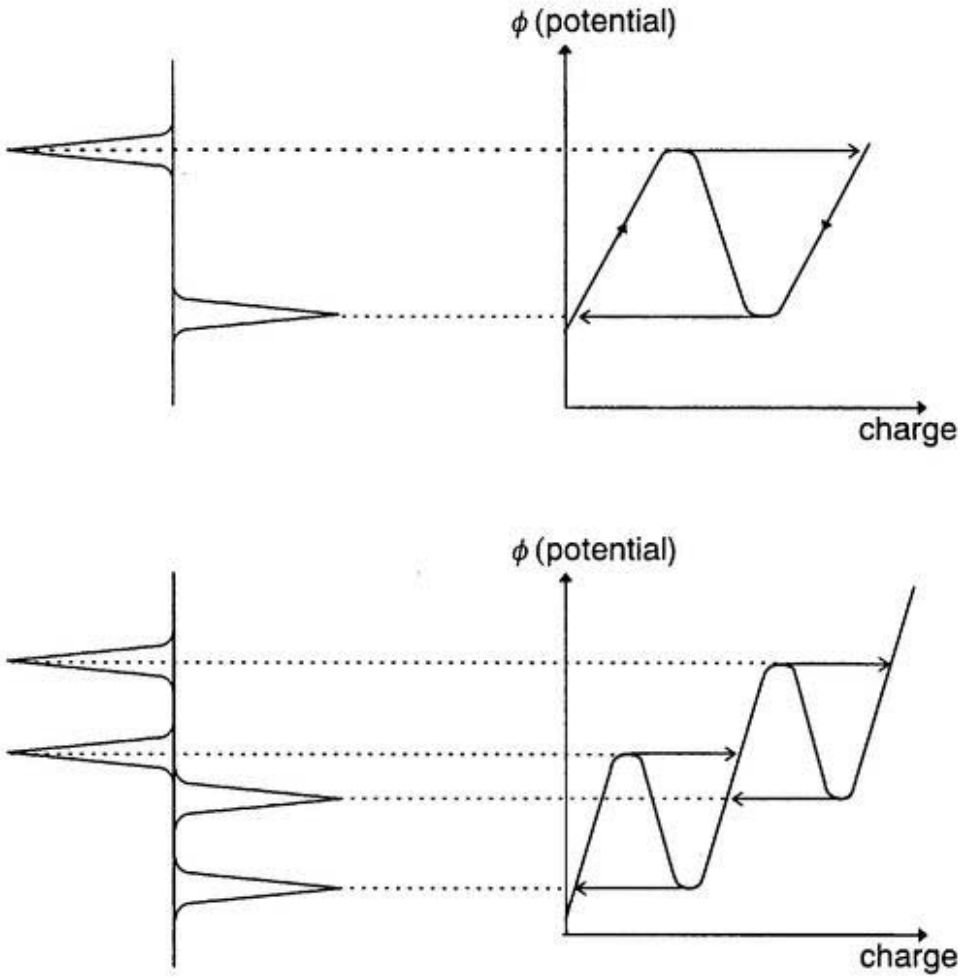

Fig. 10 Schematic picture which shows the relation between N-shaped free energy and peak position

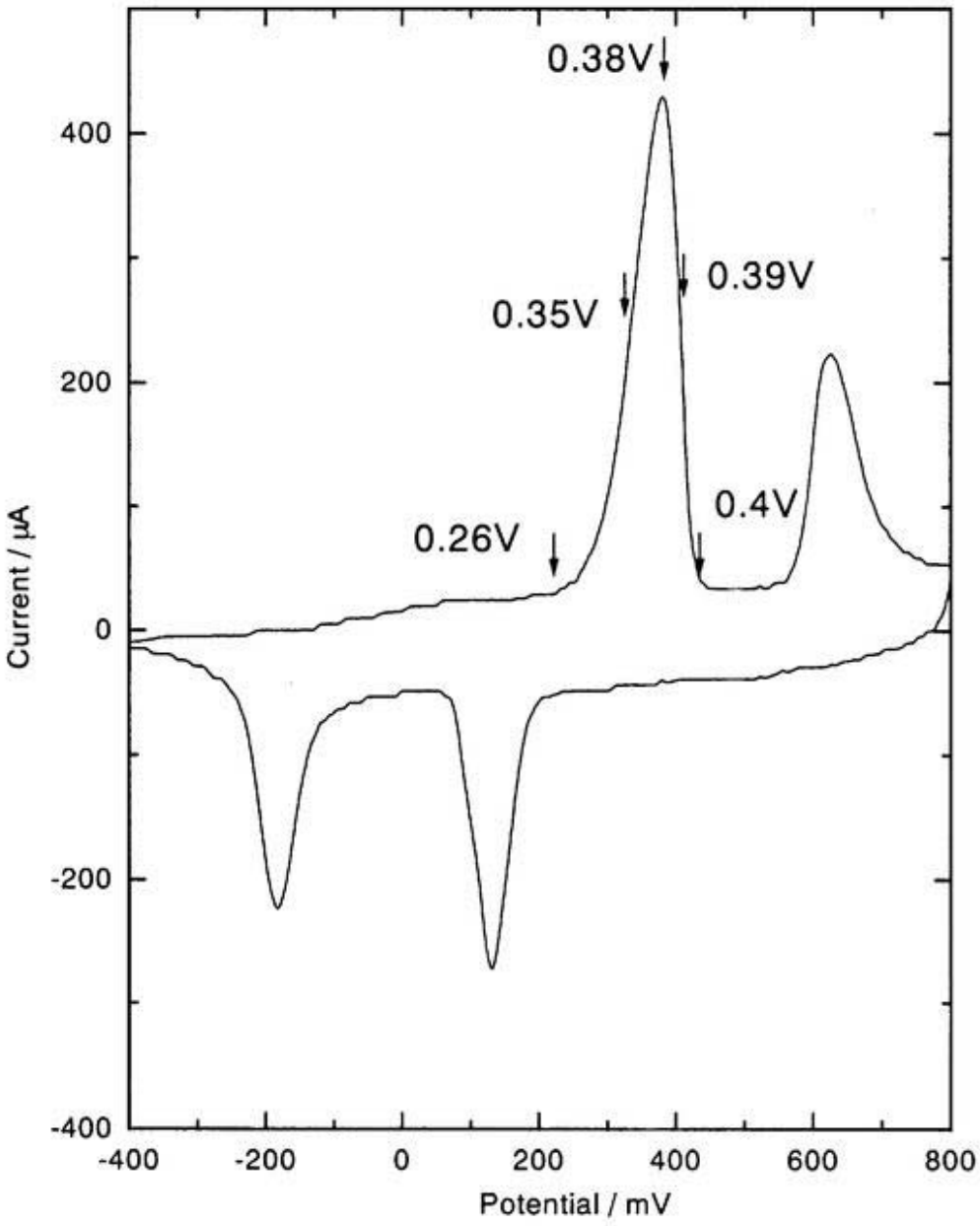

Fig. 11 Oxidation potentials of $PtPc(PF_6)_x$-PBC

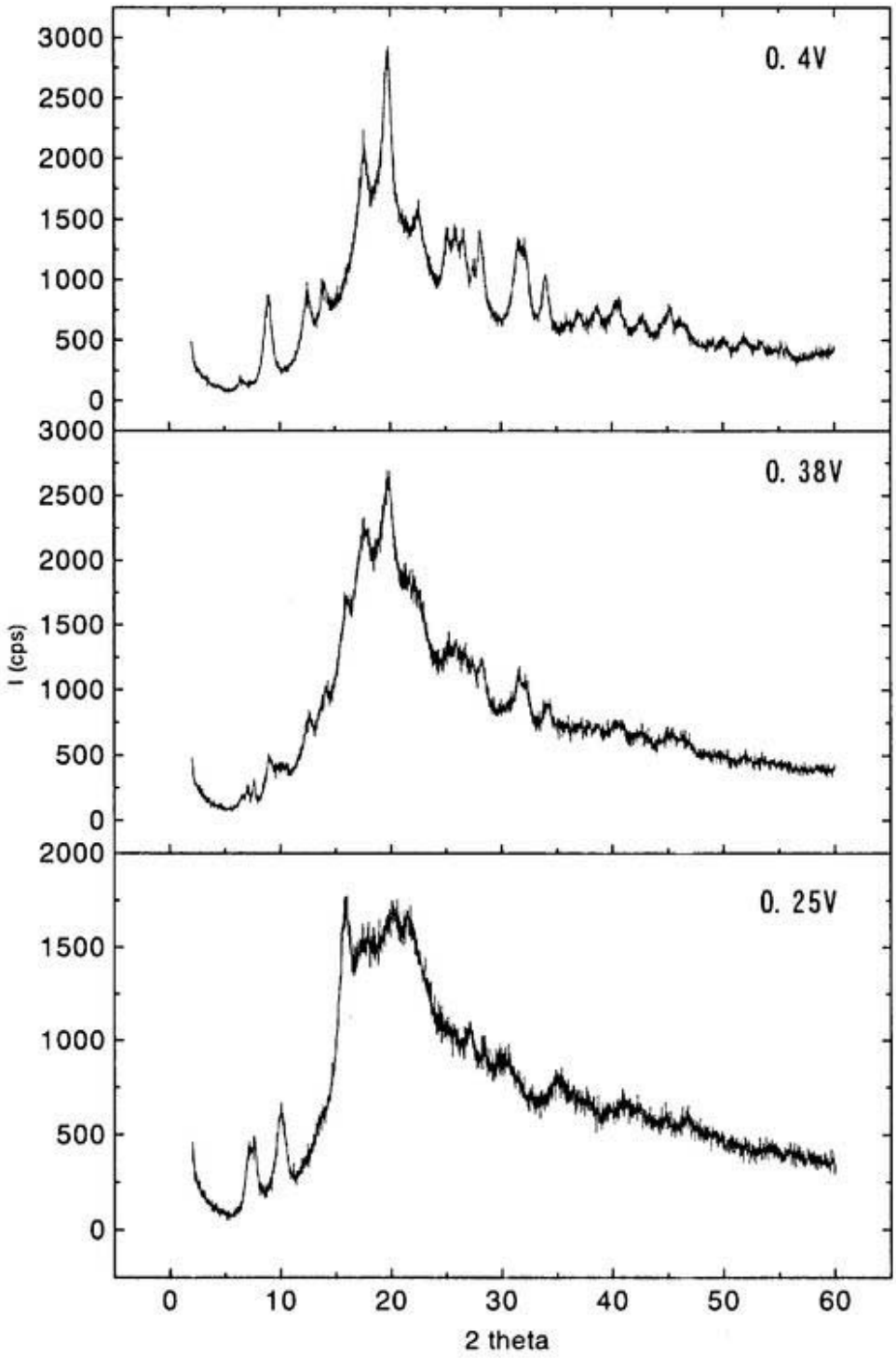

Fig. 12 Powder X-ray pattern of $PtPc(PF_6)_x$-PBC

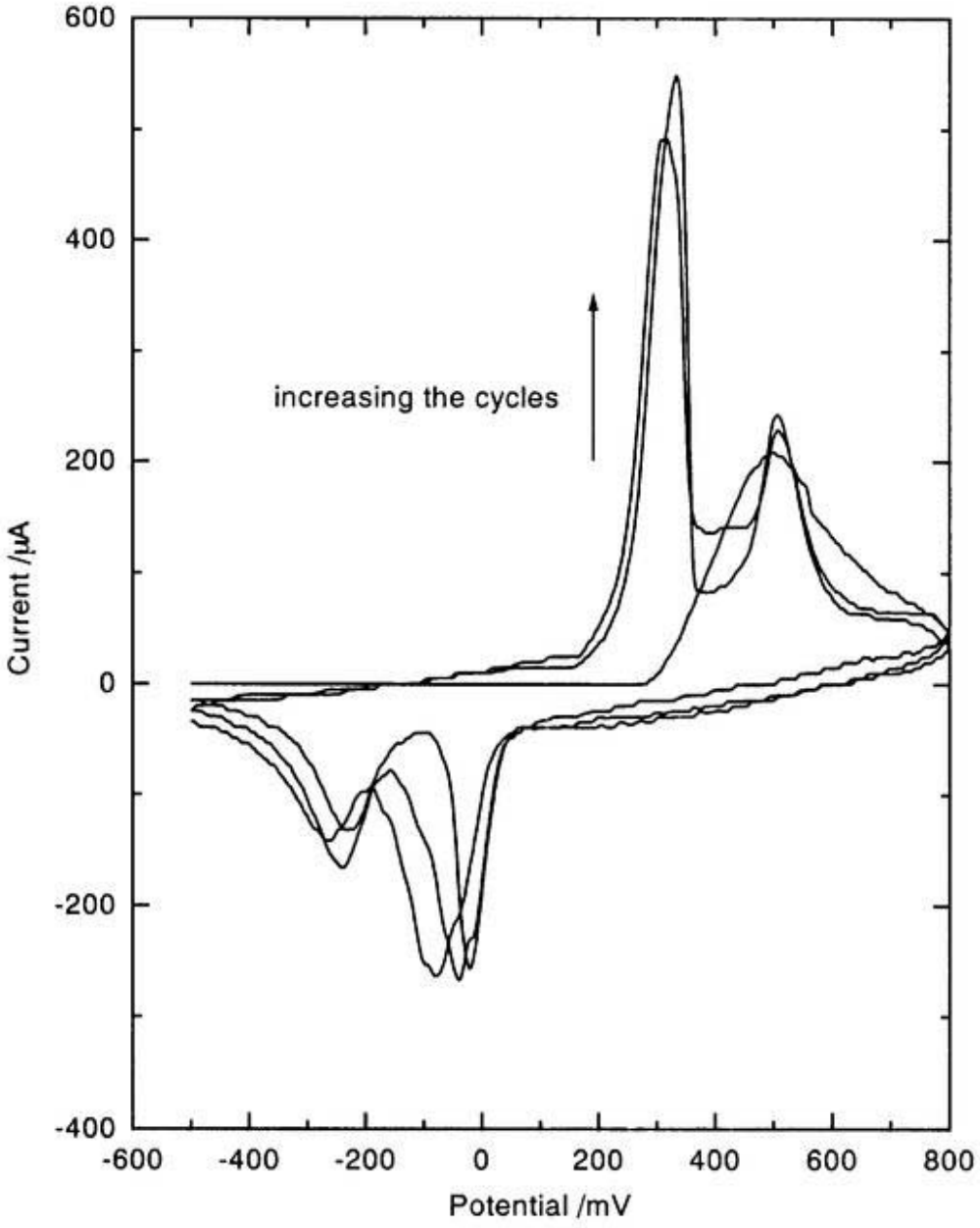

Fig. 13 Voltamograms of $NiPc(PF_6)_x$-PBC

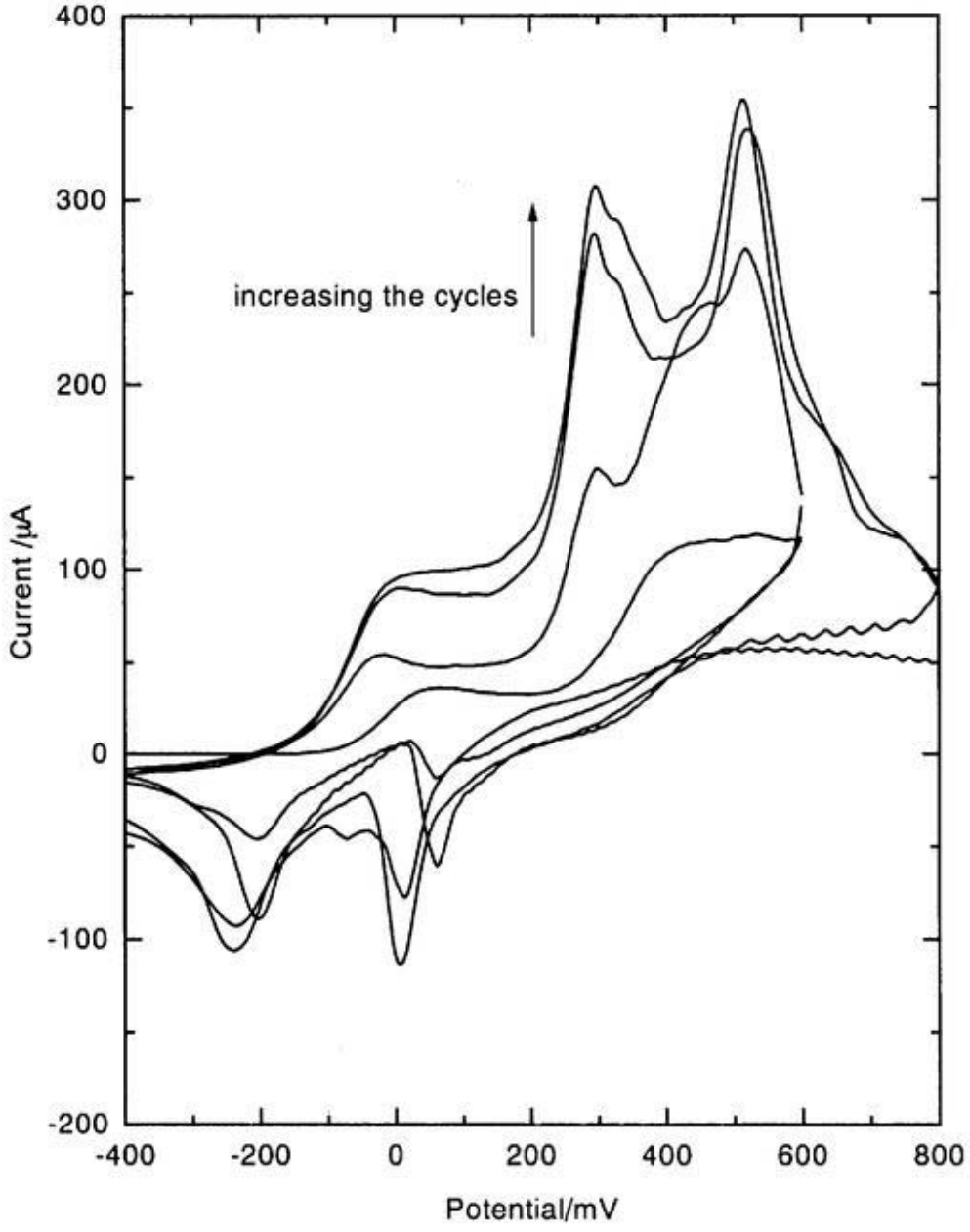

Fig. 14 Voltammograms of $NiPc(AsF_6)_x$-PBC

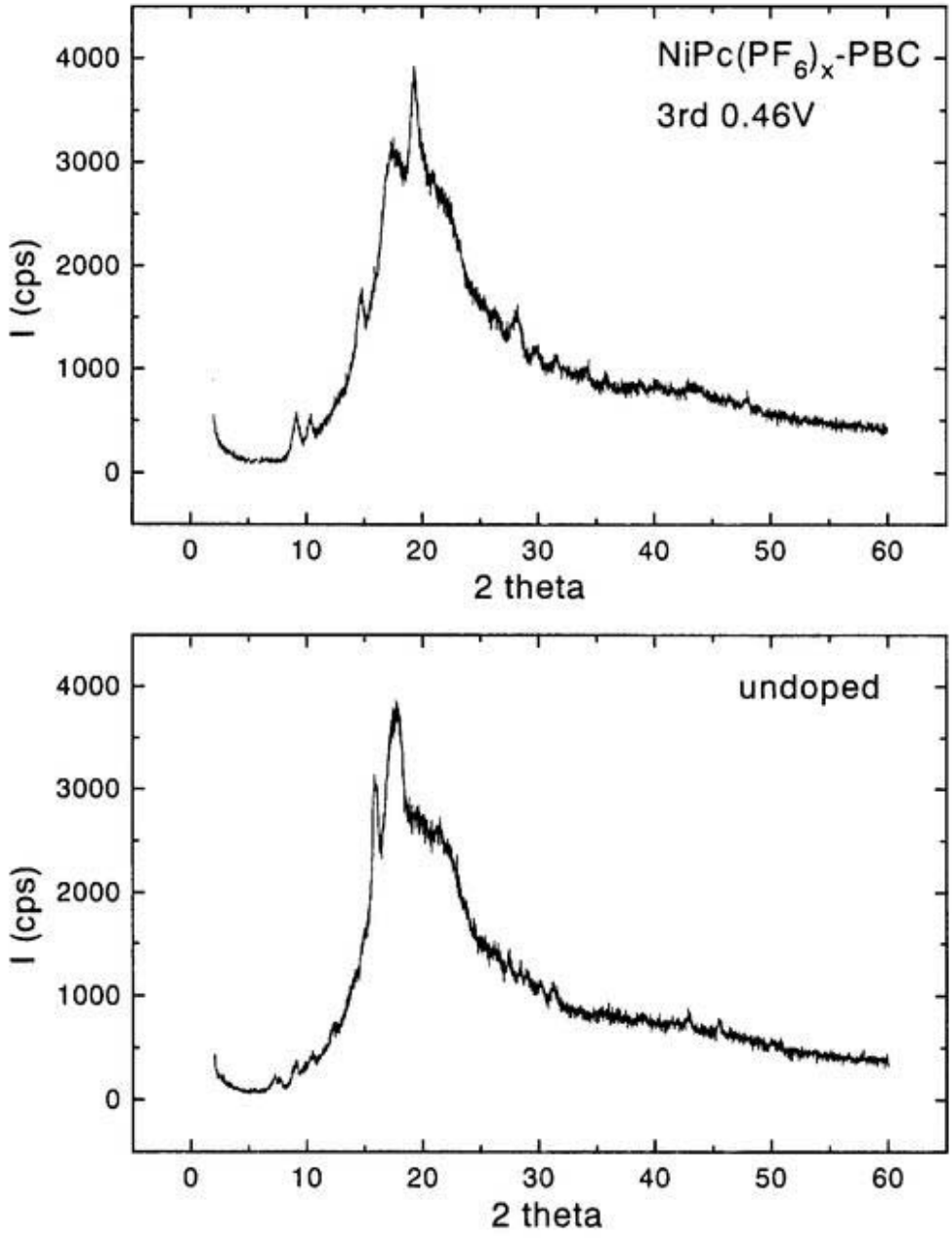

Fig. 15 Powder X-ray pattern of $NiPc(PF_6)_x$-PBC

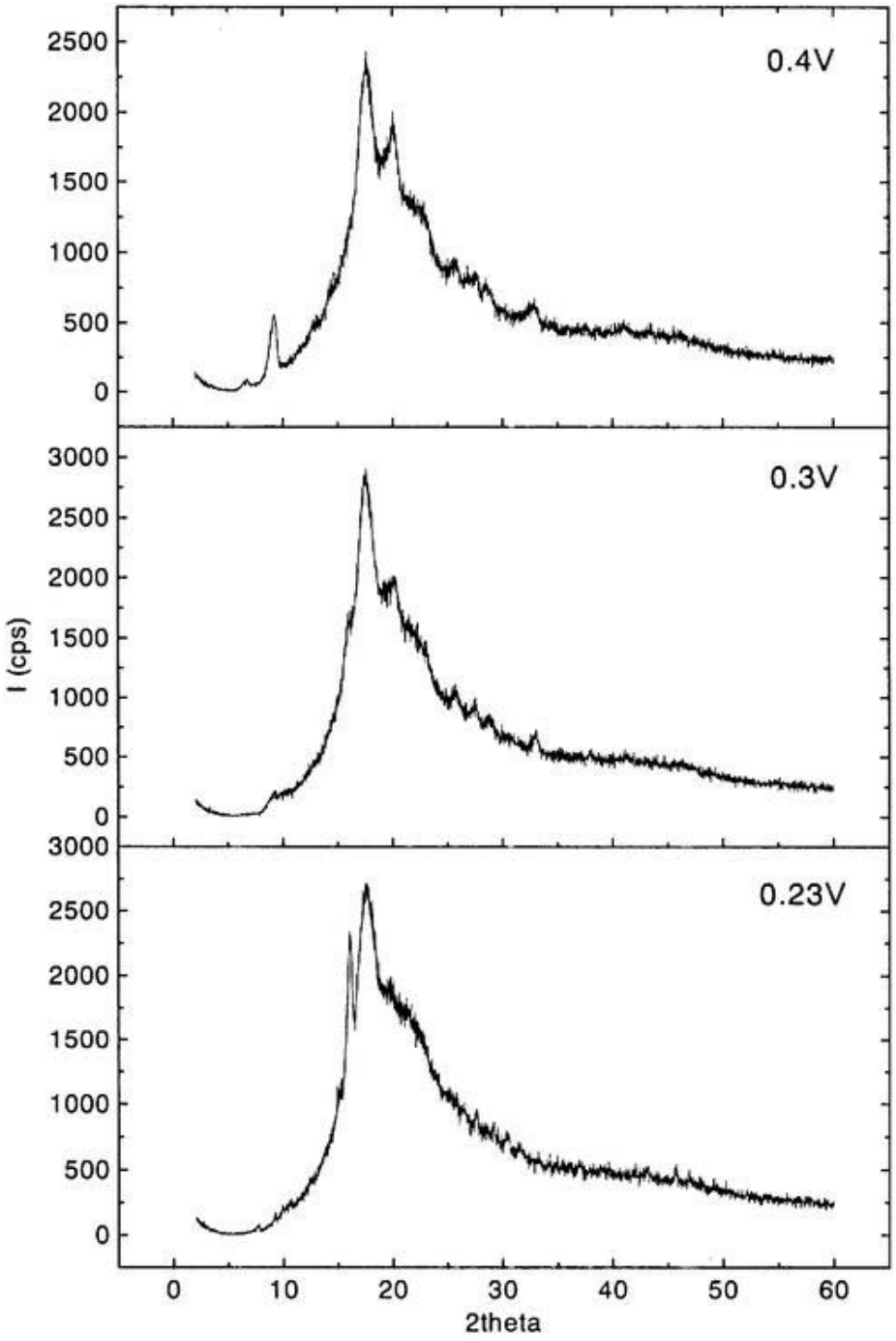

Fig. 16 Powder X-ray pattern of $NiPc(AsF_6)_x$-PBC

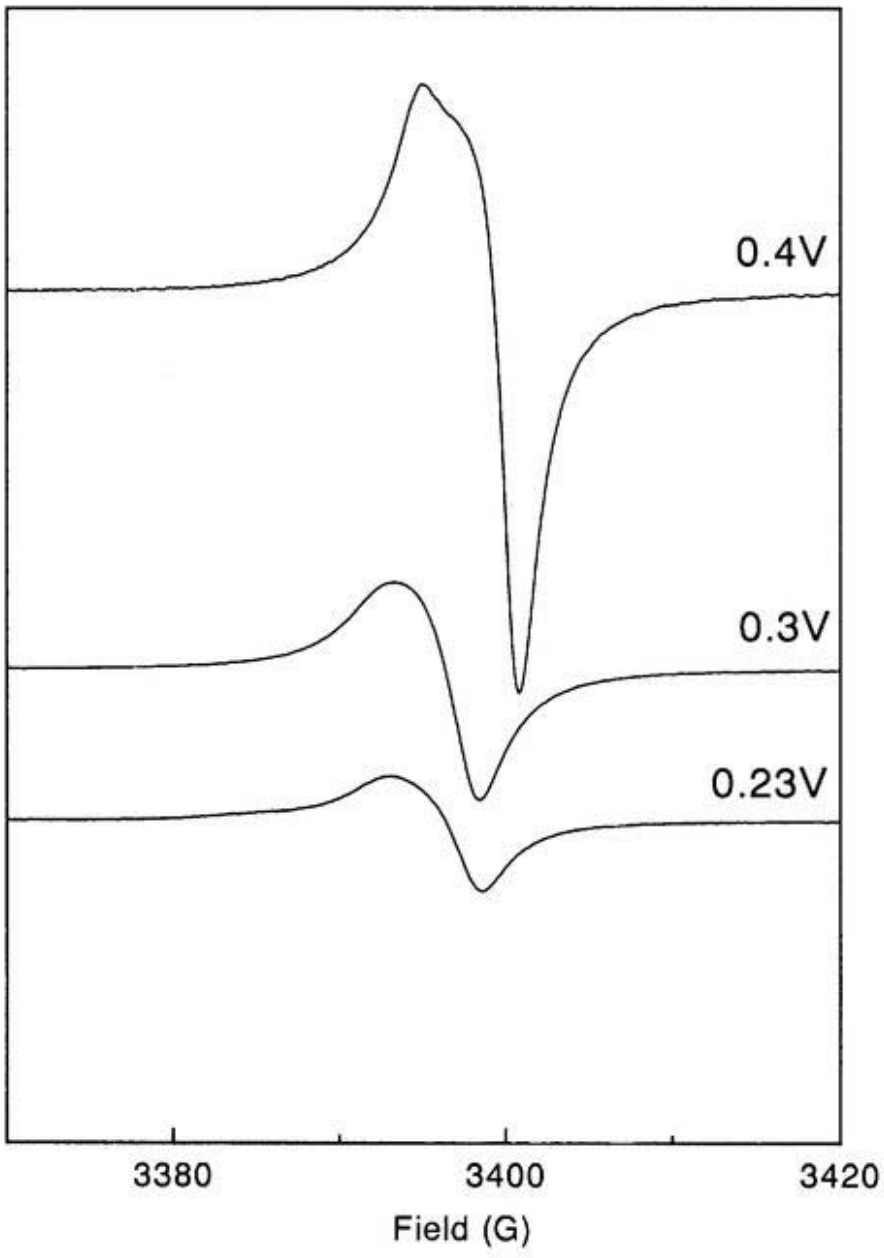

Fig. 17 ESR signals of $NiPc(AsF_6)_x$-PBC

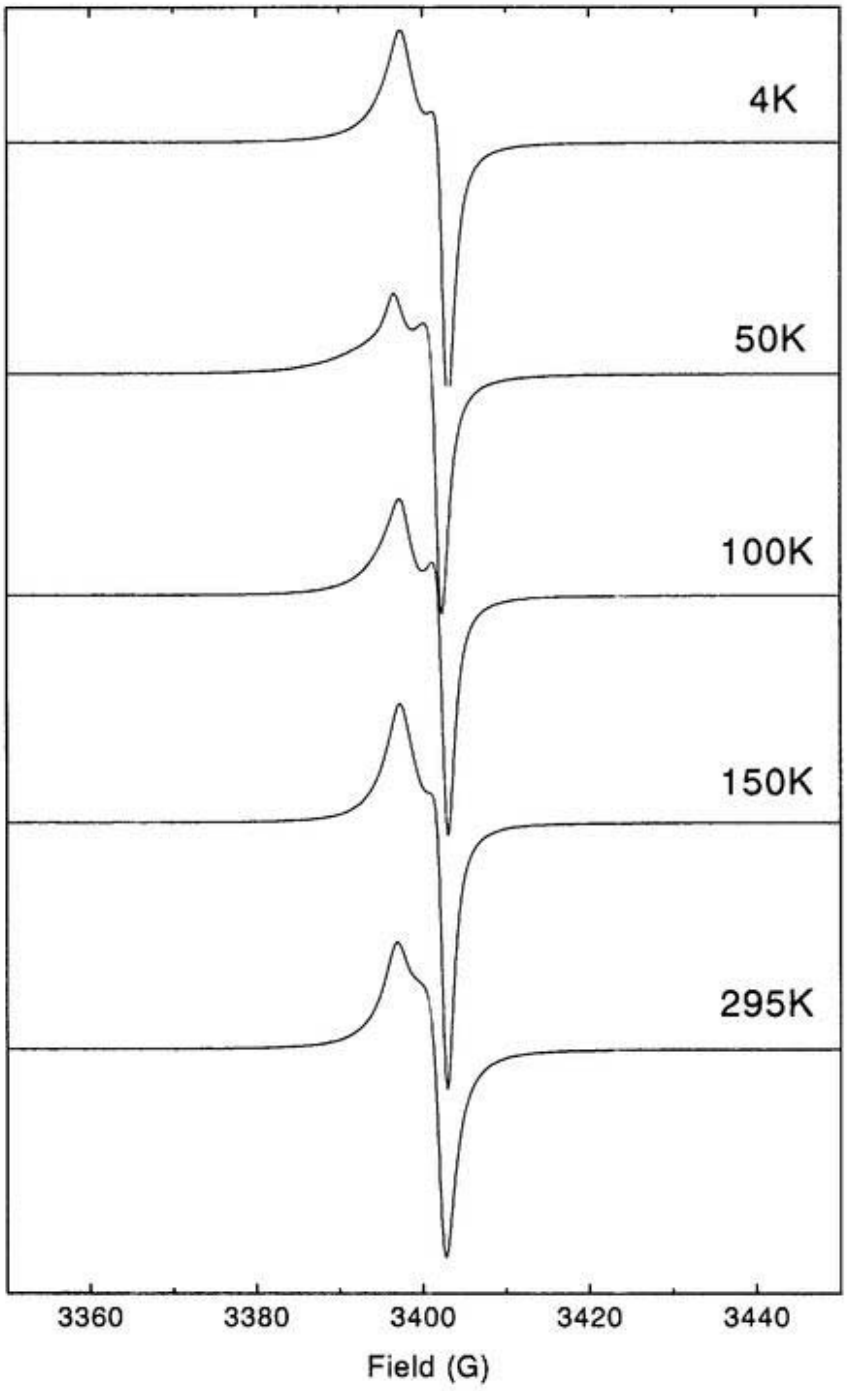

Fig.18 Temperature-dependent ESR signals of $NiPc(AsF_6)_{0.5}$

cycle \ Peak		Anodic 1	Anodic 2	Cathodic 1	Cathodic 2
1st	position(V)	0.43		-0.17	0.11
	i_p(mA)	0.538		0.175	0.306
2nd	position(V)	0.36	0.63	-0.18	0.13
	i_p(mA)	0.405	0.189	0.174	0.223

Table. 1 Peak position and current

Table. 2 The results of ICP analysis (Pt:203.646nm, P:253.565nm)

	Pt(ppm)	*P(ppm)*		*ratio Pt:P=1:x*	
0.5V PtPc(PF6)x					
97101602	14.0093	1.7889	7.831237	0.804246701	After washing with pure water
	15.5536	1.6008	9.716142	0.648225049	
	15.7416	1.9134	8.22703	0.76555528	
97101601	19.3682	2.7835	6.958218	0.905152226	
	20.8473	3.2293	6.455672	0.975614476	
970925	4.1039	0.7633	5.376523	1.171434882	Before washing with pure water
	4.046	0.8763	4.61714	1.364101205	
	4.1207	0.5235	7.871442	0.800138832	
970924	3.6878	0.8627	4.274719	1.473370932	
	4.1566	0.9039	4.598518	1.369625434	
	4.2331	0.8726	4.851135	1.298303835	
0.7V PtPc(PF6)x					
970924	8.9842	6.3599	1.412632	4.45851811	
	9.966	6.4883	1.535996	4.100432798	
	9.7418	6.6464	1.465726	4.297015546	
970925	8.5593	4.8471	1.76586	3.566673791	
	8.9138	5.0276	1.772973	3.552364254	
	8.7272	4.8884	1.785288	3.527861005	
97101602	1.1041	0.6152	1.794701	3.509357209	
	1.0659	0.534	1.996067	3.155327584	
	1.12	0.554	2.021661	3.115382682	

Chapter 4

Optical spectra of mixed crystals of phthalocyanine conductors

Y. Yonehara, K. Yakushi
Optical spectra of phthalocyanine salts
Synth. Met., in press.

Part 1

Optical spectra of phthalocyanine charge transfer salts;

$NiPc(AsF_6)_{0.5}$ and $CoPc(AsF_6)_{0.5}$

4-1-1 Introduction

The most essential characteristic of the charge-transfer salts of phthalocyanine is the double-chain and two-band structure: a metal d-chain and macrocycle π-chain coexist within the same molecular column and a narrow 3d-band is located near the Fermi level of a wide π-band.[1] These two bands do not hybridize each other because of the symmetrical difference. As for most of the phthalocyanine conducting salts except for CoPcI,[2] the π-band acts as the conducting pathway.

$NiPc(AsF_6)_{0.5}$ shows a metal-insulator transition at 40 K. In this system, high pressure induces a charge transfer from 3d-band to π-band.[3] Upon increasing pressure, the non-metallic phase of $NiPc(AsF_6)_{0.5}$ evolves up to almost room temperature around 1 GPa. As described Chapter 1, this non-metallic transition is different from the Mott transition induced by electron-electron correlation by the result of thermopower measurement.[4] However, an anomaly was observed around 40 K in the heat capacity measurement, and low temperature X-ray experiment also indicated the possibility of the structural transition. Therefore, there is still a possibility that some structural change occurred around the transition temperature. The vibronic mode is very sensitive to the lattice dimerization, so it has been used as a probe of small lattice dimerization.[5] The first motivation in this section is the detection of the lattice distortion by reflectance spectroscopy.

In contrast to metallic $NiPc(AsF_6)_{0.5}$, $CoPc(AsF_6)_{0.5}$ shows semiconducting behavior even at ambient temperature in spite of the same band filling and isomorphous crystal structure to $NiPc(AsF_6)_{0.5}$.[6] In the case of $CoPc(AsF_6)_{0.5}$, no clear evidence for lattice distortion is found in the same way as $NiPc(AsF_6)_{0.5}$ below 40 K. These

difference are compared with electrical resistivity, thermopower, and magnetic susceptibility. Figure 1 shows the difference of the transport properties between $NiPc(AsF_6)_{0.5}$ and $CoPc(AsF_6)_{0.5}$. The different point between these two compounds is the following: the 3d-orbital of the central metal is singly occupied in $CoPc(AsF_6)_{0.5}$ (S = 1/2) whereas fully occupied in $NiPc(AsF_6)_{0.5}$. Therefore, magnetic coupling between π- and d-electrons would be responsible for the non-metallic ground state of $CoPc(AsF_6)_{0.5}$. This difference is considered from the theoretical standpoint using one-dimensional Heisenberg-Kondo lattice model, the next-nearest-neighbor repulsion among π-electrons end the magnetic coupling between π- and d-electrons are essential to open a charge gap.[7] The second motivation in this section is the characterization of the band structure of $CoPc(AsF_6)_{0.5}$ by comparing the reflection spectra of the mixed crystals with $NiPc(AsF_6)_{0.5}$.

4-1-2 Experimental

Polarized reflection spectra are measured in the spectral region of 600 cm^{-1} - 30000 cm^{-1} on the single crystals of the charge-transfer salts of phthalocyanine, $Co_xNi_{1-x}Pc(AsF_6)_{0.5}$ (X = 0, 0.093, 0.25, 0.45, 0.55, 1). $NiPc(AsF_6)_{0.5}$, $CoPc(AsF_6)_{0.5}$ and $Co_xNi_{1-x}Pc(AsF_6)_{0.5}$ (X = 0.093, 0.25, 0.45, 0.55) were prepared by the electrochemical method reported before.[8] The mixed crystals were electrochemically grown using the mixture NiPc and CoPc which were co-sublimed for the purpose of purification and complete mixing. The crystal sizes of $NiPc(AsF_6)_{0.5}$, $CoPc(AsF_6)_{0.5}$, $Ni_xCo_{1-x}Pc(AsF_6)_{0.5}$ used for the measurement of optical reflectivity were 0.07×0.07×2 mm^3, 0.2×0.2×2 mm^3, and 0.07×0.07×2 mm^3, respectively. The chemical compositions of $Co_xNi_{1-x}Pc(AsF_6)_{0.5}$

(X = 0.093, 0.25, 0.45, 0.55) were determined by EPMA, and the formation of the mixed crystal was confirmed by the ESR measurement. At room temperature, $Co_xNi_{1-x}Pc(AsF_6)_{0.5}$ (X = 0.093, 0.45) did not show a narrow signal which observed in $NiPc(AsF_6)_{0.5}$ because of the strong interaction between d- and π-electrons. The details of the characterization of mixed crystals will explain in the next section.

The polarized reflectance spectrum was obtained with two spectrometers combined with a microscope: FT-IR spectrometer, Nicolet Magna 760 for 300-12000 cm^{-1} region and multi-channel detection system, Atago Macs320 for 11000-30000 cm^{-1} region. The spectra in the region from 600 to 7000 cm^{-1} were collected using a globar light, MCT detector, KBr beam splitter, and wire-grid polarizer; 4000-10000 cm^{-1} region was measured using a halogen lamp, MCT detector, Quartz beam splitter, and Glan-Tompson polarizer; 8500-12000 cm^{-1} region were obtained using a halogen lamp, Si photodiode detector, Quartz beam splitter, and Glan-Tompson polarizer; 11000-30000 cm^{-1} region was collected using xenon lamp, photodiode array system, and Glan-Tompson polarizer. The absolute value of the reflectivity was determined by comparing the reflected light from a gold mirror (600-12000 cm^{-1}) and Si single crystal (11000-30000 cm^{-1}). The single crystal was fixed on a copper sample holder by silicone grease, and the crystal face was adjusted so as to be normal to the incident light use of a goniometer head. For the low-temperature experiment, a small goniometer head was attached to the cold head of the cryostat, Oxford CF1104s which is fixed on a XYZ stage. The sample on the goniometer head was covered by a radiation shield and vacuum shroud with KBr window. The cryostat was evacuated below 10^{-5} Pa by turbo-molecular pump before cooling the sample. To avoid the contamination on the sample

surface at low temperature, the window of the radiation shield was open only in the measurement. The absolute reflectivity was obtained by comparing the reflected light from gold mirror placed close to the sample in the cryostat, which could cancel out the spectral dependence of the transmittance of the KBr window. The reflectivity of this mirror was monitored at each temperature using the gold mirror out side of the cryostat.

4-1-3 Results and discussion

(a) Anomalous spectrum of $CoPc(AsF_6)_{0.5}$

The crystal of $NiPc(AsF_6)_{0.5}$ belongs to the orthorhombic system with the space group of *Pnc2*, the lattice parameters being a = 14.015(1), b = 28.485(2), c = 6.466(3) Å, and Z = 4.[9] The crystal of $CoPc(AsF_6)_{0.5}$ belongs to the tetragonal system with the space group of *P4/mcc*, the lattice parameters being a = 14.234(2), c = 6.296(2) Å, and Z = 2.[10]

Figure 2 shows the polarized reflectance spectra of $NiPc(AsF_6)_{0.5}$, $CoPc(AsF_6)_{0.5}$ and $Co_xNi_{1-x}Pc(AsF_6)_{0.5}$ (X = 0.093, 0.25, 0.45, 0.55). In all the salts, the stacking axis is c-axis. The plasma frequency ω_p was calculated by the integration of the conductivity spectrum which was obtained by the Kramers-Kronig transformation of the //c reflectance spectrum (Figure 3) using the sum rule described by the following equation,

$$\omega_p^{\,2} = \frac{2}{\pi\varepsilon_0}\int_{\omega_1}^{\omega_2}\sigma(\omega)d\omega$$

where ε_0 is the dielectric constant, $\sigma(\omega)$ the optical conductivity. Before the Kramers-Kronig transformation, The date below 600 cm^{-1} were extrapolated using the Hagen-Rubense method which is applicable to metal and described by,

$$R = 1 - 2\sqrt{\frac{\nu}{\sigma}}$$

where R is the reflectance, ν is the frequency, σ is the conductivity. The plasma frequency of $NiPc(AsF_6)_{0.5}$ and $CoPc(AsF_6)_{0.5}$ were 7610 cm^{-1} and 9589 cm^{-1}, respectively. For reference, the plasma frequencies of $NiPc(AsF_6)_{0.5}$ and $CoPc(AsF_6)_{0.5}$ calculated by Drude model were 7921 cm^{-1} and 11827 cm^{-1}, respectively. The Drude model of dielectric function is described following equation,

$$\varepsilon(\omega) = \varepsilon_c - \omega_p^2 / \left(\omega^2 + i\omega\tau\right)$$

where $\hbar\omega$ is the photon energy, τ is the relaxation time of the carriers, and ω_p is the plasma frequency. The first term includes the constant contributions from higher excitations. Generally, the Drude model does not take the effect of Coulomb repulsion in the low frequency region into the consideration. Hence, it is reasonable that the value calculated by the Drude model is bigger than the one calculated by the Kramers-Kronig transformation. In other words, the difference between the plasma frequency calculated by the Kramers-Kronig transformation and the Drude model is a quick guide to the strength of the electron-electron correlation. However, the Drude model does not apply to $CoPc(AsF_6)_{0.5}$ which shows semiconducting behavior even at room temperature. Therefore, in the following discussion, we use the plasma frequency calculated by the Kramers-Kronig transformation. One of the most important factor which influences the plasma frequency is the transfer integral along the conducting axis. As mentioned above, the lattice parameter of $CoPc(AsF_6)_{0.5}$ *c*-axis is 3 % smaller than that of $NiPc(AsF_6)_{0.5}$. As for $NiPc(AsF_6)_{0.5}$, the pressure dependence of the plasma frequency and lattice constant was investigated previously.[11] In the case that the pressure contracted the *c*-axis

of $NiPc(AsF_6)_{0.5}$ by 3 %, the plasma frequency showed a 4 % increase. Concretely, the observed plasma frequency was corrected considering (1) the relation between plasma frequency and lattice constant of *c*-axis[11] and (2) the increment of dielectric constant of pressure medium as shown in Figure 4.[4] The corrected plasma frequency of $NiPc(AsF_6)_{0.5}$ using the lattice constant at 0.42 GPa is shown in Table 1. Compared with corrected plasma frequency of $NiPc(AsF_6)_{0.5}$, the observed plasma frequency of $CoPc(AsF_6)_{0.5}$ shows a 26 % increase over $NiPc(AsF_6)_{0.5}$. That is, it is impossible to explain this large difference of plasma frequency between $NiPc(AsF_6)_{0.5}$ and $CoPc(AsF_6)_{0.5}$ by the difference of the transfer integral. In this connection, in the case of TTF·TCNQ, the increment of the plasma frequency caused by the 3 % lattice contraction along the conducting axis is just 4 %.[12] In this case, it is considered that the pressure merely acts to increase the transfer integral along the conducting axis (*b*-axis) without any other effects.

The plasma frequency is defined by the following equation,

$$\omega_p{}^2 = \frac{N_0 e^2}{\varepsilon_0 m^*} = \frac{\left(\frac{Z}{V}\right)e^2}{\varepsilon_0 m^*}$$

where N_0 is the carrier density, e the electron charge, m^* the effective mass, Z the number of carrier per unit cell, V the unit cell volume. In this equation, e and ε_0 are the constants. Therefore, we discussed the difference of the plasma frequency based on the following two viewpoints; (1) the difference of N_0, (2) the difference of m^*.

The difference of N_0 means the band filling difference between the two salts. Judging from the crystal structure, it is difficult to contain more than X = 0.5 anion to the composition of $MPc(AsF_6)_x$ (M = Ni, Co). Accordingly, we calculated the

composition of Ni-salts based on the supposition that the composition of the Co-salts is $CoPc(AsF_6)_{0.5}$ and the effective mass is equal in both salts. The unite cell volume of the $NiPc(AsF_6)_x$ was calculated using the value under 0.42 GPa (a = 13.59455 Å, c = 6.27215 Å). In this case, the composition of the Ni-salts was given by $NiPc(AsF_6)_{0.32}$. This composition is in good agreement with the one of Iodine salt $MPc(I_3^-)_{0.33}$.[13] However, the result of EPMA measurement gave the composition of $NiPc(AsF_6)_{0.5}$ (X = 0.5) with rather good accuracy.[8]

Therefore, another possibility is the participation of the Co $3d_z^2$ electron in the optical transition. In contrast to $NiPc(AsF_6)_{0.5}$, the $3d_z^2$ orbital of Co^{2+} is singly occupied and this orbital forms a half-filled one-dimensional band, if the correlation effect is neglected. Therefore, we examined this problem from the second viewpoint ; the difference of m^*. This means that the effective mass of Co-salt is bigger than Ni-salt in appearance due to the contribution of d-electron which is actually independent on the π-electron. In this case, the contribution of the optical transition by 3d-electron to the plasma frequency should be added to that by π-electron as shown below.

$$\omega_p(\mathrm{Co}_{obs})^2 = \omega_p(\mathrm{Co,d})^2 + \omega_p(\mathrm{Co},\pi)^2 = \frac{N_d e^2}{\varepsilon_0 m^*(\mathrm{Co,d})} + \frac{N_\pi e^2}{\varepsilon_0 m^*(\mathrm{Co},\pi)}$$

and besides, that the d-band is half-filled and π-band is 1/4-filled for hole and these two bands are independent of each other. As a result, the effective mass of d-electron was estimated to be roughly 4.3, which is 3.7 times heavier than π-electron. The plasma frequency of d-electron ω_p(Co,d) was estimated to be 5690 cm^{-1}, which is compared with 7718 cm^{-1} for $\omega_p(\mathrm{Co},\pi)$. The calculated results were summarized in Table 1. The difference of effective mass derived from π-electron between the original $NiPc(AsF_6)_{0.5}$

(not at 0.42 GPa) and $CoPc(AsF_6)_{0.5}$ comes from the difference of the unit cell volume of each salt.

According to the one-dimensional tight binding model, the bandwidth $4t$ was calculated using the following equation,

$$4t = \left(\frac{\varepsilon_0}{e^2}\right)\left(\frac{V}{Z}\right)\frac{\hbar^2 \pi \rho \omega_p{}^2}{d^2 \sin(\pi\rho/2)}$$

where d is the interplanar distance between the adjacent phthalocyanines, ρ the electron density per site. Concerning $NiPc(AsF_6)_{0.5}$, the width of π-band $4t$ was estimated to be 1.35 eV. As regards $CoPc(AsF_6)_{0.5}$, the width of π-band $4t$ was estimated to be 1.45 eV, and d-band to be 0.56 eV. In the case of $CoPc(AsF_6)_{0.5}$, however, this calculation may not necessarily be suitable because of the semiconducting property of $CoPc(AsF_6)_{0.5}$ at room temperature. The calculation was carried out neglecting the effect of on-site Coulomb. The calculated value is a rough guide to estimate the d-contribution. In a real system, the half filled d-band must produce a gap according to the one-dimensional Hubbard model. As a result, the Fermi level will not be equal between d-band and π-band. This result will be a rough estimation of the bandwidth of π and d-bands, although $CoPc(AsF_6)_{0.5}$ is actually a non-metal.

The above idea that there is some interaction between d-electrons is confirmed by the reflectance spectra of the mixed crystals, which exhibit very similar spectra to $NiPc(AsF_6)_{0.5}$. In the mixed crystals, the Co^{2+} chain is interrupted by Ni^{2+} through the introduction of NiPc, thereby 1D band formed through the interaction between neighboring Co^{2+} is destroyed. The mid-infrared absorption is probably ascribable to the charge-transfer type optical transition between the neighboring Co $3d_z{}^2$ orbital. This

optical transition contributes to the enhancement of the plasma frequency in $CoPc(AsF_6)_{0.5}$, but it is not observable in the mixed crystals.

The calculated plasma frequency and band width were summarized in Table 1 compared with the band width calculated by spin susceptibility and thermoelectric power. The spin susceptibility decreases when the band width (t) is wide and increases when the correlation between electrons (U) becomes strong. Generally, the optical band width is wider than the one calculated by the spin susceptibility because of the high excitation energy of the measurement. This fact fits in well with the results.

(b) Vibrational investigation

$NiPc(AsF_6)_{0.5}$ undergoes a metal-insulator transition around 40 K. Very recently we found an anomaly in the heat capacity at the same temperature. This result suggests a possibility of some structural change around 40 K. The vibrational spectroscopy gives some information about the structural change, for example, the vibronic mode is very sensitive to the lattice dimerization, so it has been used as a probe of small lattice dimerization. Figure 5 and Figure 6 are the temperature dependence of the reflectance spectrum of $NiPc(AsF_6)_{0.5}$ and $CoPc(AsF_6)_{0.5}$, respectively. The plasma edge becomes sharp on decreasing temperature suggesting the elongation of the relaxation time. Temperature-dependent $\sigma(\omega)$ of //*c* polarization in the vibrational range was shown in Figure 7 - Figure 8. The evolution of the vibronic (a_{1g}) modes was not clearly observed even at 10 K. The possible candidates of the vibronic modes were the 1132 cm^{-1} and 1325 cm^{-1} peaks which exhibited a dispersion-like line shape and became clearer below 50 K. However, the intensity was much weaker than usual organic conductors. The

prominent peaks at 710 cm^{-1} and 729 cm^{-1} were enlarged at low temperature. Probably these peaks were the stretching modes of AsF_6^-. This assignment was confirmed from the strong bands near this region in the $\perp c$ spectrum. Another one was the broad band at 800 cm^{-1}. Since the line shape is not dispersion-like or dip even in this region, this band is probably assigned to the out-of-plane mode of phthalocyanine. The very similar vibrational feature was observed in $CoPc(AsF_6)_{0.5}$ which was in an insulating state already at room temperature. All these observation suggested that the metal-insulator transition of $NiPc(AsF_6)_{0.5}$ accompanied extremely small or no lattice dimerization along the *c*-axis although the heat capacity experiment suggests a possibility of some structural change. The low-temperature X-ray diffraction study will be able to solve this problem. The preliminary datum of low-temperature X-ray study indicates the possibility of some kind of structural change around the metal-insulator transition temperature such as a torsion of the phthalocyanine molecular "gear" in the *a, b*-plane accompanying the change of crystal system from orthorhombic to monoclinic. Consequently, these structural change will not directly influence on the electronic state of the one-dimensional chain.

Figure 9 and Figure 10 show the conductivity spectrum of $NiPc(AsF_6)_{0.5}$ and $CoPc(AsF_6)_{0.5}$ perpendicular to *c*-axis compared with absorbance spectrum of each salt. The plasma frequency of these vibrational mode were calculated and summarized in Table 2 and Table 3. Figure 11 and Figure 12 show the temperature dependence of the vibronic mode of AsF_6^- of each salt. The large broad peak at 700 cm^{-1} was assigned to the ν_3 vibration of the AsF_6^- ion. As shown in this figure, this vibrational mode split into three bands on decreasing the temperature in the both salts.

4-1-4 Summary

We verified the possibility that d-orbital forms a one-dimensional narrow band in $CoPc(AsF_6)_{0.5}$ based on the comparison of the polarized reflectance spectra of $Co_xNi_{1-x}Pc(AsF_6)_{0.5}$ (X = 0, 0.093, 0.25, 0.45, 0.55, 1). The low temperature reflectance spectrum suggests that the extremely small or no lattice dimerization is accompanied by the metal-insulator transition of $NiPc(AsF_6)_{0.5}$.

References

[1] Y. Yonehara and K. Yakushi, *Synth. Met.* **94**, 149 (1998) .

[2] G. Quirion et al., *Phys. Rev. B*, **42**, 2831 (1990).

[3] T. Hiejima and K. Yakushi, *J. Chem. Phys.* **103**, 3950 (1995) .

[4] K. Yakushi, Y. Yonehara, 高圧力の化学と技術 Vol. **6**, 167 (1997).

[5] Y. Tokura, Y. Kaneko, H. Okamoto, S. Tanuma, T. Toda, T. Mitani, and G. Saito, *Mol. Cryst. Liq. Cryst.* **12**, 199 (1985).

[6] K. Yakushi, H. Yamakado, T. Ida, A. Ugawa, K. Awaga, Y. Maruyama, K. Imaeda, and H. Inokuchi, *Synth. Met.* **55-57**,1699-1704 (1993).

[7] T. Ogawa, K. Yonemitu, *proceedings of ICSM '98, in press.*

[8] K. Yakushi, H. Yamakado, M. Yoshitake, N. Kosugi, H. Kuroda, T. Sugano, M. Kinoshita, A. Kawamoto and J. Tanaka, *Bull. Chem. Soc. Jpn.* **62**, 687 (1989).

[9] K. Yakushi, H. Yamakado, M. Yoshitake, N. Kosugi and H. Kuroda, *Synth. Met.* **29**, F95-F102 (1989).

[10] H. Yamakado, T. Ida, A. Ugawa, K. Yakushi, K. Awaga, Y. Maruyama, K. Imaeda and H. Inokuchi, *Synth. Met.* **62**,169-178 (1994).

[11] T. Hiejima, K. Yakushi et al. *Mol. Cryst. Liq. Cryst.* Vol. **296**, pp.255-268 (1997).

[12] B. Welber, P. E. Seiden, P. M. Grant, *Phys. Rev. B* **18**, 2692 (1978).

[13] J. Schramm et al., *J. Am. Chem. Soc.* **102**, 6702 (1980).

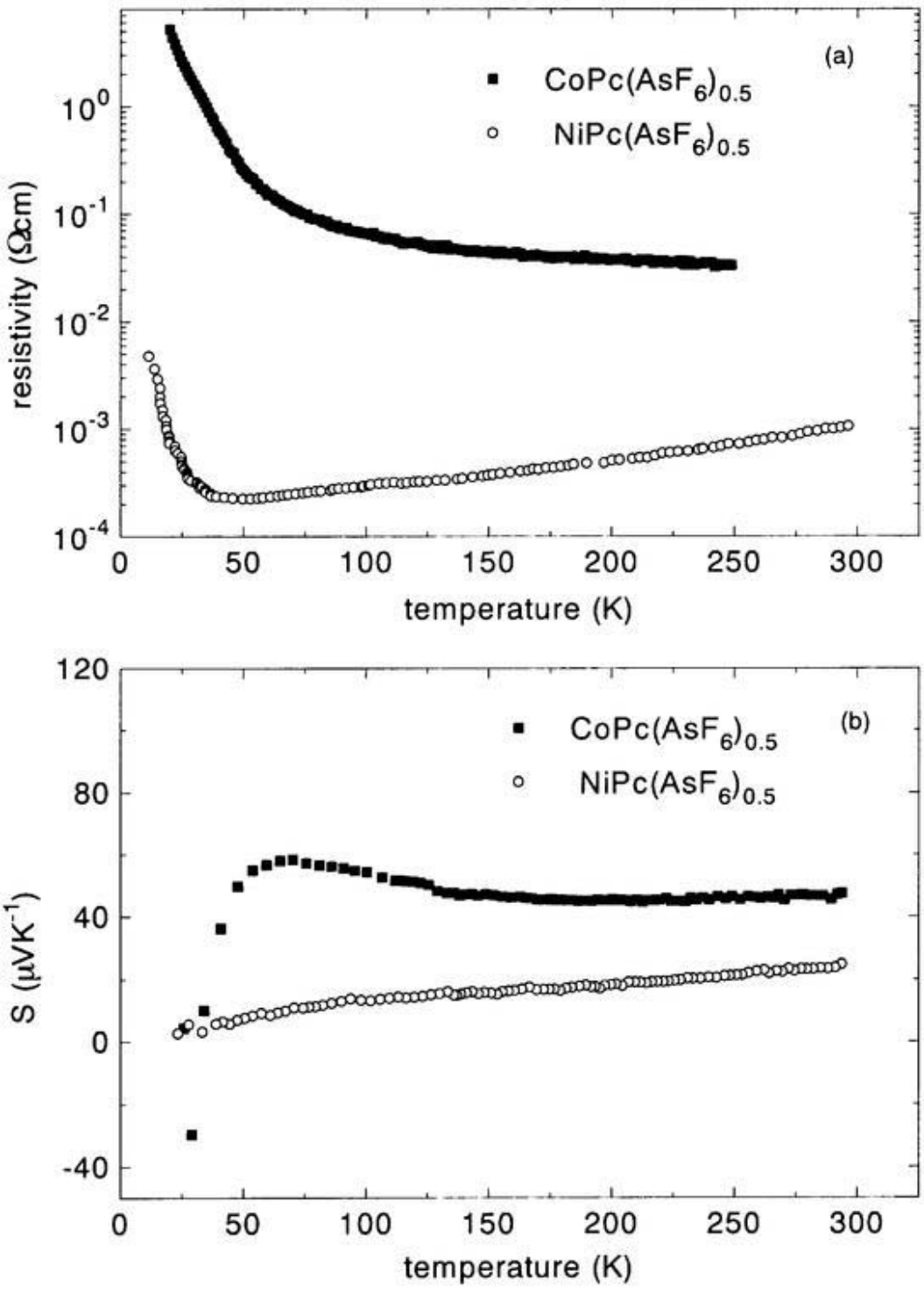

Fig. 1 Microwave resistivity at 9.5 GHz (a) and thermopower (b)

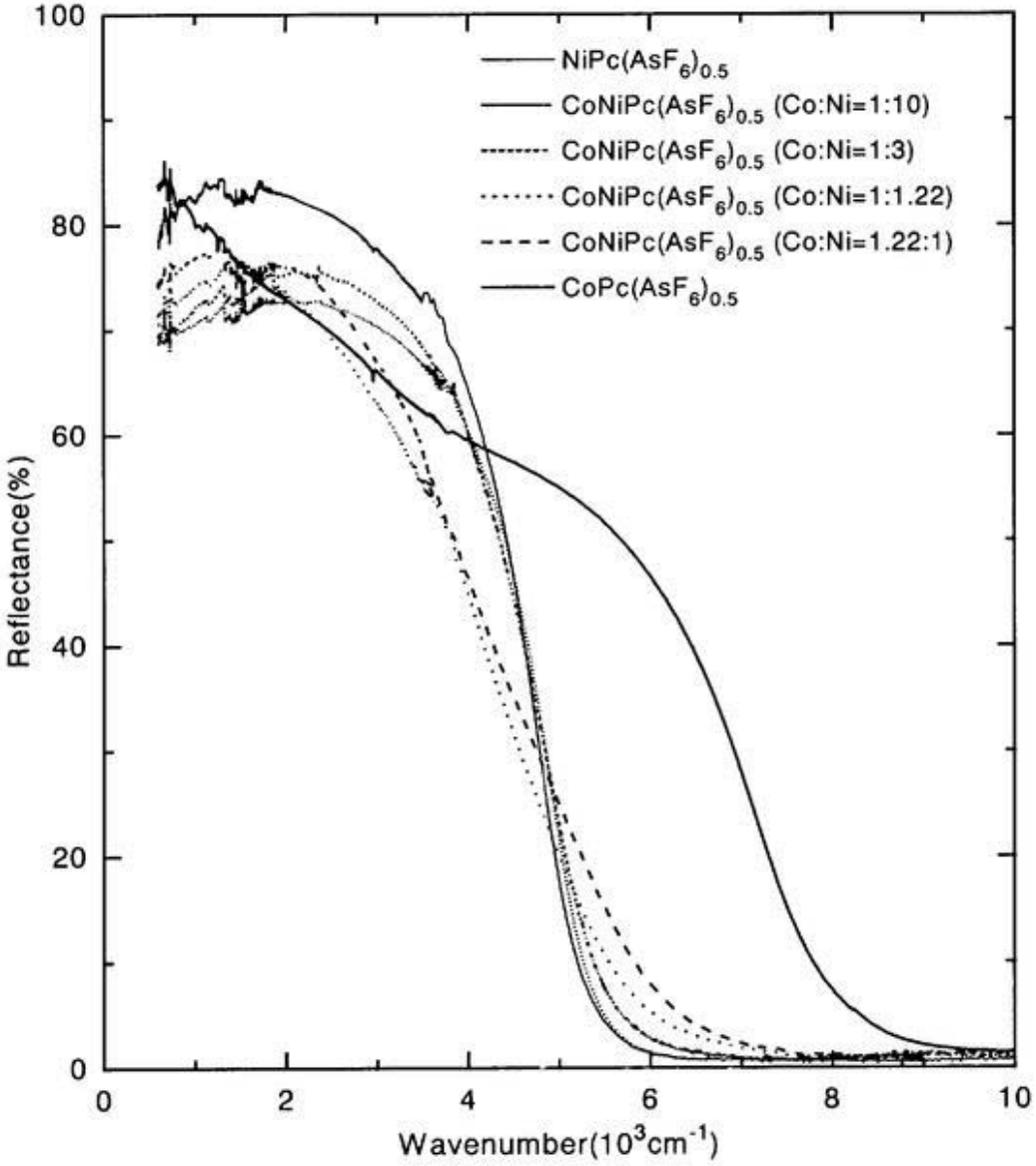

Fig. 2 Reflectance spectrum of mixed crystals

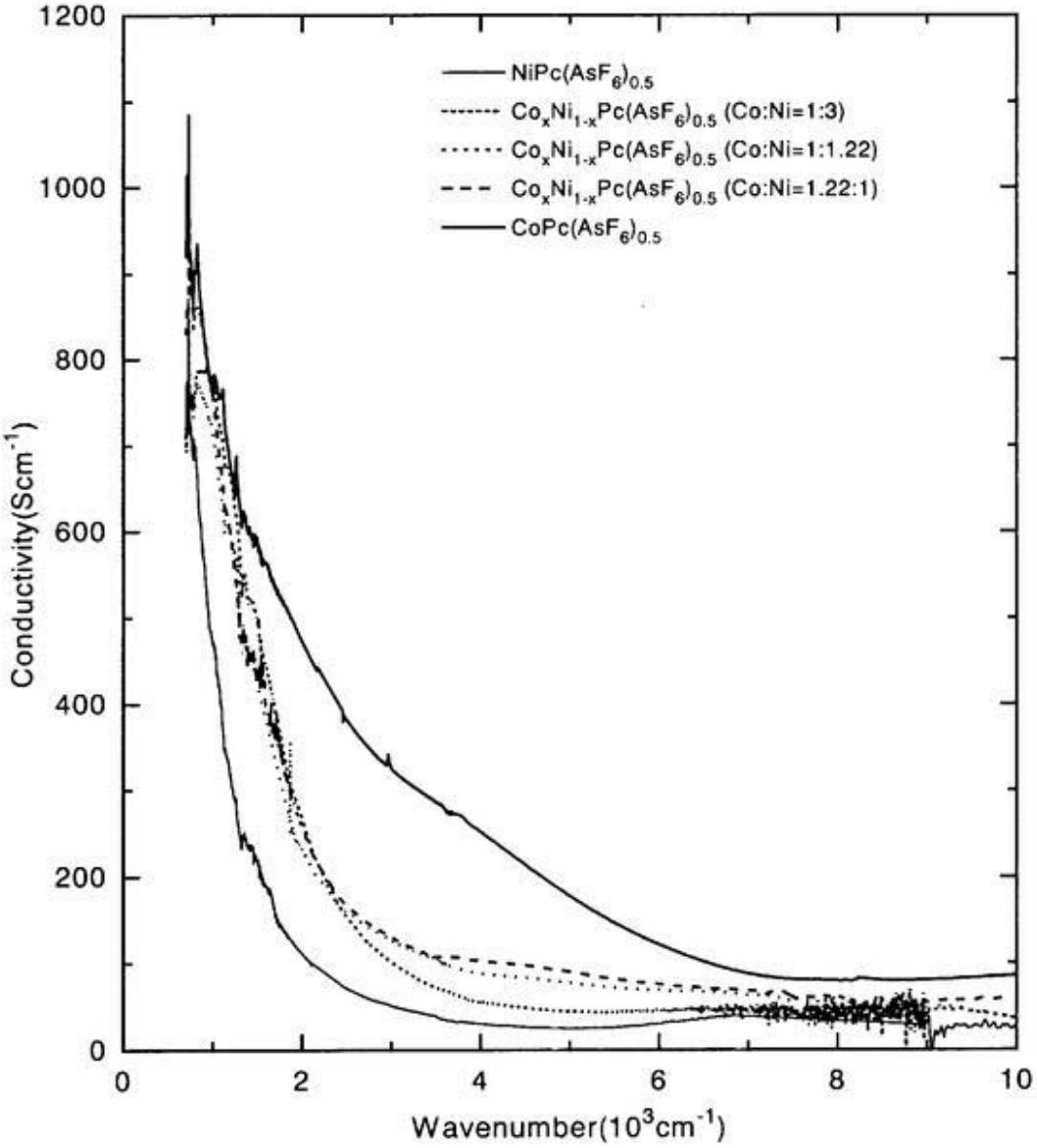

Fig. 3 Conductivity spectrum of mixed crystals

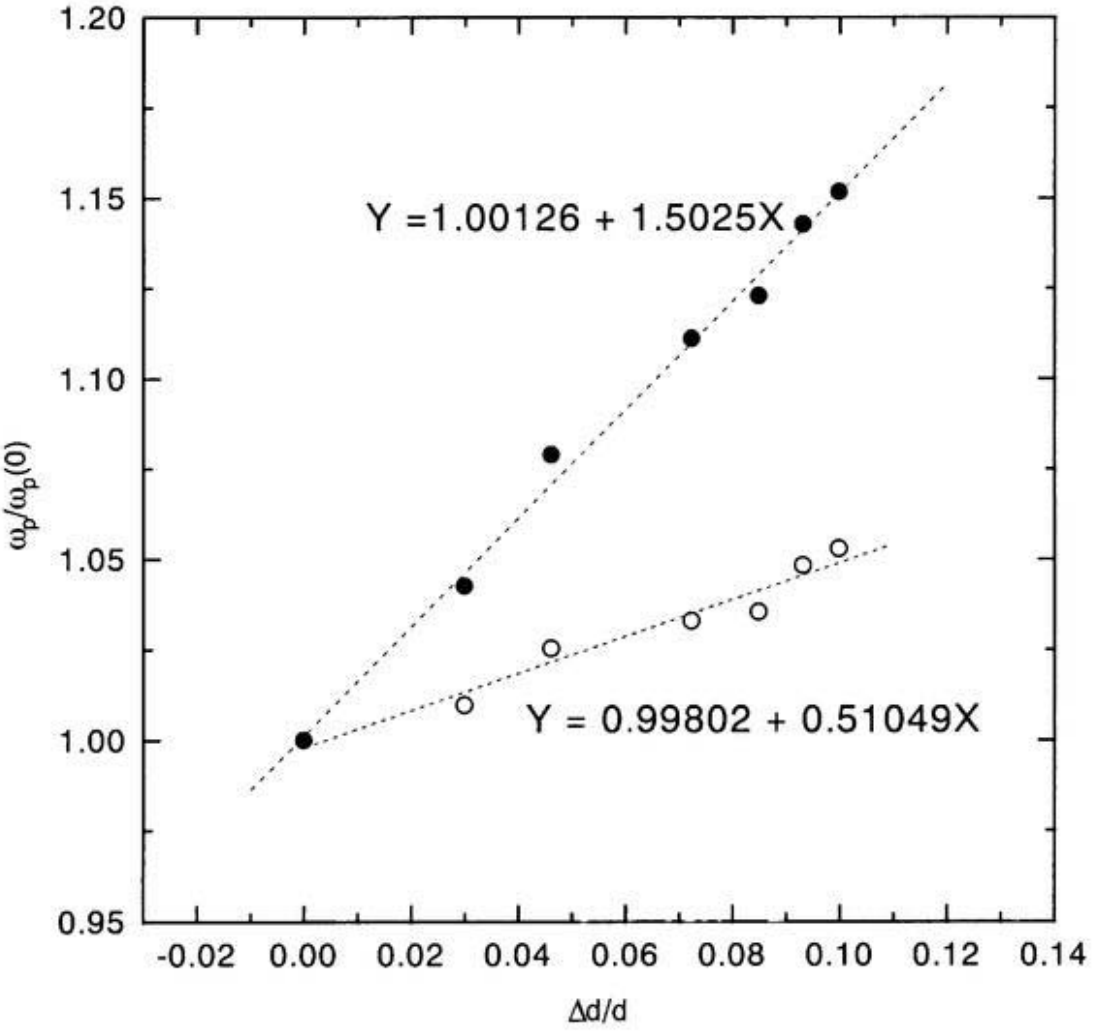

Fig. 4 Plasma frequency(ω_p) as a function of lattice parameter in the c-direction

○ before the correction of the change of dielectric function of pressure medium

● after the correction of the change of dielectric function of pressure medium

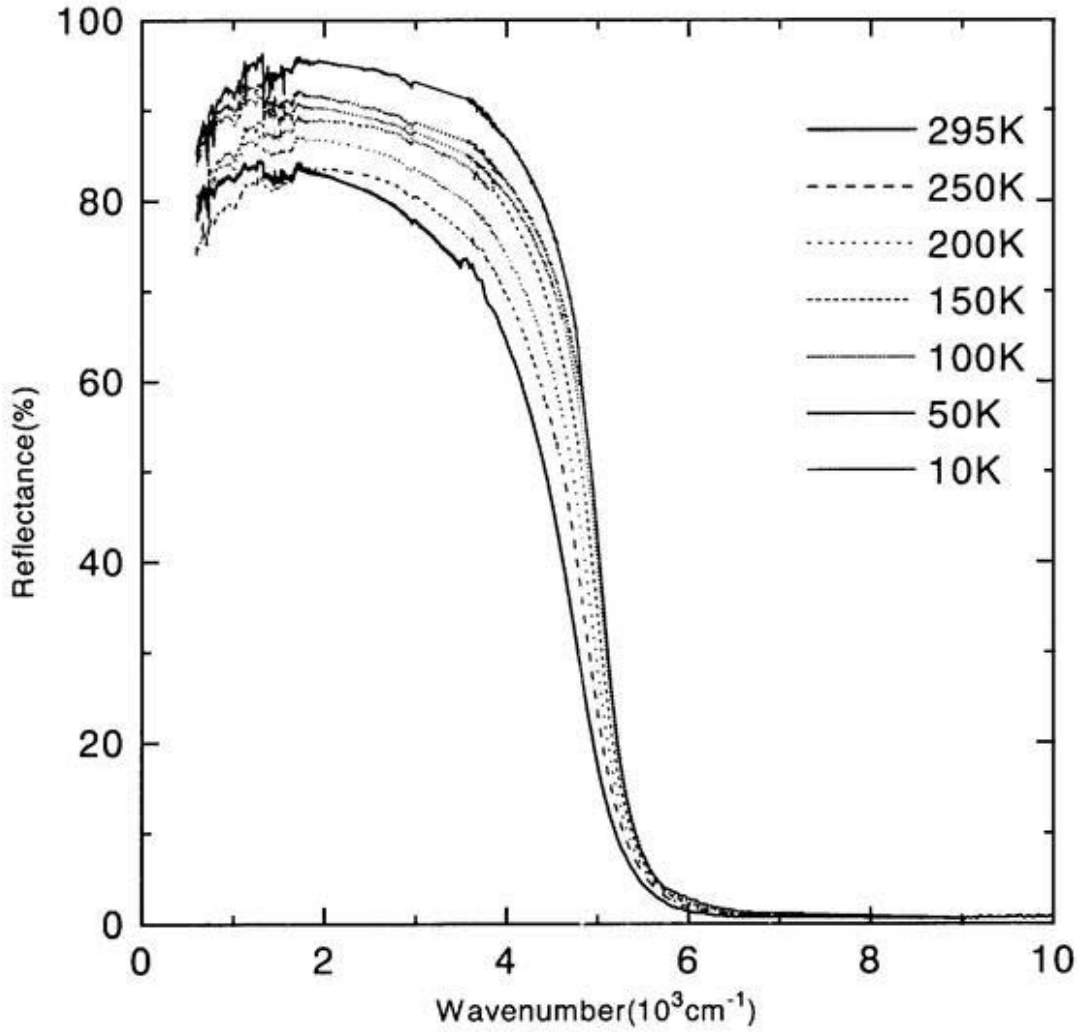

Fig. 5 Temperature dependence of refrectance spectra of $NiPc(AsF_6)_{0.5}$ parallel to c-axis

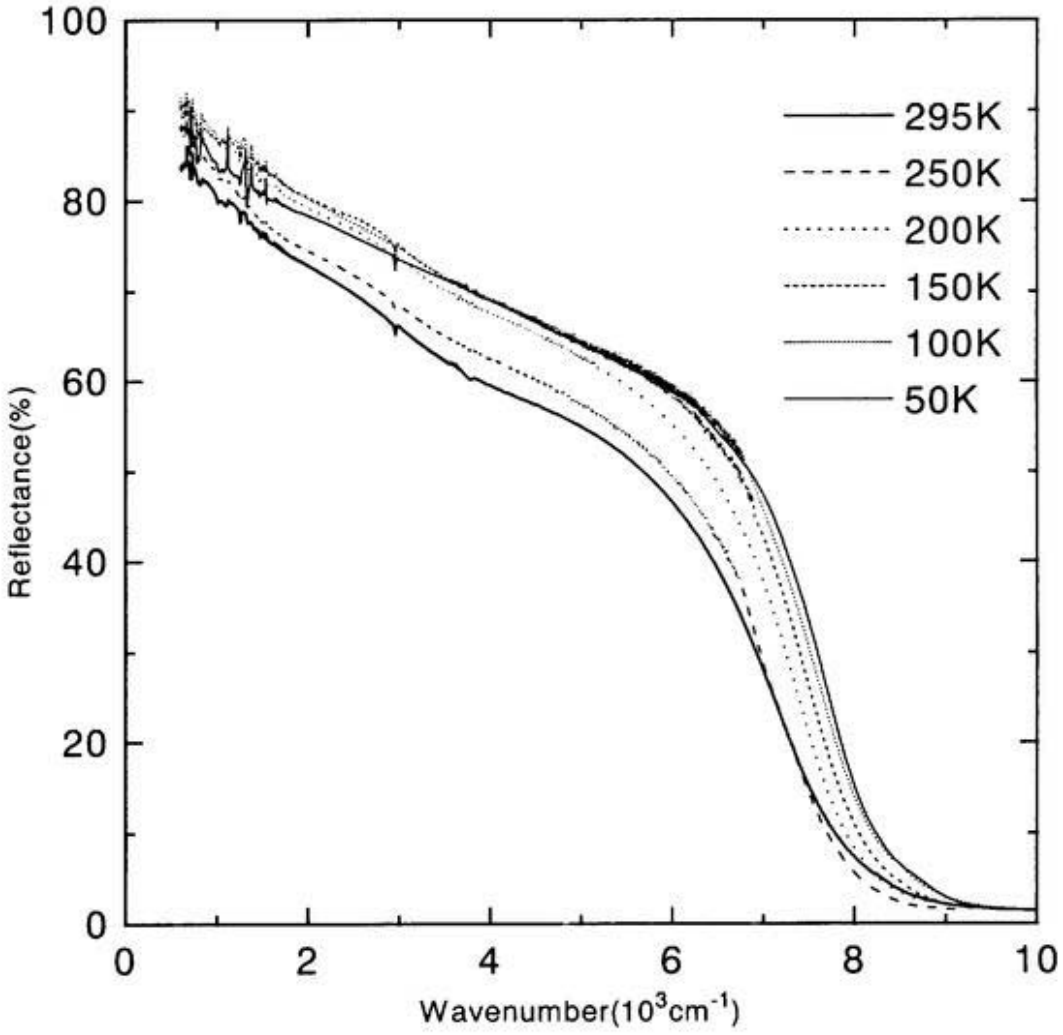

Fig. 6 Temperature dependence of reflectance spectra of $CoPc(AsF_6)_{0.5}$ parallel to c-axis

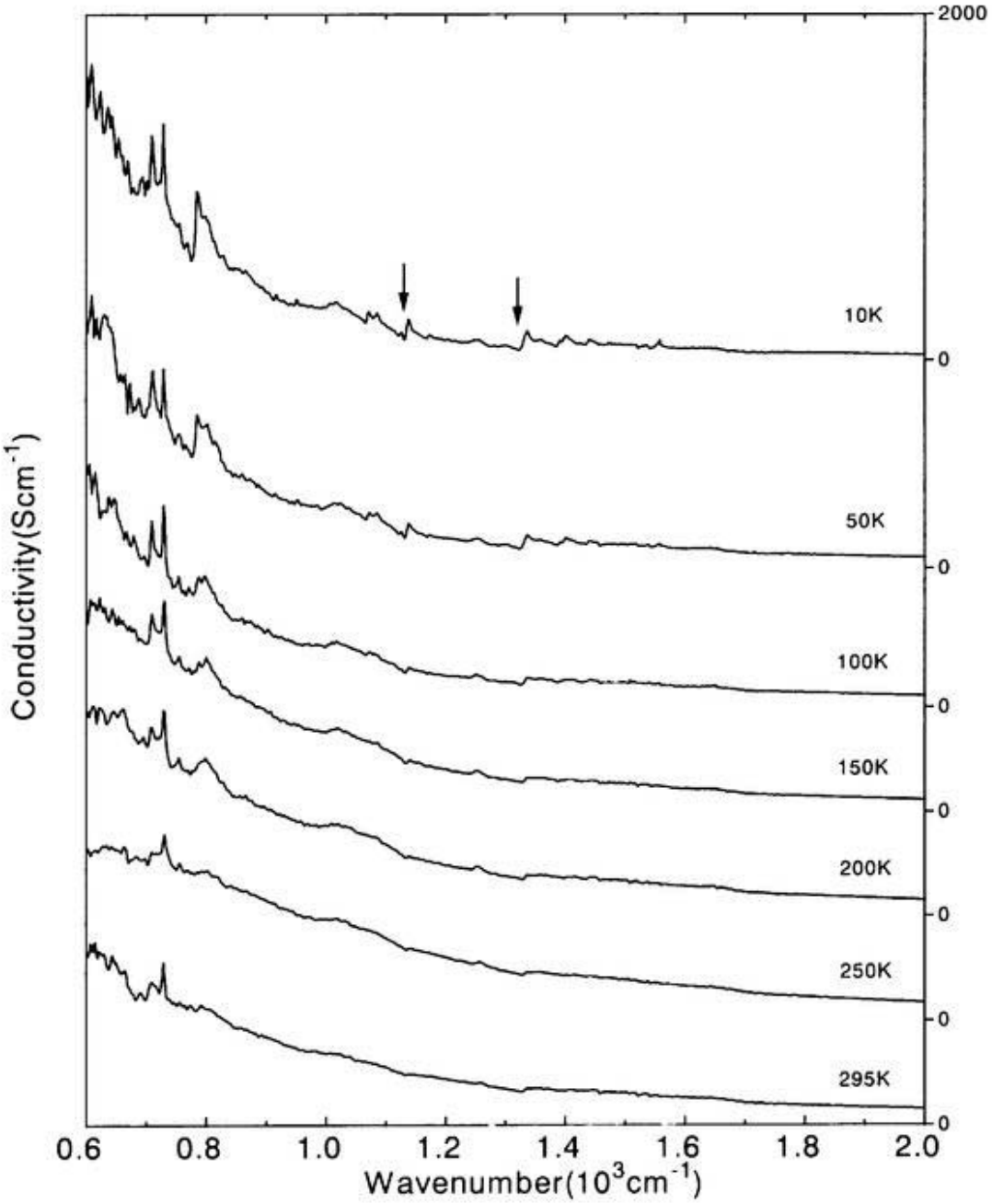

Fig. 7 Temperature dependence of conductivity spectrum of $NiPc(AsF_6)_{0.5}$ parallel to c-axis

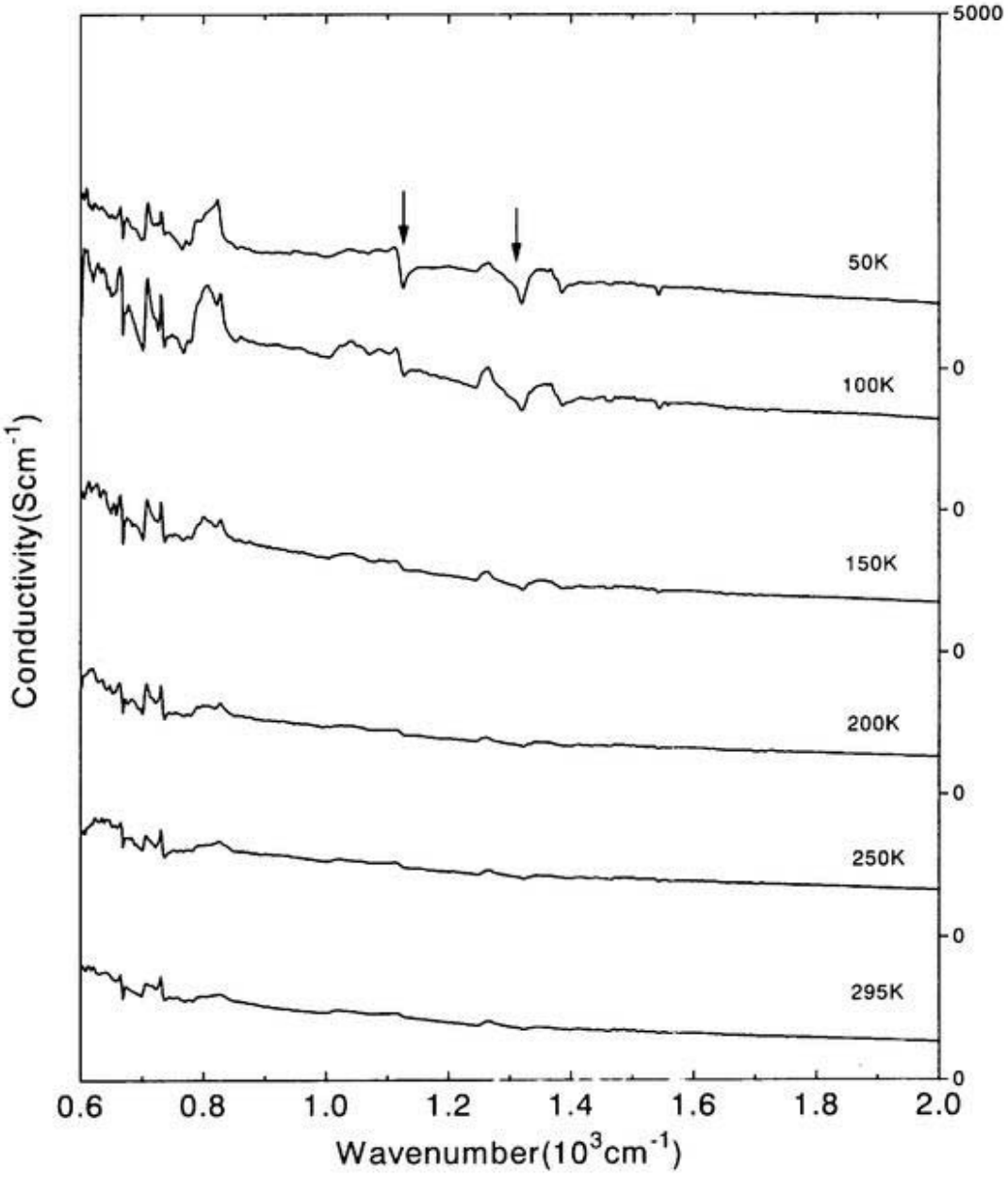

Fig. 8 Temperature dependence of conductivity spectra of $CoPc(AsF_6)_{0.5}$ parallel to c-axis

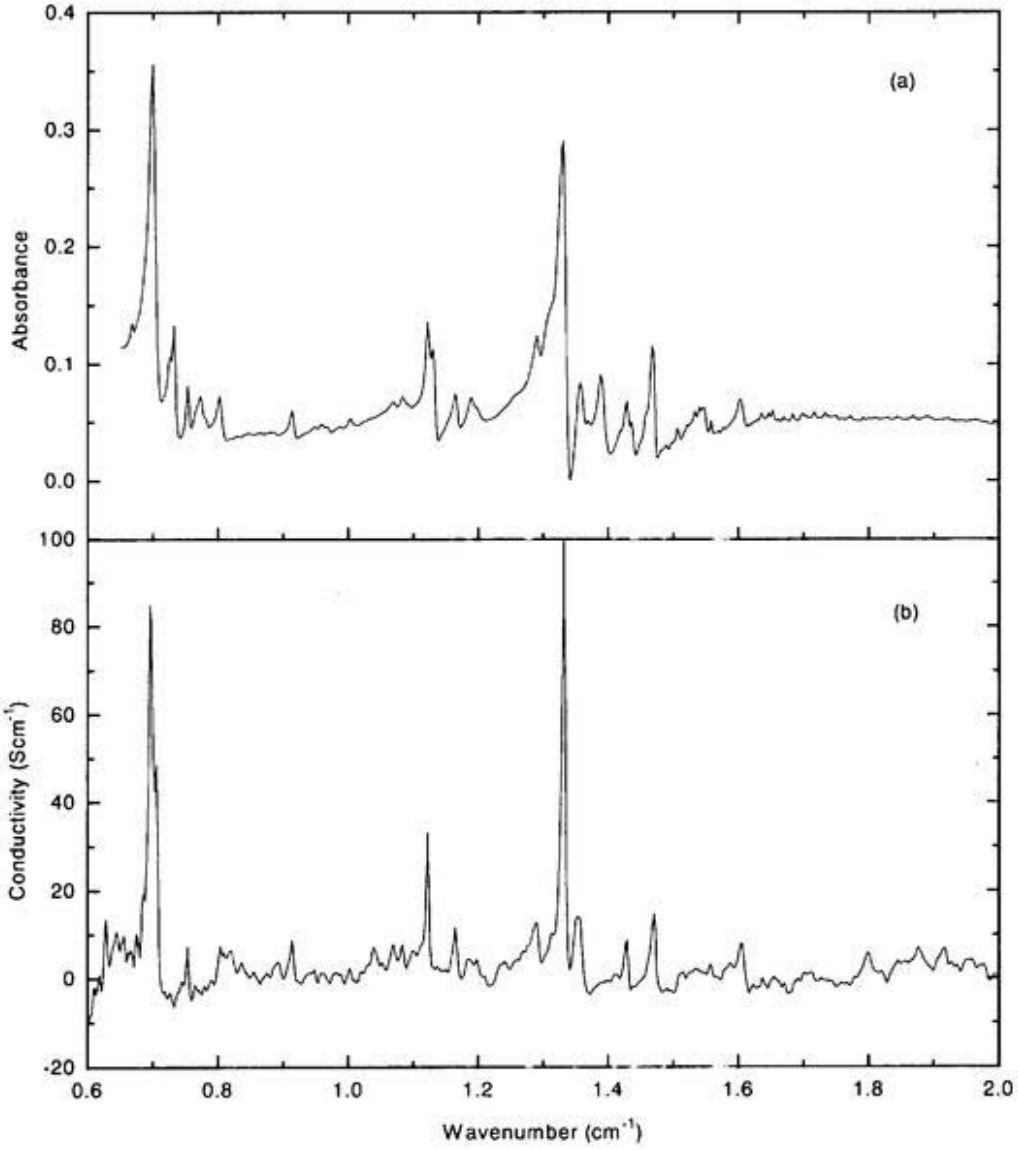

Fig. 9 Absorbance (a) and conductivity (b) spectrum of $NiPc(AsF_6)_{0.5}$

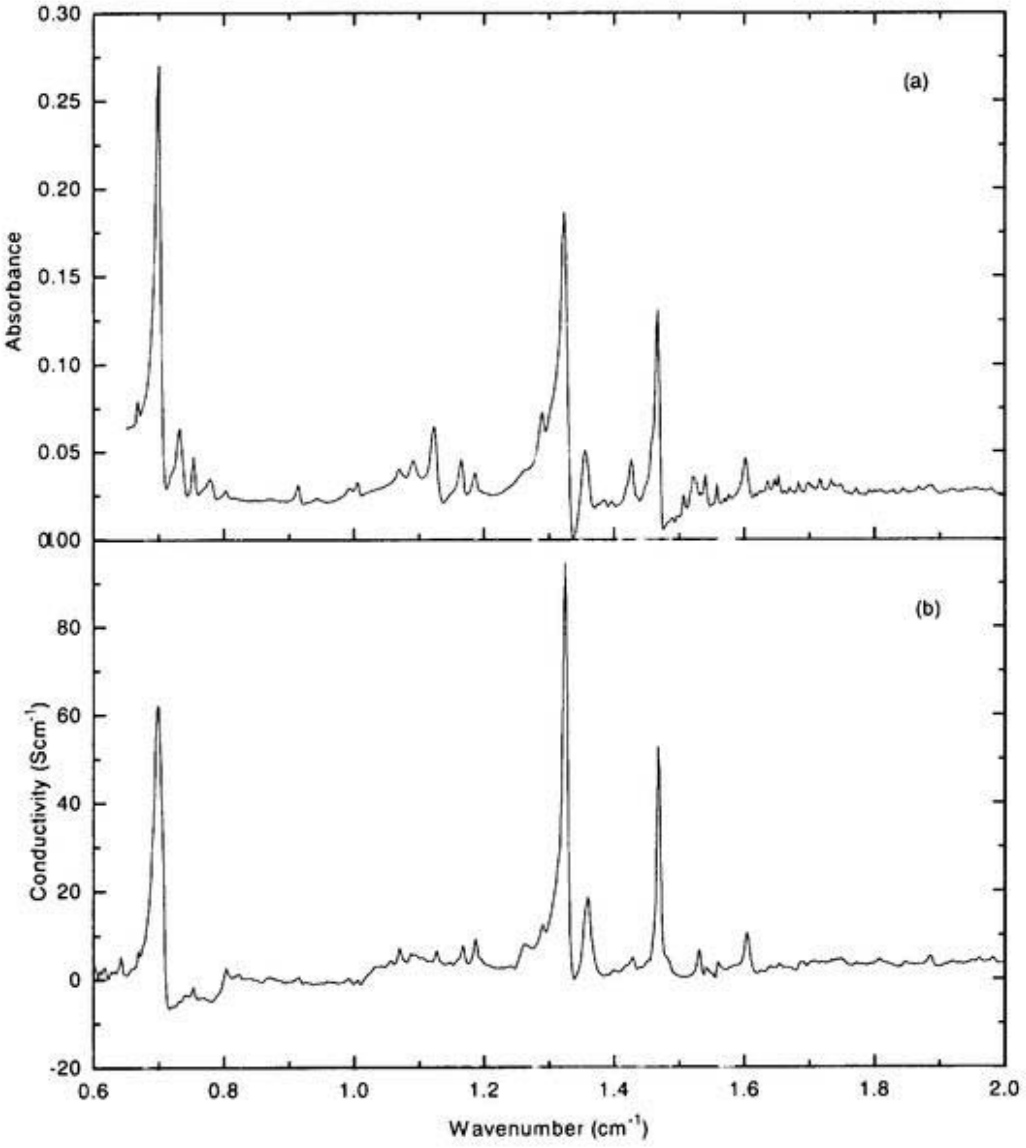

Fig. 10 Absorbance (a) and conductivity (b) spectrum of $CoPc(AsF_6)_{0.5}$

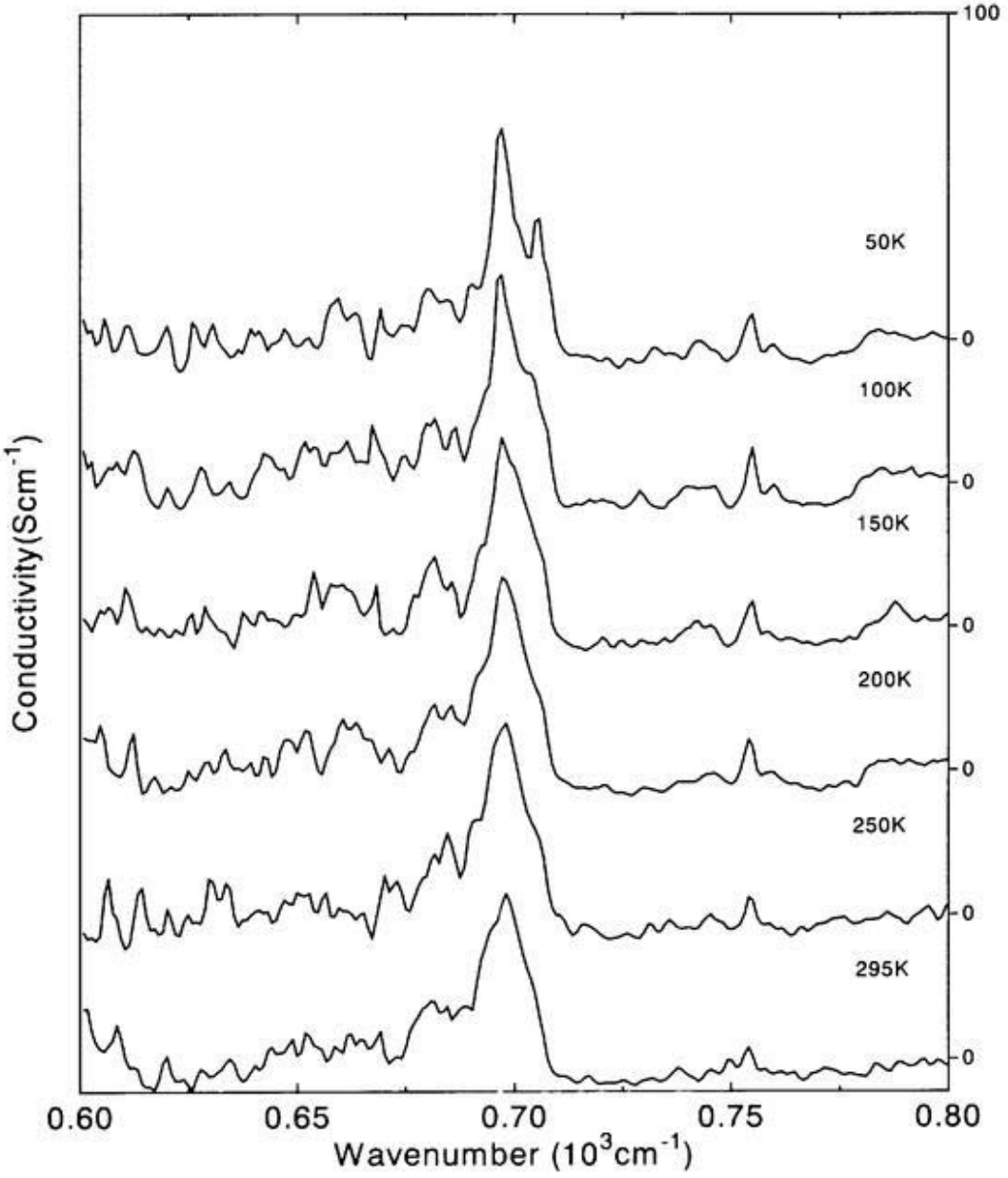

Fig. 11Temperature dependence of conductivity spectra of $NiPc(AsF_6)_{0.5}$ perpendicular to c-axis

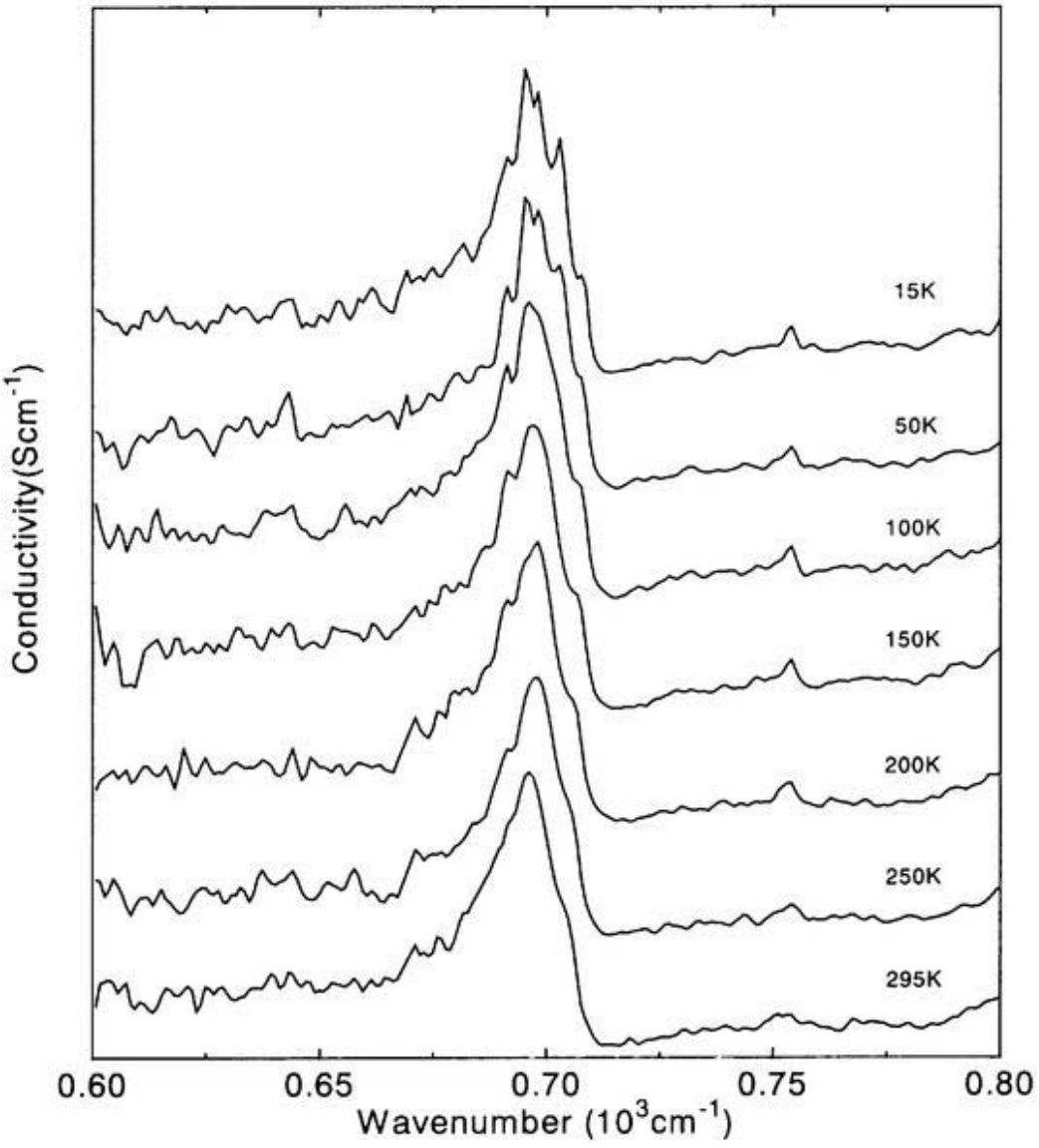

Fig. 12 Temperature dependence of conductivity spectra of $CoPc(AsF_6)_{0.5}$ perpendicular to c-axis

Table. 1 Band width of $NiPc(AsF_6)_{0.5}$ and $CoPc(AsF_6)_{0.5}$

		$\omega_p(cm^{-1})$	m^*/m_e	4t(eV)
$NiPc(AsF_6)_{0.5}$	Kramers-Kronig	7610	1.20	1.35
	0.42GPa	7917	1.18	1.44
	thermopower			1.3[※]
	spin susceptivility			0.9[※]
$CoPc(AsF_6)_{0.}$	Kramers-Kronig	9589	0.76	2.23
	π electron	7718	1.18	1.45
	d electron	5690	4.34	0.56

[※]T. Hiejima, K. Yakushi *et al. Mol. Cryst. Liq. Cryst.*, 1997, Vol. 296, pp.255-268.

Table. 2 Plasma frequency of the vibrational mode of $NiPc(AsF_6)_{0.5}$

Wavenumber (cm^{-1})	ωp (s^{-1})	ωp (cm^{-1})
628.69	7.15961E12	38.00817
644.12	6.85473E12	36.38967
655.69	4.75793E12	25.25836
674.97	2.74873E12	14.59218
696.19	3.77437E13	200.36952
705.83		
754.04	4.88611E12	25.93886
804.18	6.67715E12	35.44692
836.97	4.76537E12	25.29789
892.89	7.03652E12	37.3547
914.1	1.0298E13	54.66912
1039.46	1.15675E13	61.40808
1070.31	6.60401E12	35.05866
1083.81	6.07968E12	32.27513
1101.17	5.3253E12	28.27037
1122.38	1.57065E13	83.3809
1164.81	1.04081E13	55.25363
1186.02	1.02161E13	54.23409
1240.02	7.75758E12	41.1826
1290.16	1.57974E13	83.86361
1332.59	3.41982E13	181.54779
1353.8	1.66088E13	88.17117
1429.01	9.43303E12	50.07706
1471.44	1.49439E13	79.33262
1589.08	5.11128E12	27.1342
1606.43	1.10407E13	58.61158

Table.3 Plasma frequency of the vibrational mode of $CoPc(AsF_6)_{0.5}$

Wavenumber (cm^{-1})	ωp (s^{-1})	ωp (cm^{-1})
642.19	5.23E12	27.8
698.11	3.61E13	191.7
804.18	6.18E12	32.8
871.68	3.62E12	19.2
1070.31	5.06E12	26.9
1087.67	4.18E12	22.2
1126.24	4.74E12	25.2
1166.74	6.63E12	35.2
1187.95	8.90E12	47.2
1290.16	4.83E12	25.6
1324.87	3.71E13	197.2
1359.59	1.95E13	103.5
1400.09	2.73E12	14.5
1429.01	4.29E12	22.8
1467.58	2.52E13	133.9
1531.22	7.39E12	39.2
1542.79	4.29E12	22.8
1604.51	9.46E13	50.2

Part 2

Characterization of the mixed crystals of $NiPc(AsF_6)_{0.5}$ and $CoPc(AsF_6)_{0.5}$

4-2-1 Introduction

Cobalt phthalocyanine charge transfer salts that is one of the subject of our study is novel material because its metal ions form a linear magnetic chain surrounded by the macrocycle chain within the same one-dimensional column. These two chains make up two one-dimensional energy bands. The physics of magnetism in less than three dimensions occupies a significant place because the theory is tractable in contrast to the situation for three dimensions. The spin state of one-dimensional chain can be described by the following spin Hamiltonian,

$$H = J\sum\{\gamma\left(S_x^{\,i}\cdot S_x^{\,i+1} + S_y^{\,i}\cdot S_y^{\,i+1}\right) + S_z^{\,i}\cdot S_z^{\,i+1}\}$$

where, J is the exchange interaction between two spins. In the case that $\gamma = \infty$, it is XY model, $\gamma = 1$; one-dimensional Hisenberg model (Bonner-Fisher type), $0<\gamma<1$; XXZ model, $\gamma = 0$; Ising model.

In present study, alloys between the two porphyrinic molecular compounds non-magnetic $NiPc(AsF_6)_{0.5}$[1] and magnetic $CoPc(AsF_6)_{0.5}$[2] have been prepared and characterized and the magnetic properties were investigated.

There are many reports treating the properties of alloys between the two porphyrinic molecular conductors. Two examples will be given here to recognize the important points in handling these two chain systems related to phthalocyanine; ① phthalocyaninato nickel(Ⅱ) iodine[3] and phthalocyaninato copper(Ⅱ) iodide[4,5] ($Cu_xNi_{1-x}PcI$)[6], and ② phthalocyaninato cobalt iodide[7] and phthalocyaninato nickel iodide ($Co_xNi_{1-x}PcI$).[8] These salts were made up of the combination of three kind of parent crystals (NiPcI, CuPcI, CoPcI) which are isostructural with metal-over-metal columnar

stacks of partially (one-third) oxidized (MPc) units surrounded by chains of I_3^- counterions. However, there are two important differences between these parent crystals.

First, the site of partial oxidation is different between CoPcI and other two salts (NiPcI, CuPcI). Charge transport in CoPcI is remarkably different from that in NiPcI and CuPcI. Both NiPcI and CuPcI are organic conductors whose charge carriers are associated with the highest occupied π molecular orbital of the Pc ring. The conductivity of CoPcI at room temperature is about one-tenth that of NiPcI and is nonmetallic, decreasing continuously on cooling. These differences in charge transport arise because of the difference in the site of partial oxidation. The oxidation in CoPcI is metal-centered, and CoPcI is a metal-spine conductor whose carriers are electrons in a less than half-filled band associated with the cobalt d_z^2 orbital.

Secondly, CoPcI and CuPcI have a magnetic moment on the metal ion in the center of this molecule, whereas NiPcI does not have it. In both salts, the paramagnetic d-chain (Cu^{2+}: d^9, Co^{2+}: d^7) is diluted by introduction of diamagnetic Ni^{2+}. From a magnetic point of view, CuPcI is a novel materials because its Cu^{2+} is paramagnetic and form a linear magnetic chain embedded within a one dimensional "Fermi sea" of organic charge carriers because the site of partial oxidation is Pc ring.[2] In the case of CoPcI, although it has unpaired electron, such kind of interaction between d- and π-electrons does not exist because of the difference of the oxidation site. It is reported that the Cu^{2+} (S = 1/2) local moments of $Cu_xNi_{1-x}PcI$ remain exchange coupled even when the paramagnetic metal-ion chain incorporated within the MPc stacks is diluted with the diamagnetic Ni^{2+} ions and the Cu magnetization is also coupled to the itinerant π-

electron charge carriers, that is, the copper sites in CuPcI are exchange coupled to one another as well as to the itinerant carriers.[4] Ni^{2+} is diamagnetic and plays no direct role in the electronic or magnetic properties of the crystals. This unusual situation found also in Cu(TATBP)I (TATBP; triazatetrabenzporphyrinato)[8], results in the observation of a new type of low temperature phenomenon characterized by transitions of the coupled local moment - itinerant carrier systems.

When two parent crystals are combined to form a new mixed crystal, these two points have considerable influence with the properties of new crystals.

In our study for $Co_xNi_{1-x}Pc(AsF_6)_{0.5}$, the central chain is insulating but the π-chain makes 3/4-filled band due to the partial doping of holes by AsF_6 and thus metallic. $CoPc(AsF_6)_{0.5}$ has a magnetic moment on the cobalt ion in the center of this molecule, whereas $NiPc(AsF_6)_{0.5}$ does not have it. Consequently in $CoPc(AsF_6)_{0.5}$, itinerant π-electrons and localized unpaired d-electrons coexist. Therefore, interaction of unpaired electrons on Co^{2+} may include direct one between neighboring Co^{2+} site (J_{dd_dir}) , the one coupled to π-electrons ($J_{\pi d}$), and super exchange interaction through π-electrons (J_{dd_ind}) in the same way as CuPcI. As described in Chapter 4 part 1, the properties of parent compounds are very different from each other although both of the parent crystals belong to nearly isostructural system and ligand-centerd oxidation having the same band-filling. $NiPc(AsF_6)_{0.5}$ shows metallic behavior between 295 to 40 K under ambient pressure. $CoPc(AsF_6)_{0.5}$ exhibits nonmetallic behavior even at room temperature. The oxidized site of $CoPc(AsF_6)_{0.5}$ is not metal but Pc-ring unlike CoPcI which also exhibits nonmetallic behavior. Therefore, the origin of the nonmetallic phase of $CoPc(AsF_6)_{0.5}$ may be different from CoPcI. The interaction between unpaired d- and itinerant π-

electrons may play an important role on this nonmetallic property. Judging from the result of the reflectance measurement, d-electrons in the one-dimensional chain seems to have some orbital overlap in the one-dimensional metal chain, that is, there is a charge transfer transition in the one-dimensional d-band. The study of mixed crystals is very significant. It means not only interrupting the interaction between d-electrons to investigate the property of the interaction but also filling in the blanks between both electrical extremities; metallic $NiPc(AsF_6)_{0.5}$ and nonmetallic $CoPc(AsF_6)_{0.5}$.

4-2-2 Experimental

The mixed crystals were electrochemically grown using the mixture NiPc and CoPc which were co-sublimed for the purpose of purification and complete mixing. The sample and positional dependence of the atomic ratio between Co and Ni of the single crystal was measured by means of EPMA using JEOL superprobe 733. The cobal (Nilaco) were used as the standard materials of Co and Ni atoms. EPMA was performed at few points on each crystal by the use of the electron beam of 1μm.

X-ray diffraction data of $Co_xNi_{1-x}Pc(AsF_6)_{0.5}$ (Co : Ni = 1 : 3) were collected at room temperature with a Rigaku AFC-7R. The crystal structures were solved by the Patterson methods (SAPI) and refined by the full-matrix least-squares method using teXan software.[9, 10] X-ray diffraction data of $Co_xNi_{1-x}Pc(AsF_6)_{0.5}$ (Co : Ni = 1 : 1.22) were collected at room temperature with a RAXISII. The crystal structures were solved by the Direct methods (SAPI91) and refined by the full-matrix least-squares method using SHELXS 86 and teXan software. The detailed conditions were summarized in Table 1 and Table 2.

Raman scattering spectrum measurements were made at ambient temperature on mixed crystals of $Co_xNi_{1-x}Pc(AsF_6)_{0.5}$ (X = 0, 0.093, 0.25, 0.45, 0.55, 1). Raman scattering spectrum was measured in back-scattering geometry on a Renishaw Ramascope System-1000 excited by a He-Ne laser with a wavelength of 632.8 nm using the microscope with an object lens, Mitsutoyo M Plan Apo50×. The laser power was decreased by neutral filter down to 0.2 mW and was focused on the 2 μm ϕ area of the single crystal. The incident light is polarized parallel to the *c*-axis and all polarization was collected for the scattered light.

ESR measurements were carried out at X-band on a Bruker ESP-300E, equipped with a cryostat of Oxford Instrument ESR900 combined with the temperature controller ITC4.

The magnetic susceptibility was measured with a SQUID magnetmeter of Quantum Design MPMS-2 and MPMS-7 in the temperature range 2 - 300 K with applied field of 1 T.

4-2-3 Results and discussion

Figure 1 shows the result of EPMA analysis for the four kinds of mixed crystals. Three crystals were investigated for each composition. There was a marked tendency for the cobalt composition of performed crystal. The contents of cobalt of performed crystal is lower than expected one from the starting material except for the Co : Ni = 1 : 10 crystals. This is probably attributable to the lower solubility of CoPc compared with NiPc.

The atomic parameters of $Co_xNi_{1-x}Pc(AsF_6)_{0.5}$ (Co :Ni =1 : 3, Co :Ni =1 : 1.22)

were complied in Table 3 and Table 4. Figure 2 and Figure 3 show side and top views of these mixed crystals. Table 5 shows the lattice constants of the Co : Ni = 1 : 3 and 1 : 1.22 crystals compared with pure $NiPc(AsF_6)_{0.5}$ and $CoPc(AsF_6)_{0.5}$. The oscillation and Weissenberg photographs indicated that the Co : Ni = 1 : 1.22 crystal belonged to the tetragonal system. The intermolecular distance of $NiPc(AsF_6)_{0.5}$ is long in comparison with $CoPc(AsF_6)_{0.5}$. This difference is responsible for the electronic structure of the central metal ion. Ni^{2+} has 8 electrons and forms a low-spin complex by the influence of coordination atoms. Therefore, $NiPc(AsF_6)_{0.5}$ does not have unpaired electron. In comparison with $NiPc(AsF_6)_{0.5}$, $CoPc(AsF_6)_{0.5}$ has unpaired electron on the central Co ion because Co^{2+} has 7 electrons and forms a low-spin complex. Hence, in the case of $CoPc(AsF_6)_{0.5}$, there is exchange interaction between unpaired electrons on the adjacent Co ions. As a result of this interaction, the intermolecular distance of $CoPc(AsF_6)_{0.5}$ becomes shorter than that of $NiPc(AsF_6)_{0.5}$. This tendency is observed in the case of iodine salts and tetrabenzopolphyrin radical salts as shown in Table 6. The adjacent Co ions completely overlap each other along the *c*-axis because of the exchange interaction between unpaired electrons, as a result, $CoPc(AsF_6)_{0.5}$ takes the tetragonal crystal system. The d-orbital of Ni^{2+} in $NiPc(AsF_6)_{0.5}$ is fully occupied. Therefore, the repulsion between fully occupied d-orbital results in the zigzag stacking of Ni ions and thereby the unit cell involves two NiPc columns in NiPc salts giving the orthorhombic crystal structure. The intermolecular distance of the mixed crystals Co : Ni = 1 : 3 and 1 : 1.22 are 3.211 and 3.20 Å, respectively. These are just intermediate between pure $NiPc(AsF_6)_{0.5}$ and $CoPc(AsF_6)_{0.5}$. Moreover, the Co : Ni = 1 : 3 crystal shows a little big intermolecular distance than 1 : 1.22 crystal. This is a quite reasonable result to support

the formation of the mixed crystal.

Fig. 5 and Fig. 6 show the polarized Raman spectra of single crystals of $Co_xNi_{1-x}Pc(AsF_6)_{0.5}$ (X=0, 0.093, 0.25, 0.45, 0.55, 1). In $\perp c$ spectrum of all the mixed crystals, there appear a characteristic band around 1541-1563 cm^{-1} that seems to be an overlapping pattern of pure $NiPc(AsF_6)_{0.5}$ and $CoPc(AsF_6)_{0.5}$. From this spectrum, it is not clear that the resulting crystals are real mixed crystals, that is, there is a possibility that Co and Ni sites of $Co_xNi_{1-x}Pc(AsF_6)_{0.5}$ exist for segregated domains. In //*c* spectrum of mixed crystals, three completely new bands which were not observed in the spectrum of pure $NiPc(AsF_6)_{0.5}$ and $CoPc(AsF_6)_{0.5}$ appeared at 185, 370, and 740 cm^{-1}. The noticeable points are that the new bands were observed only when the polarized direction is parallel to *c*-axis, and the new bands were connected with each other by the relation between fundamental and its overtone. These experimental results suggest that the resonance effect which is related to the transition parallel to *c*-axis occurs. Unfortunately, due to the complexity in the structure of the macrocycle ring, theoretical assignments for the metal-ligand vibration are almost impossible and thus, very few data have been reported so far. Consulting the results of infrared spectra of Pc derivatives, metal dependent gerade bands were observed in this energy region and the band around 300 cm^{-1} and 180 cm^{-1} are attributed to the M-N + in-phase motion of pyrrole and aza groups, and M-N out of-phase motion, respectively as shown in Fig. 7. If we suppose that the gerade intramolecular vibration mode relating to central metal coupled with the charge transfer state which should appear in the //*c* spectrum only when the Ni and Co ions are located in the neighboring position each other as shown in Fig. 7, the appearance of new bands in the //*c* spectrum may be an evidence of the formation of the

mixed crystal. In this experiment, He-Ne laser (638.2 nm) was used for the exciting laser. This energy is correspond to 15802 cm^{-1}, therefore, if the suggestion described above is correct, the charge transfer between Ni and Co ions should observe around 16000 cm^{-1} in the //*c* spectrum. To confirm this suggestion, additional optical research in the visible region will be required.

$CoPc(AsF_6)_{0.5}$ itself does not show any signal because of the strong spin-lattice interaction that is the most important mechanism causing spins to turn over in many solids through the spin-orbit coupling. The spin-orbit coupling is the interaction between the magnetic field produced by the orbital or spatial movement of the electron and the magnetic moment of the electron spin. Another reason of the broadening of the signal is the modulation of the dipolar interaction between spins. The random flipping of neighboring nuclear spins in a dilute paramagnetic crystal gets the spins out of phase with each other and in this way broadens the resonance line. In a more concentrated sample the random flipping of neighboring electron spins causes a stronger broadening. The width of homogeneously broadened lines can be estimated from the uncertainly principle,

$$\Delta E \Delta t \geq \frac{\hbar}{2} \quad \text{or} \quad g\mu_0 \Delta H \Delta t \geq \frac{\hbar}{2}$$

ΔE is the uncertyainty (standard deviation) in our determination of the energy, Δt is the lifetime of the spin state, and ΔH is the line width. This equation says that the longer the electron remains in an energy state, the less is the uncertainty in the energy and therefore in the field at resonance. Consequently the longer the lifetime of the state, the narrower is the resonance line. In contrast to $CoPc(AsF_6)_{0.5}$, $Co_xNi_{1-x}Pc(AsF_6)_{0.5}$ (Co : Ni = 1 : 10)

crystal show a single, rather broad ESR signal whose g-value shows angular dependence. Figure 8 is the ESR spectra of $Co_xNi_{1-x}Pc(AsF_6)_{0.5}$ (Co : Ni = 1 : 10) crystal at 3.5 K. At room temperature, $Co_xNi_{1-x}Pc(AsF_6)_{0.5}$ (Co : Ni = 1 : 10) crystal did not show any signal and a broad signal was observed below *ca.* 160 K. This result is also one of the evidence of the formation of the mixed crystal. It means that the dipolar interaction between Co ions was obstructed by the introduction of diamagnetic Ni ions. The dipolar energy is roughly estimated by the following equation,

$$\Delta E \cong \frac{\mu_1 \mu_2}{r_{12}^{\ 3}}$$

If the Co and Ni sites of $Co_xNi_{1-x}Pc(AsF_6)_{0.5}$ existed in segregated domains, then the narrow signal of pure $NiPc(AsF_6)_{0.5}$ should be observed even at the room temperature. The narrow ESR signal of $NiPc(AsF_6)_{0.5}$ is originated from the $Pc^{\cdot}$ species in the crystal. This result indicates that the two types of MPc (M = Co, Ni) are microscopically dispersed within the $Co_xNi_{1-x}Pc(AsF_6)_{0.5}$. At high values of x, the ESR methods to characterize the microscopic dispersion of Co and Ni sites in $Co_xNi_{1-x}Pc$ is complicated by two competing effects. First, lowering the concentration of paramagnetic spins by the introduction of diamagnetic NiPc molecules tend to narrow the ESR lines as this reduces the dipolar interactions between neighboring Co^{2+} sites. Secondly, the interruption of the one-dimensional CoPc chain by intervening NiPc molecules will reduce the effects of exchange, thereby tending to broaden the ESR line. At lower values of x like Co : Ni = 1 : 10, the situation becomes simpler. The small exchange interaction present within the MPc structure would have no measurable effect upon the ESR and only dipolar broadening effects should be observed. Therefore, in the future, it will be

important to investigate the composition-dependent ESR signal. The signal was fitted well by single Lorentzian function though $Co_xNi_{1-x}Pc(AsF_6)_{0.5}$ is two spins systems Co^{2+} and $Pc^{\cdot}$. The distance between central metal and π-electrons is *ca.* 2 Å. Hence, the strong exchange coupling ($J>>(g_{Co}-g_{\pi})\mu_B H_0$) between the local and carrier spins causes the ESR spectrum of a single crystal of $Co_xNi_{1-x}Pc(AsF_6)_{0.5}$ to show a single resonance.

The angular dependence of the g-value at 3.5 K was shown in Figure 9. The principal values are g//=1.95 and g $\perp$=2.95, where // and $\perp$ denote the geometrical relation between the *c*-axis of the crystal and the static magnetic field. Since the g-factor arises from a mixing of the spin-orbit interaction with the z component of the spin in the external magnetic field it stands to reason that a different g value will obtain depending on whether the external field is along either the molecular x, y, or z axes. In the case of $CoPc(AsF_6)_{0.5}$, the molecular x and y directions is equivalent and only z axis is different because the g tensor for $Co_xNi_{1-x}Pc(AsF_6)_{0.5}$ crystals is axially symmetric with the c-axis corresponding to the unique tensor axis. In addition, the g-value of $CoPc(AsF_6)_{0.5}$ varies with the nature of the ligands. For example, the g-values of Co^{2+} in Cs_3CoCl_5 are g//=2.32 and g $\perp$=2.27[11] and in neutral CoPc are g//=1.92 and g $\perp$=2.90.[12] The relation of the g-values (g// < g $\perp$) of $CoPc(AsF_6)_{0.5}$ means that the unpaired electron at Co ion is located in the $3d_z^2$ orbital. Figure 10 and Figure 11 show the temperature dependence of the signal intensity and g-values, respectively. The detailed study of the signal serves to verify the properties of d-electrons on the Co^{2+} ion. A combination of measurements of ESR and static susceptibility will give much information for the interaction of d-electrons.

The susceptibility of $CoPc(AsF_6)_{0.5}$ is much more suppressed than that of CoPc which conforms the Curie-Weiss law but significantly larger than $NiPc(AsF_6)_{0.5}$ which conforms the Pauli paramagnetism.[13] This means that the antiferromagnetic interaction between molecules are much stronger in $CoPc(AsF_6)_{0.5}$. The Curie-Weiss law is given by following equation, and applicable to the case that there is little interaction between magnetic moments.

$$\chi(T) = \frac{g^2 \mu_B{}^2 N_A \left(\frac{N}{N_A}\right)(S+1)}{3k(T-\theta)} = \frac{C}{T-\theta}$$

The parameters of CoPc are C = 0.661 emu K / mol, θ=-3.27 K.[13] From this Curie constant, S = 1/2 is obtained, using the g-values, g// = 2.00, $g\perp$ = 3.20, which were obtained from ESR experiment.[14] In CoPc crystal, the adjacent molecule is shifted to the direction of the outer nitrogen atom and the Co ions is coordinated by four inner nitrogen atoms within the molecule and two outer nitrogen atoms of adjacent molecules, which is shown by the octahedron. The Co-N distances are 1.91 and 3.18 Å.[15] In $CoPc(AsF_6)_{0.5}$ crystal, on the other hand, molecules are stacked in a metal-over metal stacking mode. The Co ion coordinated by four inner nitrogen atoms within the molecule and two Co ions of adjacent molecules, the distance of which are 1.91 and 3.15 Å.[2] The large antiferromagnetic interaction may be attributed to (1) the direct interaction between Co ions in $CoPc(AsF_6)_{0.5}$ against the indirect interaction through the spin polarization in CoPc or (2) through the unpaid π-electron in $CoPc(AsF_6)_{0.5}$ which has a very large transfer integral (~0.3 eV) between adjacent molecules. A large anisotropy was observed in the magnetic susceptibility of the oriented crystals. The

susceptibilities with H//*c* and H ⊥ *c* constitute of the Curie component and the T-linear component. The susceptibility of $CoPc(AsF_6)_{0.5}$ is able to divide into three components as follows.

$$\chi^{//} = \chi^{//}_{spin} + \chi^{//}_{orbit} + \chi^{//}_{dia}$$

$$\chi^{\perp} = \chi^{\perp}_{spin} + \chi^{\perp}_{orbit} + \chi^{\perp}_{dia}$$

Therefore, before analyzing the data, we have to subtract the diamagnetic susceptibility ($\chi^{//}_{dia}$) coming from orbital diamagnetism which has a large anisotropy estimated from the anisotropic diamagnetic susceptibility of H_2Pc.[16] We have to estimate the orbital paramagnetism ($\chi^{//}_{orbit}$) (Van Vleck paramagnetism) which seems to be large, since a large anisotropy is observed in g-value. Especially, as for T-linear component, we should give the matter serious consideration because of its small value coming from the small amount of sample. Therefore, for the present, we considered the Curie-like component only. We conjecture that the Curie ascribed to $(CoPc)_2^+$ which exist as a lattice defect.[13] The Curie constant was obtained by the least-squares fitting using the function of $\chi(T) = A + B \cdot T + C/T$. The Curie constant of CoPc, $Co_{0.45}Ni_{0.55}Pc(AsF_6)_{0.5}$, $CoPc(AsF_6)_{0.5}$ were 0.661, 0.061, and 0.0051 emuK/mol, respectively. Figure 12 shows the susceptribility of $Co_{0.45}Ni_{0.55}Pc(AsF_6)_{0.5}$. The molar concentration of $(CoPc)_2^+$ species of $CoPc(AsF_6)_{0.5}$ was estimated to be 2.2 %.[13] As compared with this, the molar concentration of the defects of $Co_{0.45}Ni_{0.55}Pc(AsF_6)_{0.5}$ was estimated to be 9.8 % using the g-values obtained by the ESR measurement of $Co_{0.01}Ni_{0.99}Pc(AsF_6)_{0.5}$ (Co : Ni = 1 : 10). Ni ion does not have spins, therefore, one fifths of the Co spins are remaining after introduction of diamagnetic Ni ions. Judging from the amount of introduced Ni ions, it is difficult to think that all spins are offset each other through the direct AF interaction.

Co and Ni ions should be mixed. Hence, the existence of the indirect AF interaction through the π-electron is expected. As mentioned last Chapter, the direct interaction between d-electrons seems to be interrupted by the introduction of Ni ions and the plasma edge shifts to the side of $NiPc(AsF_6)_{0.5}$ itself in spite of the low concentration of the Ni ions. To estimate the degree of indirect interaction through the π-electrons, the exact analysis of the T-linear component will be unavoidable.

References

[1] K. Yakushi, H. Yamakado, M. Yoshitake, N. Kosugi, H. Kuroda, T. Sugano, M. Kinoshita, A. Kawamoto, and J. Tanaka, *Bull. Chem. Soc. Jpn.*, 62, 687 (1989).

[2] H. Yamakado, T. Ida, A. Ugawa, K. Yakushi, K. Awaga, Y. Maruyama, K. Imaeda, and H. Inokuchi, *Synth. Met.* 62, 169(1994).

[3] (a) C. J. Schramm, R.P. Scaringe, D. R. Stokakovic, B. M. Hoffman, J. A. Ibers, and T. J. Marks, *J. Am. Chem. Soc.*, 102, 6702 (1980). (b) J. Martinsen, R. I. Greene, S. M. Palmer, and, B. M. Hoffman, *J. Am. Chem. Soc.*, 105, 677 (1983).

[4] M. Y. Ogawa, J. Martinsen, S. M. Palmer, J. L. Stanton, J. Tanaka, R. L. Greene, B. M. Hoffman, and J. A. Ibers, *J. Am. Chem. Soc.*, 109, 1115 (1987).

[5] Soonchil Lee, M. Yudkowsky, W. P. Halperin, M. Y. Ogawa, and B. M. Hoffman, *Phys. Rev. B*, 35, 5003 (1987).

[6] M. Y. Ogawa, S. M. Palmer, K. Liou, G. Quirion, J. A. Thompson, M. Poirier, B. M. Hoffman, *Phys. Rev. B*, 39, 10682 (1989).

[7] J. Martinsen, J. L. Stanton, R. L. Greene, J. Tanaka, B. M. Hoffman, *J. Am. Chem. Soc.*, 107, 6915 (1985).

[8] K. K. Liou, M. Y. Ogawa, T. P. Newcomb, G. Quirion, M. Poirier, B. M. Hoffman, and J. A. Ibers (unpublished).

[9] G. M. Sheldrick, *Acta Crystallogr., Sect. A*, 46, 467 (1990).

[10] TeXsan Single Crystal Structure Analysis Package, Molecular Structure Corporation, 1985;1992.

[11] K. D. Bowers and J. Owen, *Rept. Prog, Phys.*, 18, 304(1955).

[12] J. F. Gibson, D. J. E. Ingram, and D. Schonland, *Disc. Faraday Soc.*, 26, 72(1958).

[13] K.Yakushi, abstruct of IMS research meeting？（分子研研究会） "Development of Molecular Spinics"(1998).

[14] K. Liou, C. S. Jacobsene, and B. M. Hoffman, *J. Am. Chem. Soc.*, 111, 6616(1989).

[15] G. A. Williams, B. N. Figgis, R. Mason, S. A. Mason, and P. E. Fielding, *J. Chem. Soc. Dalton Trans.*, 1688(1980).

[16] C. G. Barraclough, R. L. Martin, and S. Mitra, *J. Chem. Phys.*, 55, 1426(1971).

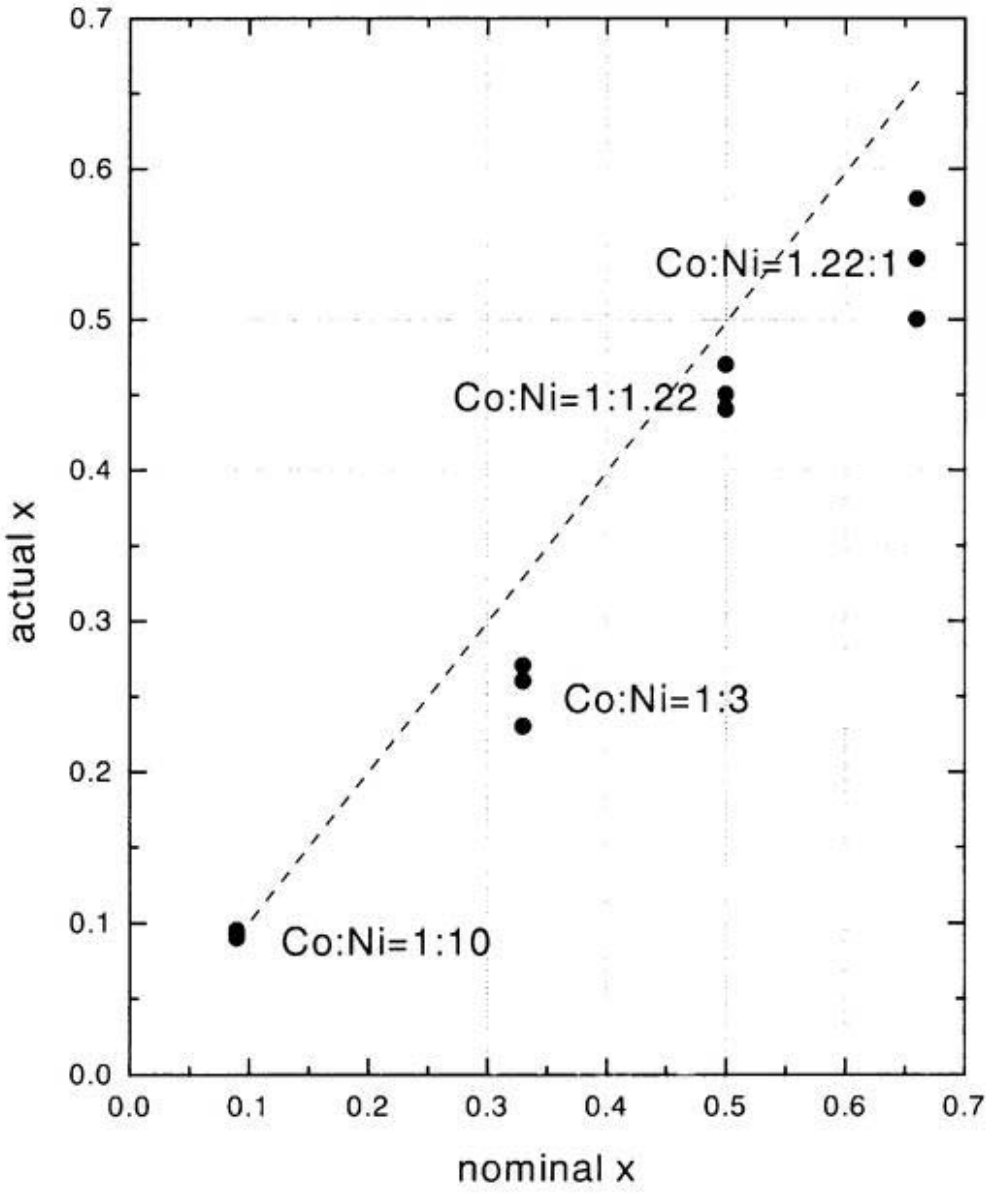

Fig. 1 Compositions of Mixed crystals, $Co_xNi_{1-x}Pc(AsF_6)_{0.5}$

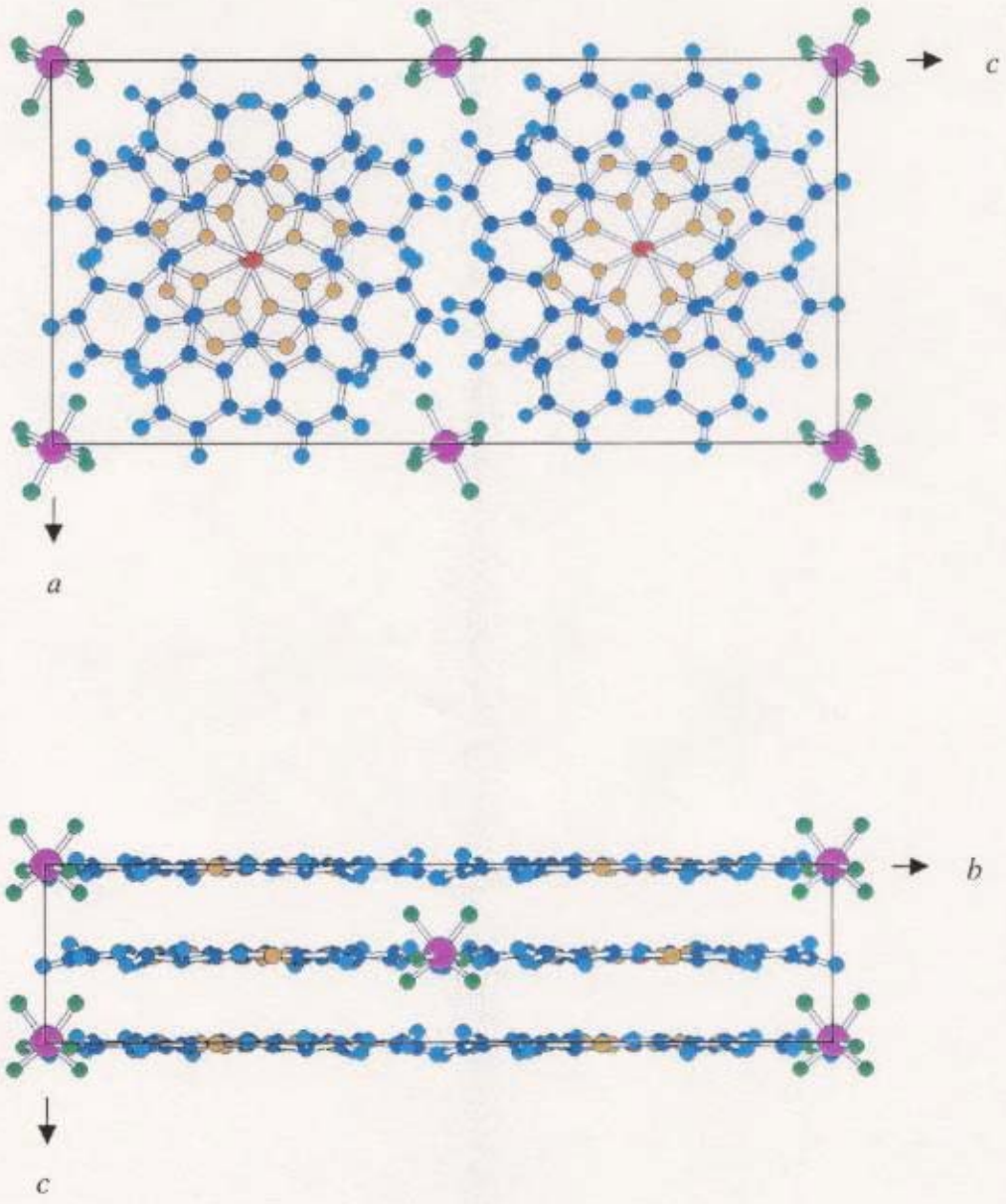

Fig. 2 Crystal structure of $Co_xNi_{1-x}Pc(AsF_6)_{0.5}$ (Co:Ni=1:3)

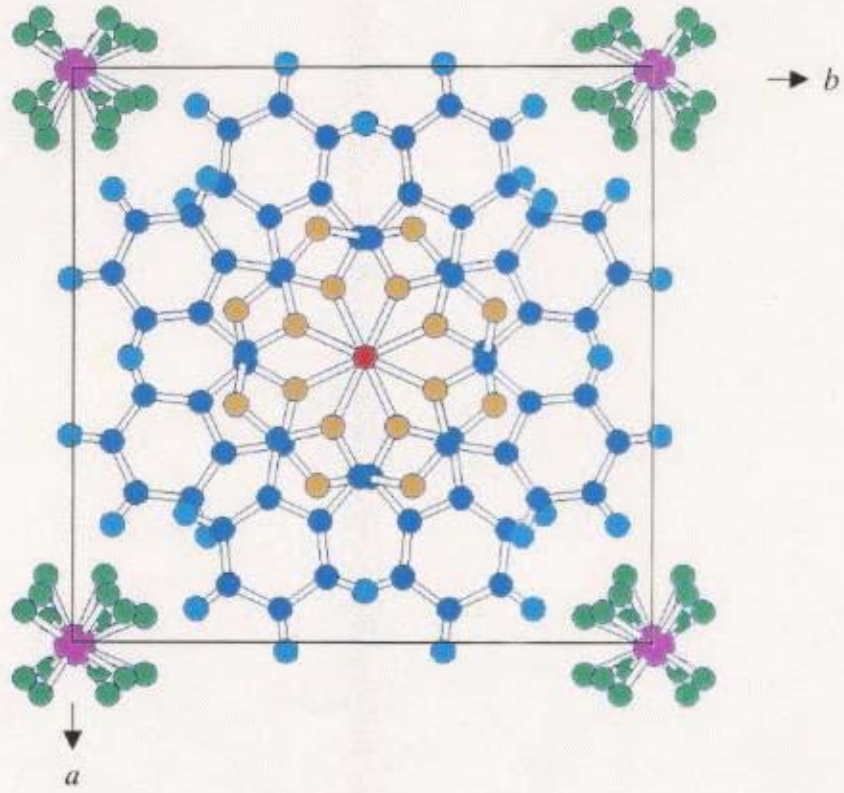

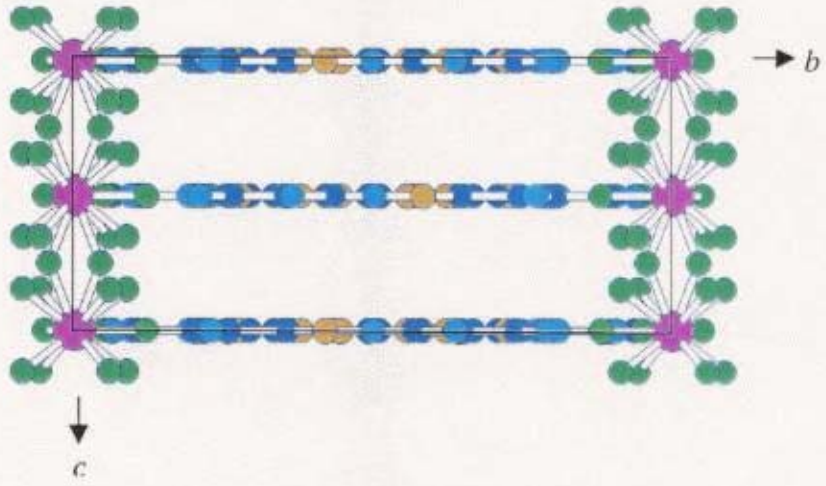

Fig. 3 Crystal structure of $Co_xNi_{1-x}Pc(AsF_6)_{0.5}$ (Co:Ni=1:1.22)

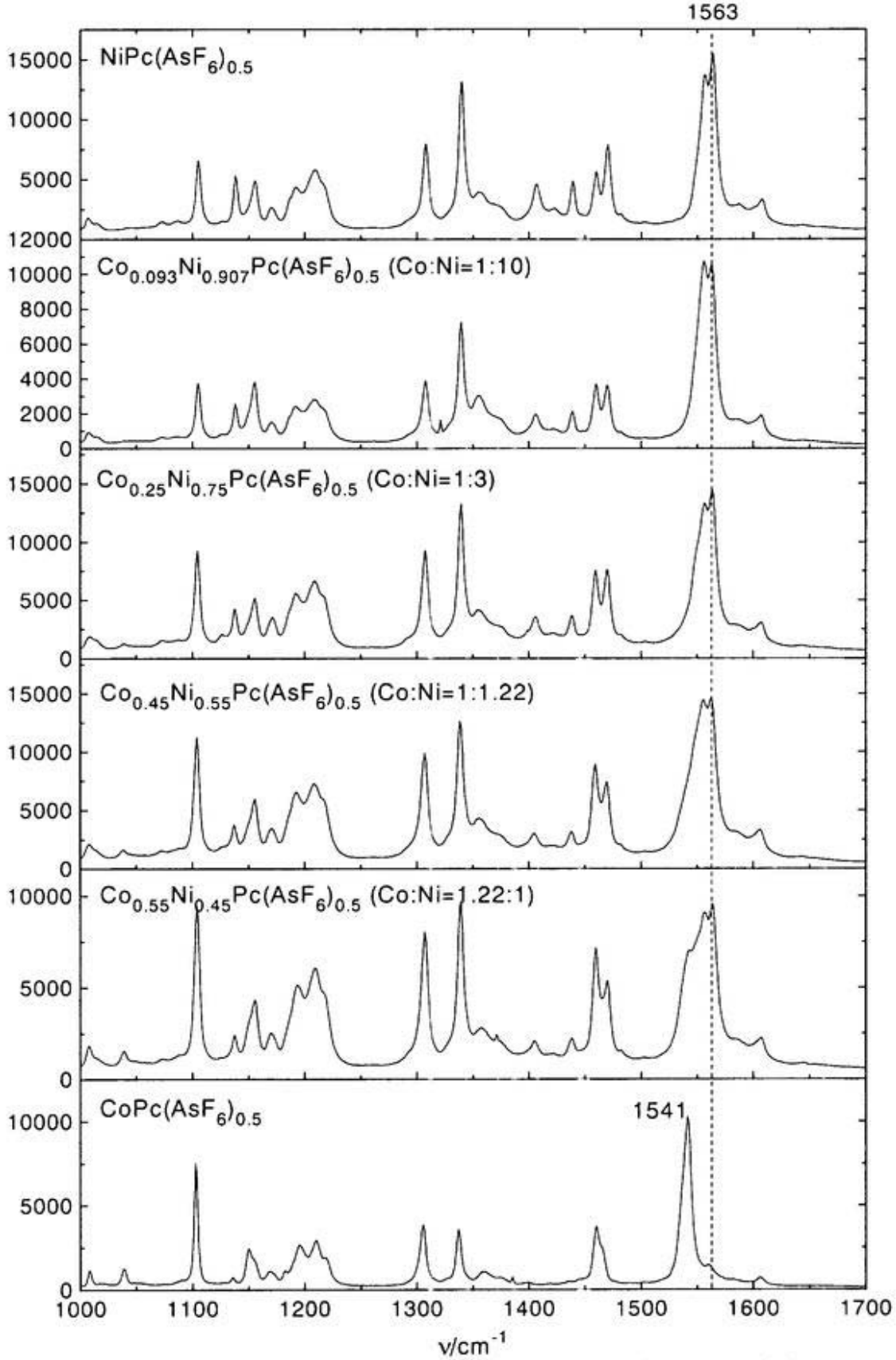

Fig. 4 Raman Spectrum of Mixed Crystals (perpendicural to c-axis)

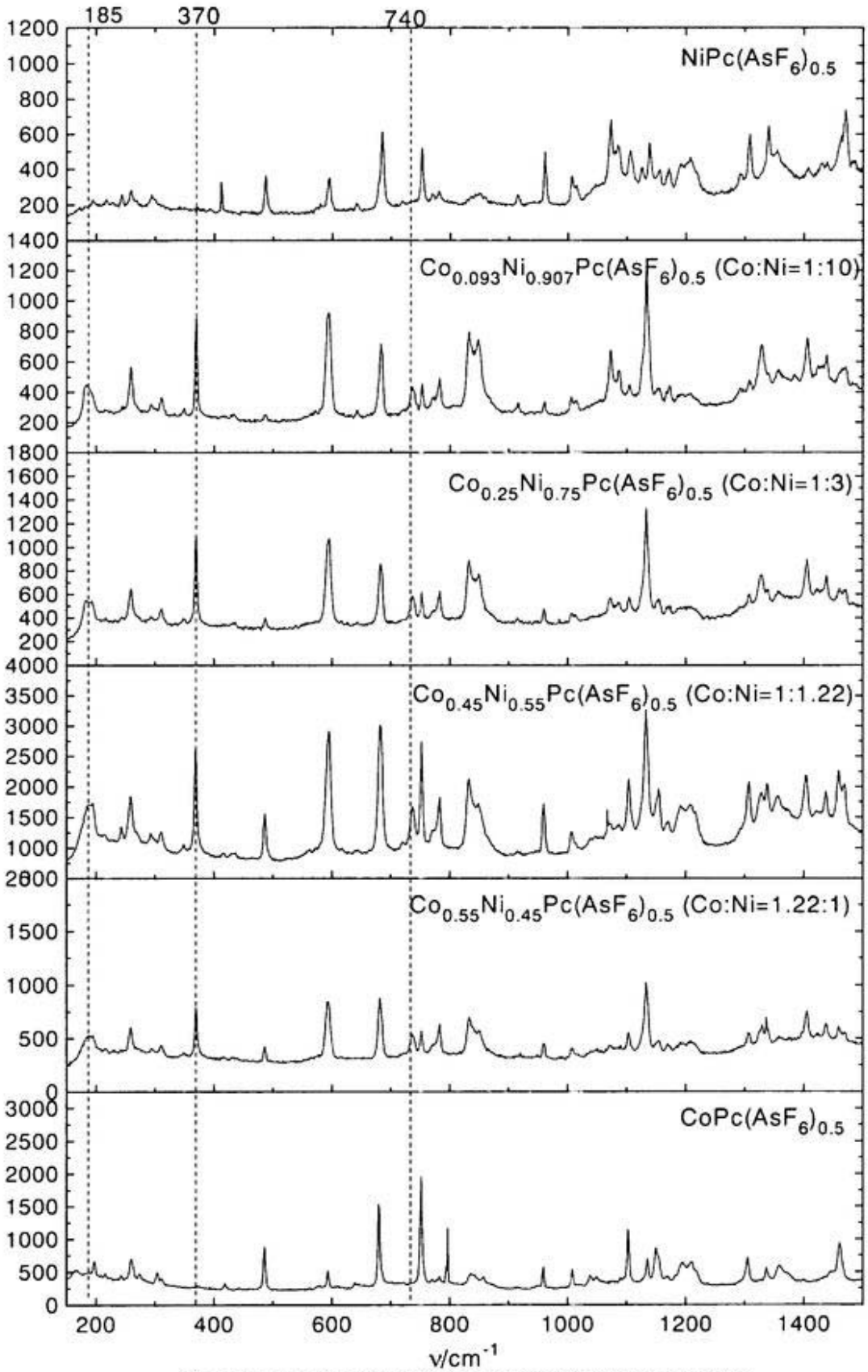

Fig. 5 Raman Spectra of Mixed Crystals (parallel to c-axis)

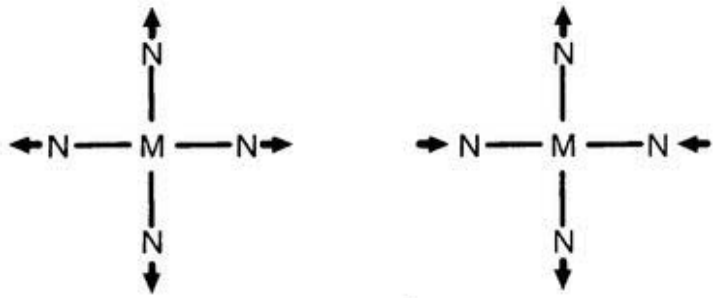

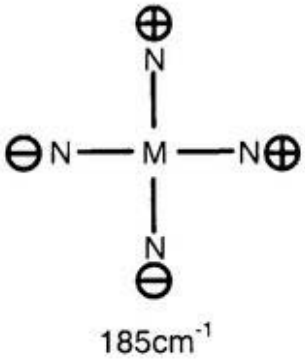

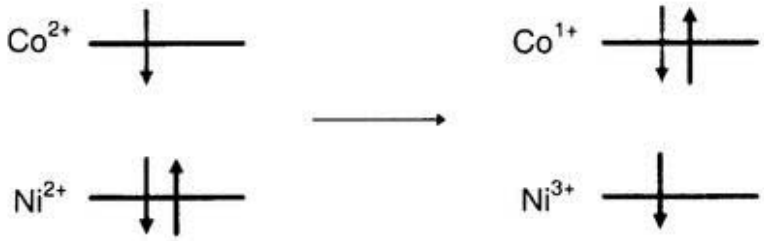

Fig. 6 The gerade modes of in-phase and out-of-phase

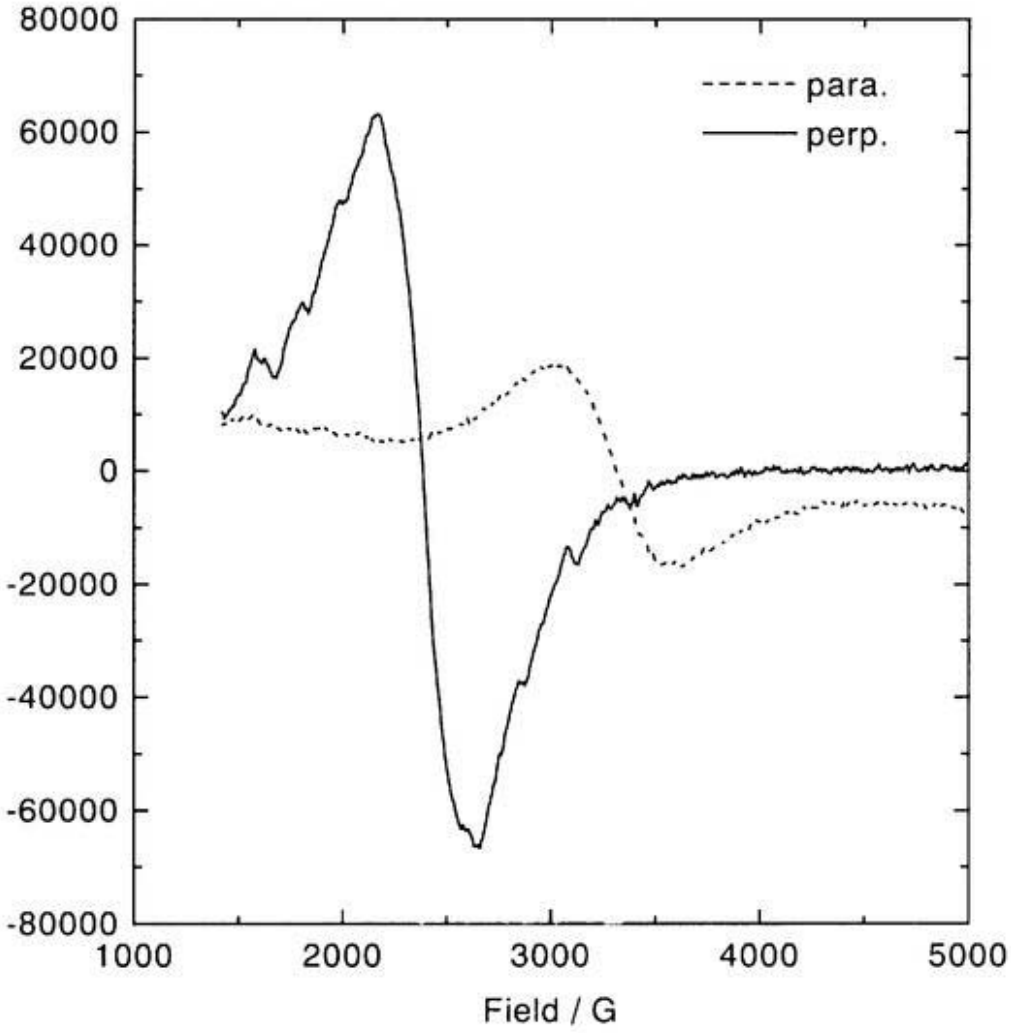

Fig.7 ESR signals of $Co_xNi_{1-x}Pc(AsF_6)_{0.5}$ (Co:Ni=1:10)

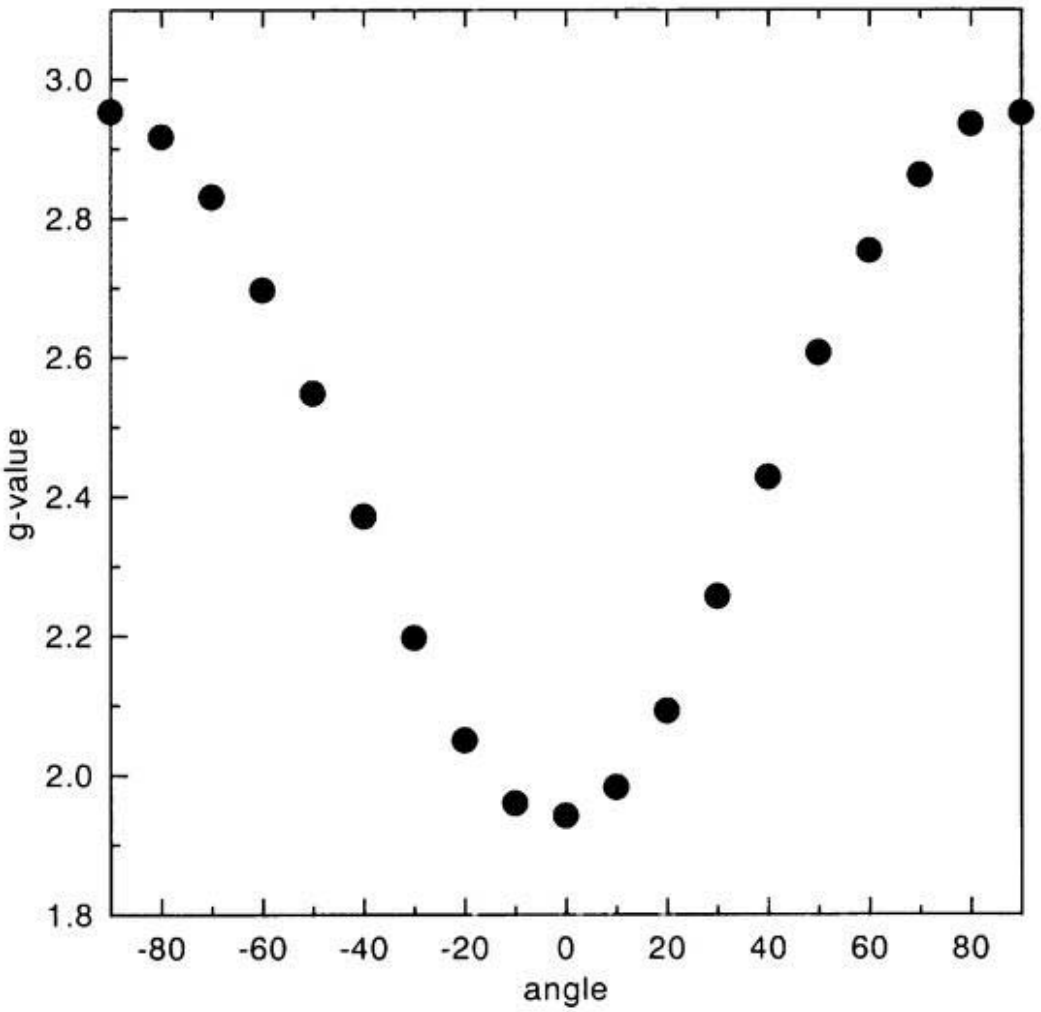

Fig. 8 Angular dependence of the g-value
of $Co_xNi_{1-x}Pc(AsF_6)_{0.5}$ (Co:Ni=1:10) at 3.5K

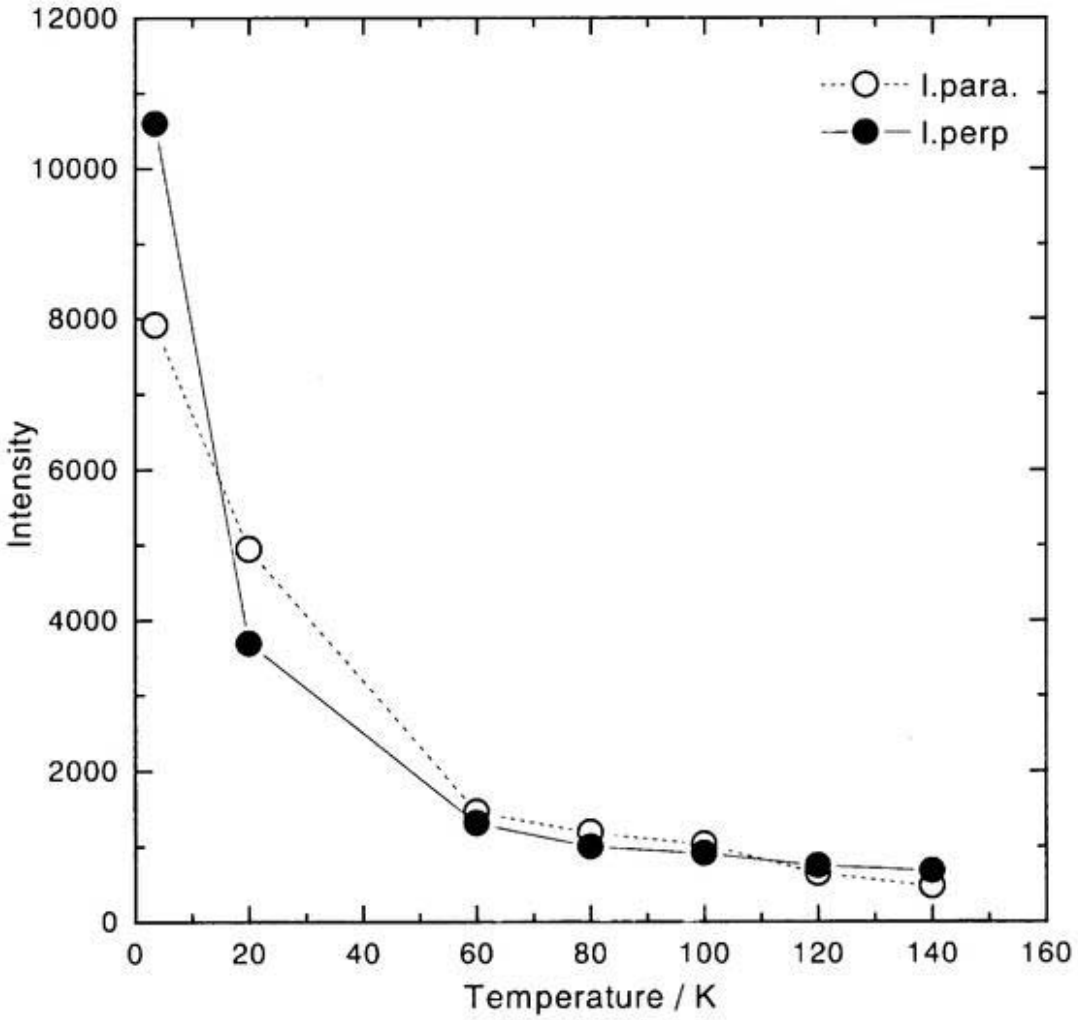

Fig. 9 The temperature dependence of the intensity of the ESR signals

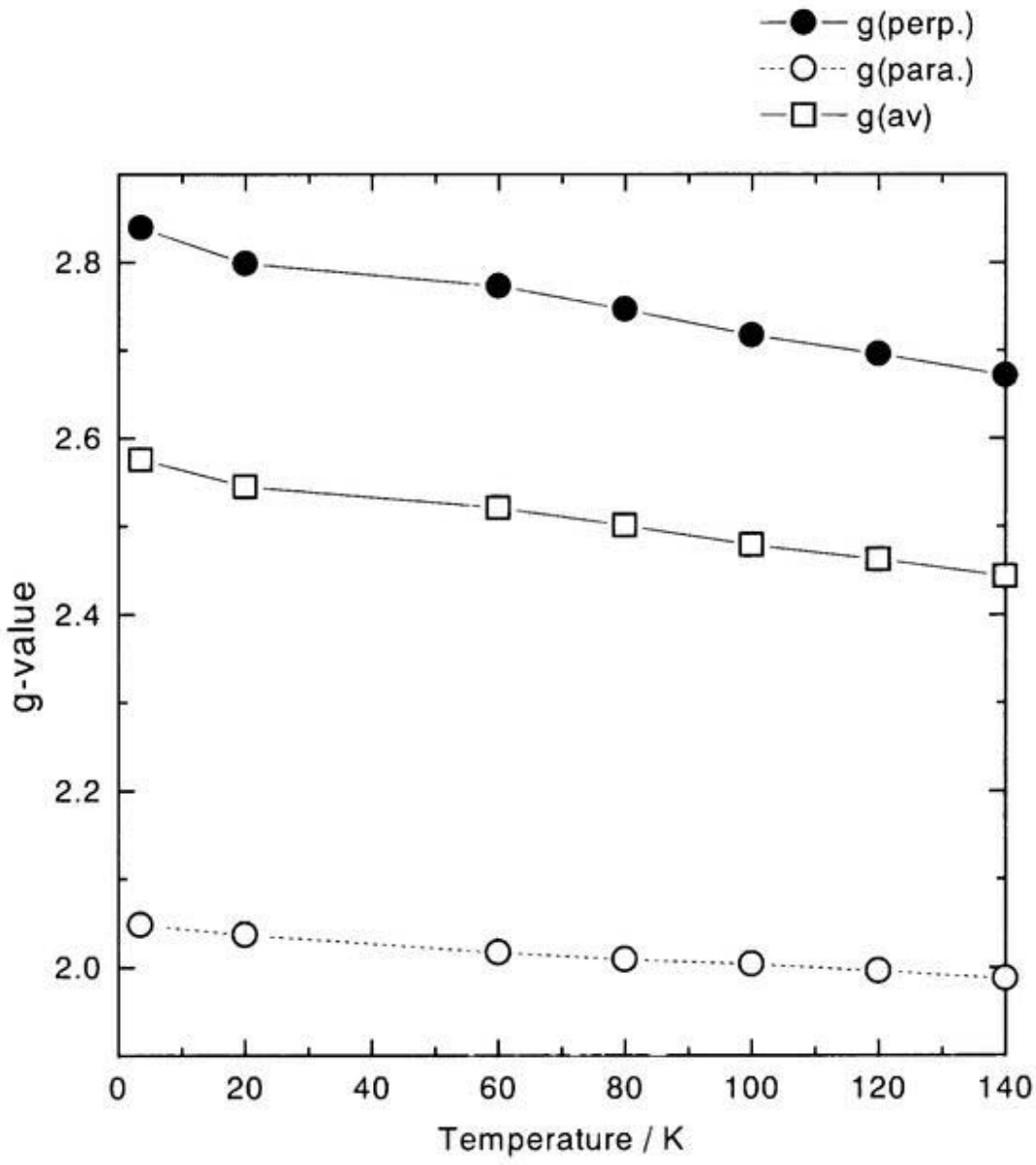

Fig. 10 Temperature dependence of g-value for $Co_xNi_{1-x}Pc(AsF_6)_{0.5}$ (Co:Ni=1:10)

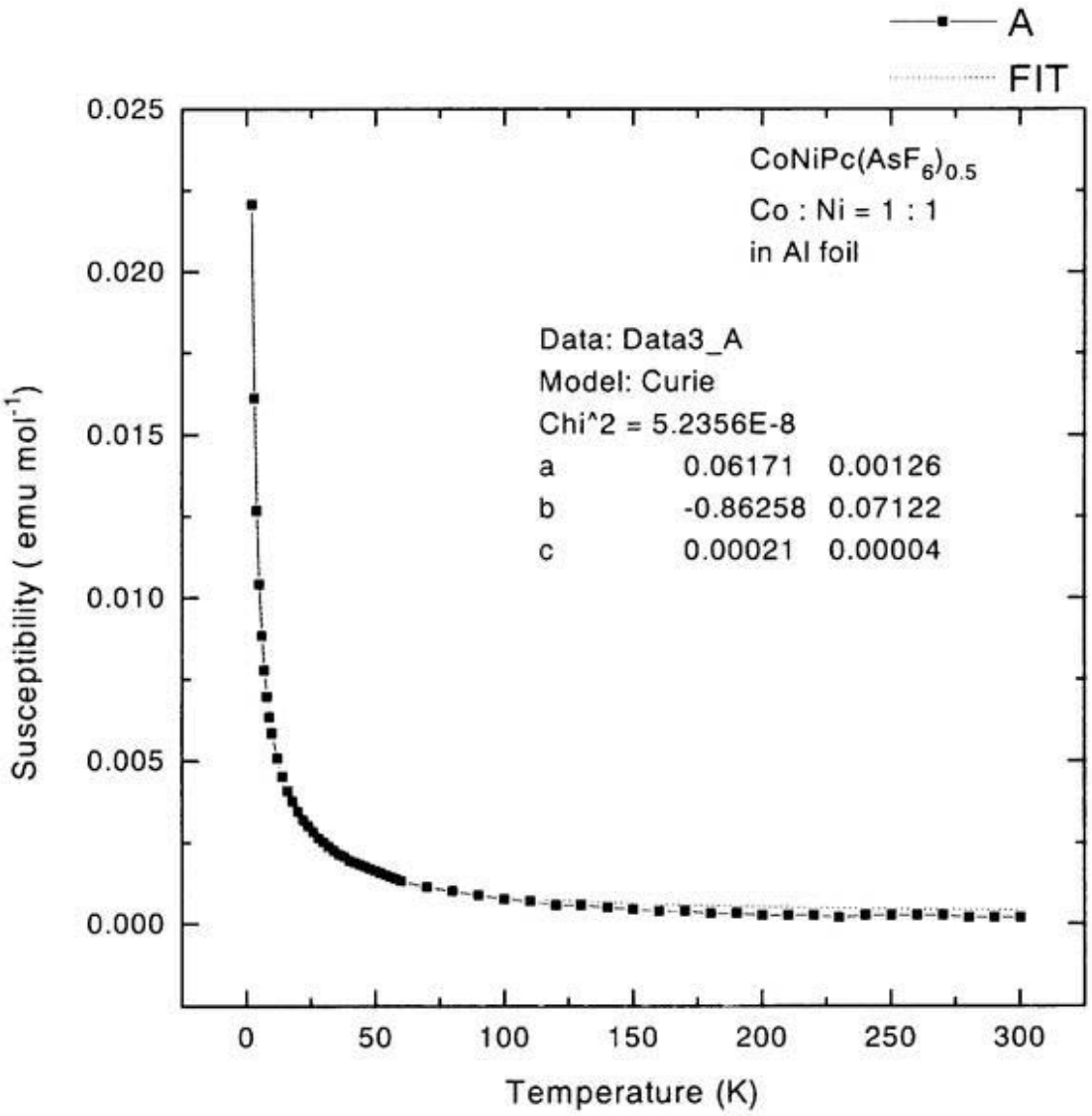

Fig. 11 Susceptibility of Mixed crystal

Table 1-1. Experimental details for $Co_xNi_{1-x}Pc(AsF_6)_{0.5}$ (Co : Ni = 1 : 3)

Crystal Data	
Empirical Formula	$C_{32}H_{16}N_8Ni_{0.75}\ Co_{0.25}As_{0.5}F_3$
Formula Weight	665.75
Crystal Dimensions	$0.03 \times 0.03 \times 0.5\ mm^3$
Crystal System	orthorhombic
Lattice Type	Primitive
No. of Reflections Used for Unit Cell Determination (2θ range)	13 (24.1-26.4°)
Omega Scan Peak Width at Half-hight	0.41°
Lattice Parameters	a = 14.032(9) Å b = 28.49(1) Å c = 6.422(4) Å V = 2567(2) $Å^3$
Space Group	Panm
Z value	4
D_{calc}	1.722 g / cm^3
F_{000}	1341.00
$\mu(MoK_\alpha)$	14.39 cm^{-1}

Intensity Measurements	
Diffractometer	Rigaku AFC7R
Radiation	NoK_α (λ =0.71069 Å) graphite monochromated
Attenuator	Zr foil (factor = 7.33)
Take-off Angle	6.0°
Detector Aperture	3.0 mm horizontal 3.0 mm vertical
Crystal to Detector Distance	235 mm
Voltage, Current	50 kV, 100 mA
Temperature	23.0 ℃
Scan Type	ω
Scan Rate	8.0° / min (in ω) (up to 5 scans)
Scan Width	(0.90 + 0.30 tan θ)°
$2\theta_{max}$	55.1°

No. of Reflections Measured	Total: 3406
	Unique: 3405 (R_{int} = 5.553)
Corrections	Lorentz-polarization

Structure Solution and Refinement	
Structure Solution	Patterson Methods (SAPI)
Refinement	Full-matrix least squares
Function Minimized	$\Sigma w(\|Fo\| - \|Fc\|)^2$
Least Squares Weights	$w = \frac{1}{\sigma^2(Fo)} = \left[\sigma_c{}^2(Fo) + \frac{p^2}{4} Fo^2 \right]^{-1}$
p-factor	0.0040
No. Observations (I > 3.00σ(I))	827
No. Variables	271
Reflection / Parameter Ratio	3.05
Residuals: R ; Rw	0.091 ; 0.129
Goodness of Fit Indicator	4.85
Max Shift / Error in Final Cycle	3.97
Maximum peak in Final Diff. Map	0.94 e^- / $Å^3$
Maximum peak in Final Diff. Map	-0.69 e^- / $Å^3$

Table 1-2. Experimental details for $Co_xNi_{1-x}Pc(AsF_6)_{0.5}$ (Co : Ni = 1 : 3)

Crystal Data	
Empirical Formula	$C_{32}H_{16}N_8Ni_{0.75}\ Co_{0.25}As_{0.5}F_3$
Formula Weight	665.79
Crystal Dimensions	$0.03\times0.03\times0.5\ mm^3$
Crystal System	orthorhombic
Lattice Type	Primitive
Indexing Images	222339568 stills @ 0.0minutes
Detector Position	0.00 mm
Detector Swing Angle	0.00 °
Pixel Size	NaN mm
Lattice Parameters	a = 14.033(4) Å
	b=28.54(1)Å
	c = 6.435(2) Å
	V = 2576.8101 $Å^3$
Space Group	Pnc2 (#30)
Z value	4
D_{calc}	1.716 g / cm^3
F_{000}	1341.00
$\mu(MoK_\alpha)$	14.33 cm^{-1}

Intensity Measurements	
Diffractometer	RAXISII
Radiation	MoK_α (λ =0.71070 Å)
	graphite monochromated
Detector Aperture	200 mm×200 mm
Data Images	41 exposures @ 0.0 minutes
Oscillation Range	0.0°
Detector Position	0.00 mm
Detector Swing Angle	0.00°
Pixel Size	0.000 mm
$2\theta_{max}$	51.4°
No. of Reflections Measured	Total: 2276
Corrections	Lorentz-polarization

	Secondary Extinction (coefficient: 4.24814e-06)

Structure Solution and Refinement	
Structure Solution	Direct Methods (SAPI91)
Refinement	Full-matrix least squares
Function Minimized	$\Sigma w(\|Fo\| - \|Fc\|)^2$
Least Squares Weights	$w = \frac{1}{\sigma^2(Fo)} = \left[\sigma_c{}^2(Fo) + \frac{p^2}{4} Fo^2 \right]^{-1}$
p-factor	0.0250
No. Observations (I > 3.00σ(I))	1739
No. Variables	388
Reflection / Parameter Ratio	4.48
Residuals: R ; Rw	0.068 ; 0.088
Goodness of Fit Indicator	2.71
Max Shift / Error in Final Cycle	2.17
Maximum peak in Final Diff. Map	0.95 e^- / $Å^3$
Maximum peak in Final Diff. Map	-0.52 e^- / $Å^3$

Table 2. Expereimental details for $Co_xNi_{1-x}Pc(AsF_6)_{0.5}$ (Co : Ni = 1 : 1.22)

Crystal Data	
Empirical Formula	$C_{32}H_{16}N_8Ni_{0.75}\ Co_{0.25}As_{0.5}F_3$
Formula Weight	665.79
Crystal Dimensions	$0.03\times0.03\times0.5\ mm^3$
Crystal System	tetragonal
Lattice Type	Primitive
Indexing Images	222339568 stills @ 0.0minutes
Detector Position	0.00 mm
Detector Swing Angle	0.00 °
Pixel Size	NaN mm
Lattice Parameters	a = 14.226(2) Å
	c = 6.414(1) Å
	V = 1298.0699 $Å^3$
Space Group	P4/mcc (#124)
Z value	1
D_{calc}	1.704 g / cm^3
F_{000}	669.00
$\mu(MoK_\alpha)$	13.58 cm^{-1}

Intensity Measurements	
Diffractometer	RAXISII
Radiation	MoK_α (λ =0.71070 Å)
	graphite monochromated
Detector Aperture	200 mm × 200 mm
Data Images	52 exposures @ 0.0 minutes
Oscillation Range	0.0°
Detector Position	0.00 mm
Detector Swing Angle	0.00°
Pixel Size	0.000 mm
$2\theta_{max}$	51.3°
No. of Reflections Measured	Total: 1113
	Unique: 664 (R_{int} = 0.064)
Corrections	Lorentz-polarization
	Secondary Extinction

(coefficient: 4.24814e-06)

Structure Solution and Refinement	
Structure Solution	Direct Methods (SAPI91)
Refinement	Full-matrix least squares
Function Minimized	$\Sigma w(\|Fo\| - \|Fc\|)^2$
Least Squares Weights	$w = \frac{1}{\sigma^2(Fo)} = \left[\sigma_c{}^2(Fo) + \frac{p^2}{4} Fo^2 \right]^{-1}$
p-factor	0.0300
No. Observations (I > 3.00σ(I))	436
No. Variables	70
Reflection / Parameter Ratio	6.23
Residuals: R ; Rw	0.070 ; 0.073
Goodness of Fit Indicator	2.14
Max Shift / Error in Final Cycle	0.03
Maximum peak in Final Diff. Map	0.67 e^- / Å^3
Maximum peak in Final Diff. Map	-0.68 e^- / Å^3

Table 3-1. Atomic coordinates and equivalent temperature facters B(eq) for $Co_xNi_{1-x}Pc(AsF_6)_{0.5}$ (Co : Ni = 1 : 3)

atom	x	y	z	B(eq)
As(1)	0.0000	0.5000	0.5000	8.5664
Ni(1)	0.4883	0.7459	0.0000	2.2321
Co(1)	0.4880	0.7458	0.0000	0.9971
F(1)	0.1069	0.5271	0.5000	14.4201
F(2)	0.0361	0.4636	0.3057	16.9180
N(1)	0.6078	0.7180	0.0000	1.5568
N(2)	0.5713	0.6371	0.0000	2.0995
N(3)	0.4338	0.6858	0.0000	1.2200
N(4)	0.2649	0.7040	0.0000	2.0780
N(5)	0.3671	0.7730	0.0000	2.0409
N(6)	0.4057	0.8551	0.0000	1.2565
N(7)	0.5460	0.8037	0.0000	2.0924
N(8)	0.7102	0.7861	0.0000	2.1409
C(1)	0.6943	0.7405	0.0000	2.0102
C(2)	0.7744	0.7068	0.0000	2.2333
C(3)	0.8701	0.7134	0.0000	2.8351
C(4)	0.9256	0.6732	0.0000	4.5517
C(5)	0.8849	0.6289	0.0000	3.9794
C(6)	0.7881	0.6232	0.0000	2.7975
C(7)	0.7336	0.6624	0.0000	2.4362
C(8)	0.6314	0.6719	0.0000	3.1336
C(9)	0.4737	0.6433	0.0000	1.4995
C(10)	0.4097	0.6049	0.0000	1.7323
C(11)	0.4256	0.5564	0.0000	3.6799
C(12)	0.3409	0.5300	0.0000	4.3411
C(13)	0.2482	0.5487	0.0000	3.8223
C(14)	0.2362	0.5966	0.0000	2.9616
C(15)	0.3239	0.6257	0.0000	1.6463
C(16)	0.3370	0.6756	0.0000	2.3383
C(17)	0.2786	0.7498	0.0000	2.9207
C(18)	0.1998	0.7837	0.0000	1.0792
C(19)	0.1073	0.7779	0.0000	3.2341
C(20)	0.0470	0.8171	0.0000	3.6306

C(21)	0.0900	0.8606	0.0000	4.7412
C(22)	0.1872	0.8691	0.0000	2.7410
C(23)	0.2419	0.8263	0.0000	2.4760
C(24)	0.3450	0.8204	0.0000	2.9224
C(25)	0.5012	0.8492	0.0000	2.7242
C(26)	0.5653	0.8857	0.0000	1.9894
C(27)	0.5555	0.9342	0.0000	2.5126
C(28)	0.6321	0.9630	0.0000	4.4328
C(29)	0.7241	0.9430	0.0000	4.6647
C(30)	0.7377	0.8939	0.0000	3.5890
C(31)	0.6555	0.8676	0.0000	2.1056
C(32)	0.6419	0.8150	0.0000	1.9969
H(1)	0.8978	0.7457	0.0000	4.0000
H(2)	0.9951	0.6774	0.0000	4.0000
H(3)	0.9260	0.6016	0.0000	4.0000
H(4)	0.7618	0.5924	0.0000	4.0000
H(5)	0.4896	0.5410	0.0000	4.0000
H(6)	0.3461	0.4965	0.0000	4.0000
H(7)	0.1962	0.5268	0.0000	4.0000
H(8)	0.1710	0.6087	0.0000	4.0000
H(9)	0.0788	0.7460	0.0000	4.0000
H(10)	-0.0206	0.8124	0.0000	4.0000
H(11)	0.0433	0.8864	0.0000	4.0000
H(12)	0.2149	0.9015	0.0000	4.0000
H(13)	0.4899	0.9472	0.0000	4.0000
H(14)	0.6232	0.9977	0.0000	4.0000
H(15)	0.7775	0.9645	0.0000	4.0000
H(16)	0.8022	0.8802	0.0000	4.0000

Table 3-2 Atomic coordinates and equivalent temperature factors B(eq) for $Co_xNi_{1-x}Pc(AsF_6)_{0.5}$(Co:Ni=1:3)

atom	x	y	z	B(eq)
As(1)	0	0	0.842	8.05(4)
Ni(1)	0.48787	0.25434	0.0708	2.03(2)
Co(1)	0.48784	0.25435	0.0704	3.16(7)
F(1)	0.9548	0.0412	0.9259	9.5(2)
F(2)	0.116	0.0291	0.0531	13.6(2)
F(3)	0.9808	0.0366	0.3053	18.9(5)
N(1)	0.3639	0.2265	0.07	2.76(8)
N(2)	0.2629	0.2952	0.071	2.72(9)
N(3)	0.431	0.3153	0.079	2.43(8)
N(4)	0.5693	0.3651	0.07	3.08(9)
N(5)	0.6106	0.2825	0.07	2.34(7)
N(6)	0.7122	0.2137	0.077	2.95(9)
N(7)	0.5442	0.1941	0.077	2.74(8)
N(8)	0.4053	0.1435	0.076	2.57(9)
C(1)	0.3437	0.179	0.062	2.32(9)
C(2)	0.2416	0.1713	0.066	2.39(9)
C(3)	0.1854	0.131	0.07	3.4(1)
C(4)	0.0891	0.1373	0.081	4.3(1)
C(5)	0.0472	0.182	0.067	4.6(2)
C(6)	0.104	0.222	0.085	3.5(1)
C(7)	0.1996	0.2158	0.074	2.50(9)
C(8)	0.279	0.2491	0.076	2.46(9)
C(9)	0.335	0.3252	0.065	2.52(9)
C(10)	0.3205	0.3756	0.066	2.86(10)
C(11)	0.2361	0.402	0.075	4.1(1)
C(12)	0.2487	0.4508	0.082	4.5(1)
C(13)	0.3404	0.4708	0.05	4.0(1)
C(14)	0.4219	0.4445	0.068	4.1(1)
C(15)	0.4086	0.396	0.087	2.7(1)
C(16)	0.4774	0.3575	0.081	2.46(9)
C(17)	0.6317	0.3293	0.079	2.97(10)
C(18)	0.7327	0.3373	0.083	2.9(1)
C(19)	0.7891	0.3778	0.052	2.9(1)
C(20)	0.8849	0.3725	0.074	4.4(1)
C(21)	0.9287	0.329	0.047	3.8(2)
C(22)	0.8715	0.2872	0.067	4.3(1)

C(23)	0.7759	0.2931	0.081	2.9(1)
C(24)	0.6977	0.2593	0.082	2.44(9)
C(25)	0.6399	0.1838	0.073	2.58(9)
C(26)	0.6557	0.133	0.078	2.90(10)
C(27)	0.738	0.1064	0.07	3.6(1)
C(28)	0.7265	0.058	0.084	4.2(1)
C(29)	0.6379	0.0383	0.079	5.2(2)
C(30)	0.5523	0.0638	0.06	3.9(1)
C(31)	0.5663	0.1127	0.089	2.38(10)
C(32)	0.4964	0.1508	0.063	2.20(9)
H(1)	0.2112	0.1006	0.1067	3.8501
H(2)	0.0519	0.11	0.0383	6.1536
H(3)	0.9749	0.1843	0.0161	5.8219
H(4)	0.0797	0.2538	0.0966	3.6512
H(5)	0.1745	0.3891	0.0335	3.7913
H(6)	0.2	0.4706	0.1363	3.5054
H(7)	0.3133	0.5043	0.0111	5.2381
H(8)	0.4842	0.4585	0.0623	4.2724
H(9)	0.7621	0.4086	0.0883	3.8922
H(10)	0.92	0.3993	0.0203	6.8183
H(11)	0.9999	0.3268	0.1067	4.3727
H(12)	0.8995	0.2555	0.0805	4.5034
H(13)	0.8012	0.1199	0.0376	3.8941
H(14)	0.78	0.038	0.1136	4.4548
H(15)	0.6323	0.0036	0.0125	6.2634
H(16)	0.4986	0.0504	0.0377	4.7042

Table 4 Atomic coordinates and equivalent temperature factors B(eq) for $Co_xNi_{1-x}Pc(AsF_6)_{0.5}$(Co:Ni=1:1.22)

atom	x	y	z	B(eq)
As(1)	0.0000	0.0000	0.0000	17.5(2)
Ni(1)	0.5000	0.5000	0.0000	3.34(4)
Co(1)	0.5000	0.5000	0.0000	3.48(6)
F(1)	0.9418	0.0865	0.8469	11.4804
F(2)	0.1194	0.0501	0.0000	12.6(10)
F(3)	0.9570	0.0430	0.2500	17.6405
N(1)	0.3791	0.4446	0.0000	3.5(1)
N(2)	0.2769	0.5821	0.0000	3.7(1)
C(1)	0.3571	0.3490	0.0000	3.5(2)
C(2)	0.2557	0.3339	0.0000	3.6(2)
C(3)	0.2007	0.2539	0.0000	4.5(2)
C(4)	0.1045	0.2646	0.0000	5.4(2)
C(5)	0.0626	0.3540	0.0000	5.6(2)
C(6)	0.1184	0.4341	0.0000	4.9(2)
C(7)	0.2154	0.4227	0.0000	3.9(2)
C(8)	0.2929	0.4904	0.0000	3.8(2)
H(1)	0.2283	0.1903	0.0000	5.3744
H(2)	0.0638	0.2090	0.0000	6.7700
H(3)	0.9904	0.3638	0.0000	6.2428
H(4)	0.0937	0.5013	0.0000	6.2699

Table 5-1. Crystal data of $NiPc(AsF_6)_{0.5}$ and $CoPc(AsF_6)_{0.5}$

	$NiPc(AsF_6)_{0.5}$	$CoPc(AsF_6)_{0.5}$
	orthorhombic	tetragonal
	Pnc2	*P4/mcc*
a/Å	14.015	14.234
b/Å	28.485	
c/Å	6.466	6.296
Z	4	2

Table5-2. Crystal data of Mixed Crystals

	$Co_{0.23}Ni_{0.75}Pc(AsF_6)_{0.5}$	$Co_{0.45}Ni_{0.55}Pc(AsF_6)_{0.5}$
a/Å	14.032(9)	14.17(1)
b/Å	28.49(1)	14.17(1)
c/Å	6.422(4)	6.40(2)
	6.435-6.409	6.46-6.34

Table 6. Interplaner distance (Å) of tetragonal phthalocyanine (Pc) and tetrabenzopolphyrin (tbp) radical salts

counter anion	AsF_6^-	I_3^-	ClO_4^-	BF_4^-	
H_2Pc	-	3.251	3.246	-	
CoPc	3.148	3.123	-	-	
Co(tbp)	-	3.168	-	-	
NiPc	3.233	3.244	3.233	3.24	
Ni(tbp)	-	3.217	-	-	
CuPc	-	3.195	-	-	
PtPc	3.255	-	-	-	
LiPc					3.245

Chapter 5

Concluding remarks

The author summarized the results at the present stage, including the prospects in future.

(1) $NiPc(AsF_6)_{0.5}$

(a) metal-insulator transition under high pressure

The metal-insulator transition temperature goes up to high temperature side on increasing pressure. The thermopower under high pressure decreased linearly against temperature and did not show any anomaly around the metal-insulator transition temperature. Since thermopower is sensitive to the density of states at the Fermi level, this metal-insulator transition under high pressure is not accompanied by the opening of a gap at the Fermi level. There is a possibility that some kind of localization is related to this insulating mechanism under high pressure. Since the number of Ni^{3+} sites increases due to the metal-ligand charge transfer induced by high pressure, the insulating phase expands to the high-temperature region in a *P-T* phase diagram.

Pressure induced d-π charge transfer is regarded as the filling control by pressure. We developed the new doping method using the MPc-PBC composite film to investigate the possibility of the filling control by potential. Though we developed a new doping method based on the solid state, we could not succeed in the filling control. Recently, H. Ohnuki et al. reported metallic LB films which were fabricated by mixing bis-ethylenedioxy-tetrathiafulvalene, or BEDO-TTF and behenic acid.[1] From the viewpoint of the development of a new materials, the composite materials such as MPc-PBC and BO-BA films are noticeable.

(b) metal-insulator transition at ambient pressure

Judging from the result of the optical study for vibronic mode, the metal-insulator transition of $NiPc(AsF_6)_{0.5}$ at 40 K accompanied extremely small or no lattice dimerization along the *c*-axis.

The thermopower decreased linearly against temperature and did not show any anomaly around 40 K.

The preliminary data of heat capacity and low-temperature X-ray diffraction study indicate the possibility that this metal-insulator transition accompanied some kind of structural transition such as a torsion of the phthalocyanine molecular "gear" in the *a, b*-plane accompanying the change of crystal system from orthorhombic to monoclinic.

(2) $CoPc(AsF_6)_{0.5}$

$CoPc(AsF_6)_{0.5}$ is regarded as the narrow-gap one-dimensional semiconductor by its conducting behavior in the temperature range 20-500 K. From the theoretical viewpoint, it is pointed out that the next-nearest-neighbor repulsion among π-electrons and the magnetic coupling between π and d-electrons are essential to open a charge gap using the one-dimensional quarter-filled Heisenberg-Kondo lattice model.

The plasma frequency of $CoPc(AsF_6)_{0.5}$ is nearly 30 % larger than that of $NiPc(AsF_6)_{0.5}$. This result indicates the formation of one-dimensional d-band in $CoPc(AsF_6)_{0.5}$.

From the above-mentioned theoretical viewpoint, the formation of the d-band contributes to narrow the charge-gap. Therefore, the effect of the defects also could be a candidate of the origin of the insulating phase of $CoPc(AsF_6)_{0.5}$. In the case of one-dimensional system, it is quite right that the small defects has a great influence in

transport properties in comparison with two- or three-dimensional systems. In any case, one-dimensional system is fascinating because theory is tractable. Especially, magnetic phthalocyanine charge transfer salt is an ideal material which is endowed with low-dimensionality and magnetic interests.

(3) $Co_xNi_{1-x}Pc(AsF_6)_{0.5}$

The crystal of $Co_xNi_{1-x}Pc(AsF_6)_{0.5}$ (Co : Ni = 1 : 3) belongs to an orthorhombic system, the lattice parameters being a = 14.032 Å, b = 28.49 Å, c = 6.422 Å, and Z = 4. The crystal of $Co_xNi_{1-x}Pc(AsF_6)_{0.5}$ (Co : Ni = 1 : 1.22) belongs to a tetragonal system, the lattice parameters being a = 14.226 Å, c = 6.414 Å, and Z = 1. $Co_xNi_{1-x}Pc(AsF_6)_{0.5}$ shows characteristic three Raman bands in the spectrum palallel to c-axis. The plasma edge of $Co_xNi_{1-x}Pc(AsF_6)_{0.5}$ is close to that of $NiPc(AsF_6)_{0.5}$ in spite of the small contents of Ni ions, that is, the interaction between Co d-electrons can cut by the introduction of non-magnetic Ni ions. The magnetic researches for this mixed crystals are effective to promote our understanding for this π-d system.

---

[1] H. Ohnuki, T. Noda, M. Izumi, T. Imakubo, and R. Kato, Phys. Rev. B, 55, R10225 (1997).